NTNU – Trondheim
Norwegian University of
Science and Technology

Thermodynamic Analysis of Heat and Mass Transfer Using Entropy Production Formalism

Kjetil Bohman Sonerud

Chemical Engineering and Biotechnology
Submission date: June 2015
Supervisor: Tore Haug-Warberg, IKP
Co-supervisor: Dr.ing. Volker Siepmann, Yara International ASA

Norwegian University of Science and Technology
Department of Chemical Engineering

Abstract

The understanding of irreversible phenomena in the world around us is of great importance – not only for the intrinsic value of such understanding, but also for the industrial applications and technological benefits such an understanding brings with it. The main aim of the current work is to explore such phenomena – with emphasis on treating simultaneous mass and heat transfer – by studying the entropy production using mathematical modelling.

A model consisting of two connected subsystems containing a binary ideal gas mixture is developed and studied. In the case of a closed system, a perturbation from the equilibrium state give rise to a manifold of constant entropy given the constraints. In the case of an open system, the steady-state is maintained by external reservoir of thermal and chemical nature. The resulting internal mass and heat transfer between the two subsystems give rise to a manifold of constant entropy production given the constraints. In order to investigate these two situations, a variable step-length predictor-corrector method is developed and employed. Both types of manifolds are successfully traced.

By solving the models, a relationship of seemingly deep nature between the two types of manifolds is observed. It is shown that the projections of both manifolds into suitable coordinates in the Cartesian $\mathbb{R}^2$ plane may be described as generalised ellipses, which opens the possibility of a mapping between the two manifolds. Thus, a possible connection between the deviation from equilibrium entropy on the one hand and the constant entropy production of an open, steady-state system is established.

The results from the current work are not yet conclusive as to whether the correlation between the entropy production manifold and manifold of constant entropy may be employed to predict or describe the general behaviour of irreversible processes occurring. However, the results are seen as a promising, and further investigations are recommended.

Sammendrag

Irreversible fenomen er en viktig del av verden rundt oss. En grundig forståelse av disse er av stor betydning - både av akademisk interesse, men også med hensyn på mulige industrielle applikasjoner og teknologiske fordeler en slik innsikt bringer med seg. Hovedformålet denne oppgaven er å utforske og belyse slike fenomen – med særlig vekt på simultan masse- og varmeoverføring –ved å bruke matematisk modellering til å betrakte entropiproduksjon.

En modell bestående av to sammenkoblede delsystem er blitt utviklet, hvorav hvert delsystem inneholder en binær, ideell gassblanding. To grensetilfeller er studert. I det ene tilfellet betraktes et lukket system. Her vil en forstyrrelse av likevektstilstanden gi opphav til et manifold av konstant entropi, gitt likningene som begrenser systemet. I det andre tilfellet betraktes et åpent system som opprettholdes ved stasjonære betingelser ved hjelp av ytre reservoar som tilfører masse og varme til systemet. Her gir de irreversible prosessene knyttet til den indre masse- og varmeoverføring mellom de to delsystemene opphav til et manifold av konstant entropiproduksjon. For å kunne behandle disse to tilfellene er det utviklet en prediktor-korrektor-metode med variabel steglengde. Denne er benyttet for å kartlegge begge manifoldene, med vellykket resultat.

Ved å betrakte resultatene er det avdekket en tilsynelatende dyp sammenheng mellom de to typene manifolder. Det er vist at dersom manifoldene projiseres ned i egnede kartesiske koordinater i $\mathbb{R}^2$ kan begge beskrives som generiske ellipser. Dette åpner for å gå fra den ene manifoldbeskrivelsen til den til den andre, som igjen åpner for en mulig sammenheng mellom avviket fra likevek-

tentropi på den ene siden og konstant entropiproduksjon i et åpent, stasjonært system på den andre siden.

Basert på resultatene fra dette arbeidet er det ikke mulig å si noe entydig om hvorvidt sammenhengen mellom entropiproduksjonsmanifoldet og manifoldet for konstant entropi kan brukes til å forutsi eller beskrive den generelle oppførselen til irreversible prosesser. Resultatene betraktes imidlertid som lovende, og videre undersøkelser av dette konseptet anbefales.

Preface

Problems worthy
of attack
prove their worth
by hitting back.

PIET HEIN, "Gruk 1"

This master thesis constitutes the final part of the 5-year integrated master program in Chemical Engineering and Biotechnology at the Norwegian University of Science and Technology (NTNU). The thesis was completed during the spring semester of 2015, with Associate Professor Tore Haug-Warberg as the main supervisor and dr.ing. Volker Siepmann as co-supervisor.

The idea behind this thesis is partly a continuation of the work performed for the specialisation project during the autumn of 2014 (Sonerud, 2014). Here, a literature review was conducted, but no modelling or calculations were performed. Thus, the current work – with its focus on model implementation and computation – complements the former. Parts of the theory in the current work is a refined and improved continuation of this project, while all calculations and modelling is entirely new.

I would like to thank the Process Modeling and Control department of Yara International ASA in Porsgrunn, Norway in general, and Dr.ing. Knut Wiig Mathisen in particular. As a summer intern of 2014, I was introduced to the interesting and challenging subject of NOx absorption modelling – this lead

to the specialisation project of the autumn of 2014, which in turn lead to the current work.

Øivind Wilhelmsen and Signe Kjelstrup of the Department of Chemistry, NTNU are thanked for valuable input at the early stages of the work. Furthermore, my co-supervisor dr.ing. Volker Siepmann deserves the highest praise. His knowledge, nerdy humour and insight has been highly appreciated – our weekly meetings have been a source of inspiration.

I would like to thank my main supervisor, Associate Professor Tore Haug-Warberg, for his keen interest in and help with the current work. Long debugging sessions to 10PM did not seem to dampen the enthusiasm. The countless interesting discussions – both regarding the thesis subject and many others – have always been enjoyed. His knowledge and enthusiastic curiosity is rare. In short: my sincerest thanks for being a superior supervisor.

I would like to thank my fellow students of the Process-Systems Engineering group (room K4-230) for many discussions, lunches and laughs. A special thanks to Ingrid for proof-reading parts of the thesis, and to Kasper both for proof-reading and magic LaTeX-skills. Without you, the thesis would look a lot worse. The valuable TikZ-lessons from Tobias are also gratefully acknowledged.

Last, but not least, I am truly grateful to my family and my friends for always being there when they are needed. A special thanks to Ingvild – both for support and general awesomeness.

Declaration of Compliance

I herby declare that this is an independent work according to the exam regulations of the Norwegian University of Science and Technology (NTNU).

Trondheim, 25.06.2015

Kjetil Bohman Sonerud

Contents

List of Figures

List of Acronyms

NOTATION	DESCRIPTION
DOF	degree of freedom
EB	energy balance
EOS	equation of state
M-S	Maxwell-Stefan
MB	mass balance
N-R	Newton-Raphson
NET	non-equilibrium thermodynamics
OOP	object-oriented programming
PDE	partial differential equation
PR	Peng-Robinson
RK	Redlich-Kwong
SRK	Soave-Redlich-Kwong

List of symbols

NOTATION	DESCRIPTION	UNIT
A	Helmholtz free energy	J
a	(thermodynamic) activity	
A_{char}	characteristic contact area	m^2
C	concentration	$\text{mol}\,\text{m}^{-3}$
c_p	specific molar heat capacity at constant pressure	$\text{J}\,\text{K}^{-1}\,\text{mol}^{-1}$
c_V	specific molar heat capacity at constant volume	$\text{J}\,\text{K}^{-1}\,\text{mol}^{-1}$
D	diffusion coefficient	$\text{m}^2\,\text{s}^{-1}$
D_{tot}	total diffusion coefficient	$\text{m}^3\,\text{s}^{-1}$
f	fully developed degrees of freedom	
$\boldsymbol{F}$	general vector-valued function	
ϕ	angle in polar coordinates	rad
G	Gibbs free energy	J
H	enthalpy	J
$\Delta_f h^\circ$	standard state ideal gas enthalpy of formation	$\text{J}\,\text{mol}^{-1}$
$\underline{\boldsymbol{h}}$	molar enthalpy vector	$\text{J}\,\text{mol}^{-1}$
h	molar enthalpy	$\text{J}\,\text{mol}^{-1}$
$\bar{h}$	partial molar enthalpy	$\text{J}\,\text{mol}^{-1}$
$\Delta_{\text{vap}} h$	enthalpy of vaporisation	$\text{J}\,\text{mol}^{-1}$

NOTATION	DESCRIPTION	UNIT
J	diffusive component mass flux	$\mathrm{mol\,s^{-1}\,m^{-2}}$
$\underline{\underline{\boldsymbol{J}}}$	Jacobian	
k	heat transfer coefficient	$\mathrm{W\,m^{-1}\,K^{-1}}$
κ	condition number	
k_{tot}	total heat transfer coefficient	$\mathrm{W\,K^{-1}}$
k_{B}	Boltzmann's constant	$\mathrm{J\,K^{-1}}$
L_{arc}	arc length	
l_{char}	characteristic diffusion distance	m
$\underline{\boldsymbol{\mu}}$	chemical potential vector	$\mathrm{J\,mol^{-1}}$
μ	chemical potential	$\mathrm{J\,mol^{-1}}$
N	total mole number	mol
$\hat{N}$	total diffusive component mass flux	$\mathrm{mol\,s^{-1}}$
$\underline{\boldsymbol{n}}$	mole vector	mol
N_A	Avogadro's number	$\mathrm{mol^{-1}}$
p	pressure	Pa
$\underline{\boldsymbol{P}}_{\underline{\boldsymbol{X}}}$	gradient of a generalised thermodynamic potential with respect to $\underline{\boldsymbol{X}}$	
$\underline{\underline{\boldsymbol{P}}}_{\underline{\boldsymbol{X}}\underline{\boldsymbol{X}}}$	Hessian of a generalised thermodynamic potential with respect to $\underline{\boldsymbol{X}}$	
P	generalised thermodynamic potential	
$\hat{Q}$	total heat flux	$\mathrm{J\,s^{-1}}$
q	heat flux	$\mathrm{J\,s^{-1}\,m^{-2}}$
$\hat{Q}^{\dagger}$	discrete heat of transfer	$\mathrm{J\,s^{-1}}$
R	universal gas constant	$\mathrm{J\,K^{-1}\,mol^{-1}}$
r	radius in polar coordinates	
S	entropy	$\mathrm{J\,K^{-1}}$
$\hat{S}$	transported entropy by mass flow	$\mathrm{J\,K^{-1}\,s^{-1}}$
$\dot{S}_{\mathrm{irr}}$	internal entropy production	$\mathrm{J\,K^{-1}\,s^{-1}}$
s°	standard state ideal gas entropy	$\mathrm{J\,K^{-1}\,mol^{-1}}$
$\underline{\boldsymbol{s}}$	molar entropy vetcor	$\mathrm{J\,K^{-1}\,mol^{-1}}$

NOTATION	DESCRIPTION	UNIT
s	molar entropy	$\mathrm{J\,K^{-1}\,mol^{-1}}$
$\bar{s}$	partial molar entropy	$\mathrm{J\,K^{-1}\,mol^{-1}}$
T	(absolute) temperature	K
t	time	s
U	internal energy	J
V	volume	$\mathrm{m^3}$
x	general Cartesian x-coordinate	
$\underline{\boldsymbol{x}}_{\mathrm{ext}}$	generalised extensive variable	
$\underline{\boldsymbol{x}}_{\mathrm{int}}$	generalised intensive variable	
x	mole fraction	
y	general Cartesian y-coordinate	

List of sub- and superscripts

NOTATION	DESCRIPTION
con	connection between subsystem 1 and 2
eq	state of thermodynamic equilibrium
gas	gas phase
i	component *i*
ig	ideal gas
init	initial value
j	subsystem *j*
liq	liquid phase
red	reduced coordinate
ref	reference
rsvr	reservoir
ss	steady-state
tot	total

Chapter 1

Introduction

> In science it is always necessary to abstract from the complexity of the real world and in its place to substitute a more or less idealized situation that is more amenable to analysis.
>
> K. G. DENBIGH[1]

In the natural sciences, a fundamental desire is to describe, understand and predict the behaviour of the world around us. In the pursuit of such understanding and knowledge, we need *models* – mental, mathematical or otherwise – that act as glasses through which we observe and make sense of the way Nature operates. Models help us systematise and sort our knowledge and experiences.

The choice of model must reflect the desired outcome – no model, however advanced, is a perfect replica of the real world we live in. Models are human inventions – *a model does not equal reality* (Zumdahl, 2009). For a model to be used effectively, one must understand both its weaknesses and its strengths, and ask only the appropriate questions. In other words, one most choose a model that is *sufficiently accurate in describing the processes and phenomena of interest – and only expect the model to answer questions related to these*.

[1] Introduction to *"The Thermodynamics of the Steady State"*, (Denbigh, 1951)

Modelling irreversible processes: no single best way?

Despite the huge success of classical equilibrium thermodynamics, the world we live in is fundamentally irreversible – in the strictest sense, no true equilibrium exists.[2] Essentially everything – from the smallest cells in our bodies to the largest industrial process plants – is governed by irreversible phenomena.

Thus, the understanding of irreversible phenomena in the world around us is of great importance – not only for the intrinsic value of such understanding, but also for the industrial applications and technological benefits such an understanding brings with it. The NOx absorption process – e.g. that of Yara International ASA – which is a part of the nitric acid production is one industrial example where irreversible transport phenomena and chemical reactions are of key importance (Pradhan et al., 1997; Chatterjee and Joshi, 2008). There are many more; one other example being that of (multicomponent) distillation, as described by e.g. Kooijman and Taylor (1995) or Taylor et al. (1994). It may be argued that understanding irreversible phenomena – and when they must be treated as such, i.e. that an equilibrium approach is insufficient – is at the heart of applied chemical engineering (Wesselingh, 1997). The importance of such an understanding can not be underestimated.

> "Much remains to be done, but the utility of transport phenomena can be expected to increase rather than diminish. Each of the exiting new technologies blossoming around us is governed, at the detailed level of interest, by the conservation laws and flux expressions, together with information on the transport coefficients."
> –(Bird et al., 2007)

The aim of the current work is to explore the nature of irreversible phenomena – more specifically, those of simultaneous mass and heat transfer – with emphasis on *principles* rather than *pragmatic application*. The latter is an important part of chemical engineering – many heuristics and empirical correlations yield results

[2] This is, of course, a question of *time-scale* for any practical purposes. Systems with irreversible processes that are sufficiently slow in the time-scales of interest may be *treated as though they were at equilibrium*. However, as Earth is an open system with respect to energy – there is a continuous influx of energy from the Sun, which in turn stems from the irreversible processes of nuclear fusion – no state of true equilibrium may exist.

and rules of thumb that are of great importance in the chemical process industry. However, such an approach will seldom lead to insight into the fundamentals, such as the possibility of relating the thermodynamics of reversible phenomena and the theory of irreversible transport phenomena. It is such insight – or rather, a small step towards it – that is the main goal of this thesis.

This may seem like one step backwards – by nature, simplified systems must be studied. Why not use models that mimic the real world with the greatest possible precision? To paraphrase Otto Redlich: it is often helpful to take a few steps backwards when challenging subjects are treated in order to pave the road for subsequent progress.[3] The hope is that such insight will eventually lead to progress both in real-world practise and theoretical knowledge – both are of great value.

It is noted that the interest in transport phenomena in particular and rate phenomena in general seems to have increased in the last half of the 20th century and this far into the 21st (Bird, 2004). This seems to stem from an ever-increasing desire to understand Nature – not only for its intrinsic value, but also because of the industrial applications and benefits that follow. As computing power is ever more available and the regulations on emissions, energy expenditure and HSE are increasing, the need for and availability of models to represent the real world is larger than ever before.

However, there seems to be no single-agreed upon approach to modelling such rate problems. The classical texts on separation processes in chemical engineering such as (Geankoplis, 2003) frequently employs the assumption that phenomena that are inherently irreversible – such as distillation – may be treated as though an equilibrium is locally instilled. The latter gives rise to the celebrated concept of the *equilibrium tray*. In order to describe the behaviour and operation of real separation processes, empirical correction factors must regularly be employed. It is argued that such an approach often lead to unphysical and un-

[3] OTTO REDLICH (1896-1978) made numerous contributions to science, with the Redlich-Kwong equation of state (EOS) being the best-known to most chemical engineers. The full quotation paraphrased above: *"It is the ability of retracing to the fundamentals that distinguishes the technologist from the technician, who applies well established formulae according to old examples. Whenever a really new problem arises and the established model fails, the technologist has to go back step by step in order to find the point of departure from where he must start to blaze a new trail."* (Redlich, 1976)

realistic descriptions, especially so for multicomponent mixtures (Krishna and Wesselingh, 1990).

In what may be argued to be *the* classic text in engineering transport phenomena – (Bird et al., 2007) – dimensionless quantities and empirical relations are emphasised. While such an approach is certainly of great practical value, the underlying phenomena may often be obscured at first sight.[4] A similar approach is taken by (Jakobsen, 2008), with emphasis on the implications for chemical reactor modelling.

Other authors take a different approach; in the field of non-equilibrium thermodynamics (NET), the consistent treatment of coupled, irreversible phenomena is at the very centre (Denbigh, 1959; de Groot and Mazur, 1984; Kjelstrup et al., 2010). The framework extends classical equilibrium thermodynamics, employing the pioneering work of Onsager[5] to describe the nature of irreversible processes as a sum of force-flux relations. A brief outline of the subject will be given in Chapter 3. Others again focus on certain aspects of irreversible phenomena – such as the Maxwell-Stefan (M-S) approach to mass transfer outlined by (Krishnamurthy and Taylor, 1985*a*,*b*; Krishna and Taylor, 1993). This approach has proved to be especially successful for multicomponent mass transfer applications, e.g. in separation processes such as distillation.

It is frequently emphasised in the literature that classical thermodynamics is a science of *states*, not *rates* (Callen, 1985; Kondepudi, 2008). In other words, while reversible processes[6] are adequately treated, the irreversible processes such as mass and heat transfer are seen as being outside the scope of thermodynamics. Whether this is taken as true or not – the aforementioned NET framework may

[4] The author wishes to emphasise that this must not be seen as criticism towards (Bird et al., 2007) – the text is extensive and excellently written, presenting the mathematical analogy between the treatment of momentum, mass and energy transport in a rigorous way. The main point is mainly to contrast this classical engineering approach with that of other, related frameworks to underpin the fact that there seems to be *no single way of treating irreversible phenomena in the available literature.*

[5] American-Norwegian scientist and 1968 Nobel laureate Lars Onsager (1903-1976) is often credited with being the father of irreversible thermodynamics due to his discovery of the *reciprocal relations* (Onsager, 1931*a*,*b*) bearing his name that are at the core of the subject (Callen, 1985).

[6] It should be emphasised that while no real process is truly reversible, many processes evolve through a series of quasi-equilibrium states – where any irreversible processes are of negligible importance – such that they may be treated as though the were equilibrium processes. This notion will be further explored in the context of the model development in Chapter 4.

serve as an illustration that such a restriction may not be the full story – it must be emphasised that the *time and space invariant state of equilibrium governed by classical thermodynamics will always be a limiting case for any irreversible process.* In other words, one may state that thermodynamics provide boundaries that must be respected – all irreversible processes should cease at the state of equilibrium, since the driving forces for such phenomena are necessarily zero at this state (Sandler, 1989; Callen, 1985). All models used to describe irreversible phenomena – whichever are chosen and for whatever reason – should converge to the state of thermodynamic equilibrium in the *absence of external constraints* and *given sufficient time*.[7] This state may never be realised on the relevant time scales – and the pragmatic engineer may thus be inclined to dismiss the whole point as being of no practical implication. However, it is proposed - - that *consistence with classical thermodynamics* is still of both great interest and importance in any modelling of irreversible phenomena. Employing models that are consistent in their description of Nature must be seen as a major benefit – such models are *robust* in the sense that they may be used to describe the steady-state scenario and the equilibrium situation alike.

Thesis objective

The aim of the current work is to investigate the modelling of irreversible phenomena in general – with emphasis on mass and heat transfer in particular – using driving forces that are consistent with classical equilibrium thermodynamics. In addition, avoiding a detailed integration of the transport equations over the connecting volume is sought to be avoided – the *gradients* of a true continuous description are approximated by the *differences* of lumped description.

[7] The notion of *sufficient* is of great importance – whether relaxation towards equilibrium is a fast or slow process differs with vast orders of magnitude. As an example, mechanical equilibrium in gaseous systems is often assumed to be instantaneous on the relevant time scales of most chemical engineering applications (de Groot and Mazur, 1984) – this assumption will be employed as part of the model development in Chapter 4. In contrast, a commonly cited example of the opposite is that of diamond – this carbon structure is thermodynamically unstable at standard temperature and pressure. In other words, the diamond jewellery is a non-equilibrium system waiting to relax back to its most stable form – that of graphite. However, since the activation energy barrier for this phase transition is very high, the rates of this process is extremely slow on the time scales relevant to a human life. Thus, the diamond may - with justice - be regarded as a stable compound for all practical purposes (Kjelstrup and Helbæk, 2006)

In order to achieve this, a two-compartment system of a binary ideal gas mixture is studied. Simultaneous mass and heat transfer is treated, assuming that there is no direct coupling[8] between the two – in other words, the phenomena are considered to be superposed. The set of equations governing the composite system gives rise to *manifolds of constant entropy* – for the closed system – and *manifolds of constant entropy production* – for the open system maintained at a steady-state. Tracing out these manifolds is a central part of the current work, using a self-developed, generalised predictor-corrector method implemented in PYTHON. The tracing of the constant entropy production manifold is performed using different phenomenological transport laws in order to observe and explore the implications of the different formulations. Since ensuring *consistency* is seen as important, it is verified that the proposed model obey the *a priori* inferred relations between the different formulations of the entropy production, as well as that of the integrated entropy production along the path of relaxation towards a state of equilibrium from that of a non-equilibrium state. These notions are further explored in Chapter 2 and Chapter 4.

The main focus is on *principles* and *understanding* at the cost of *practical engineering results*. Thus, this thesis will not provide an improved method or correlation for predicting transport phenomena as observed in real process plants – the aim is not a *valid* model. Rather, the intention is to explore whether a thermodynamically consistent formulation of such irreversible processes is feasible, and if we can learn anything new about the nature of such phenomena by exploring them in such a framework. Model *consistency* – and thus model *verification* are regarded as highly important.

Thesis structure

The theory of classical thermodynamics that is applicable to the current work is outlined in Chapter 2. This chapter also contains a discussion of the role of entropy in the modelling of irreversible phenomena, and how the entropy balance may be exploited for consistency checking in the latter context. Further-

[8] In other words, that the Soret and Dufour effects are negligible. These concepts – and their implications for the results – will be further discussed in Chapter 3.

more, an overview of the relevant transport phenomena theory for simultaneous mass and heat transfer is given in Chapter 3. Next, the model development – including model structure, constraint equations and modelling assumptions – is outlined in Chapter 4 The numerical method developed for the manifold tracing – a variable step-length predictor-corrector method – is presented in Chapter 5. Employing this to solve the developed models yields the results discussed in Chapter 6. Lastly, concluding remarks and suggestions for further work are given in Chapter 7.

The bigger picture

It is interesting to reflect on the topic of the current work in the context of the slightly bigger picture of general irreversible phenomena. It should be explicitly noted that the thesis objectives outlined above deviate from those of the original scope. The initial purpose of the current work was to explore how the combination of mass and heat transport and chemical reactions might be treated in a consistent manner for a gas-liquid interface – assuming that these were to be treated as irreversible, i.e. that the rates of the processes would have to be explicitly accounted for. Such a situation represents the reality for many problems relevant to the chemical engineer – including the process of NOx absorption that is a part of the nitric acid production used as a step in modern fertilizer manufacturing. The latter was the subject of the literature study conducted by the author as part of the specialisation project of the autumn 2014 (Sonerud, 2014), and the continuation of this by computational modelling was seen as an attractive topic.

The notion of tracing and exploring the entropy (production) manifolds that ended up being central in the current work were originally seen as an interesting idea only, and creating a proof-of-concept model to investigate this was expected to be a relatively swift process. However, it was realised that the complexity of both developing and solving the models necessary to shed light on this idea – even using idealisations such as ideal gas or simplified phenomenological laws – was largely underestimated by the author. As such, the original goal of treating chemical reactions was moderated, and the present goal of treating mass and

heat transfer only arose.

This experience underscores the seemingly established fact from the literature that a consistent treatment of multiple simultaneous irreversible processes is highly complex. Thus, the question of whether this is due to the inherent nature of these phenomena or the way we – as scientists and chemical engineers – approach them arises. The large increase in degrees of freedom of a true non-equilibrium problem treated as time and space variant – e.g. in terms of the amount of experimental parameters that are required – seems to give support to the former. However, the seemingly varying nature of the different attempts to describe such problems indicates that the optimal approach is not yet found.

In this context, the value of a proper focus on *structure* and *abstraction* is appreciated. These powerful principles apply to both programming and science alike – and especially so when the two subjects are combined as in the case of computer modelling in a thermodynamic context. While solving the *particular* is usually much more accessible, the true power of modelling arises with a focus of *generality* – in the sense that the same model or formulation may be employed to solve, explore and illuminate a diverse set of problems and challenges. This is often hard to achieve or formulate – a focus on structure and abstraction is demanding – but the eventual pay-off is often proportionally rewarding.

Chapter 2

Thermodynamics

> Thermodynamics is two laws and a little calculus.
>
> K. A. DILL & S. BROMBERG[1]

It may be argued that the impressive power of classical thermodynamics to handle a wide array of problems first and foremost stems from its *generality* – with a relatively small number of postulates, concepts and the necessary mathematical tools, a vast number of theoretical and practical problems may be treated and solved. The purpose of this chapter is to provide the necessary thermodynamic and mathematical background that enable the subsequent modelling and exploration of irreversible phenomena in later chapters. In doing so, the postulatory approach of (Haug-Warberg, 2006*b*) and (Callen, 1985) is followed – both are recommended for any reader interested in a more thorough discussion of the concepts presented below.

Classical thermodynamics is the study of energy and its conversion from one form to the other – in situations as diverse as that of living cells and industrial refrigeration cycles (Atkins, 2010). It is a macroscopic science, abstracting the detailed properties of the myriads of interacting atoms and molecules that comprise the system in question to a few state variables. For an illustrative example of the abstractive powers of classical thermodynamics, consider a balloon filled

[1] Chapter 6 in *"Molecular Driving Forces: Statistical Thermodynamics in Biology, Chemistry, Physics, and Nanoscience"*, (Dill and Bromberg, 2010)

with helium (He) at standard temperature and pressure.[2] At first, one might imagine that in order to describe the *macroscopic* state of this ensemble of atoms, the *microscopic* position and momentum of each atom would have to be known – a number of variables of the order 1×10^{23}. However, from the point of view of classical thermodynamics, this system may be fully characterised by three variables only – (T, V, N) – where T is (absolute) temperature, V is volume and N is the number of moles of He.[3] To say that this is an enormous reduction in the amount of data needed to fully describe the macroscopic state of the system is an understatement. Put differently, most of the microscopic coordinates are not of interest from the macroscopic point of view – most of the $\approx 1 \times 10^{23}$ degrees of freedom cancel out.

2.1 Fundamental postulates of classical thermodynamics

The purpose of this section is to present the fundamental postulates of classical equilibrium thermodynamics on which the rest of this chapter resides. Choosing the internal energy formulation as a starting point, it is postulated that there exists an *extensive* thermodynamic state function $U(S, V, \underline{\boldsymbol{n}})$ - the fundamental equation - such that

$$\mathrm{d}U = \left(\frac{\partial U}{\partial S}\right)_{V,\underline{\boldsymbol{n}}} \mathrm{d}S + \left(\frac{\partial U}{\partial V}\right)_{S,\underline{\boldsymbol{n}}} \mathrm{d}V + \sum_{i=1}^{m} \left(\frac{\partial U}{\partial N_i}\right)_{S,V,N_{j\neq i}} \mathrm{d}N_i \qquad (2.1)$$

The *extensive* variables of the system are the independent variables of eq. (2.1), with S being the entropy of the system, V being the volume of the system and $\underline{\boldsymbol{n}}$ being the mole vector of the m components of the system. In the internal energy formulation, these are the *canonical*[4] variables.

[2] The standard state pressure is normally assumed to be 1 bar – or 1×10^5 Pa – and the standard temperature is 298.15 K – or 25 °C

[3] In fact, the *intensive state* of this system may be described by only two variables, e.g. T and p. However, in order to fully account for the extensive state of the system, a third variable related to the *size of the system* is needed – e.g. the number of moles of He in the above example.

[4] Following (Siepmann, 2006), the canonical variables are the natural variables of a thermodynamic state function. By employing the Legendre transform described in Section 2.2, it is possible to go from one canonical representation to another without loss of information

Defining the partial derivatives of internal energy with respect to the extensive variables – the *intensive* variables of the system – as

$$\left(\frac{\partial U}{\partial S}\right)_{V,\underline{\boldsymbol{n}}} \triangleq T \tag{2.2}$$

$$\left(\frac{\partial U}{\partial V}\right)_{S,\underline{\boldsymbol{n}}} \triangleq -p \tag{2.3}$$

$$\left(\frac{\partial U}{\partial N_i}\right)_{S,V,N_{j\neq i}} \triangleq \mu_i \tag{2.4}$$

with T being the (absolute) temperature, p being the pressure and μ_i being the chemical potential of component i, it is possible to restate eq. (2.1) as

$$\mathrm{d}U = T\,\mathrm{d}S - p\,\mathrm{d}V + \sum_{i=1}^{m} \mu_i\,\mathrm{d}N_i \tag{2.5}$$

The understanding of the intensive variables as the ones that are independent of the size of the system, while the extensive variables scale with the size of the system corresponds to the more formal definition of the concepts as Euler homogeneous of zeroth and first order, respectively. The latter is further discussed in Section 2.3.

Another important postulate is that the internal energy is *additive* – a composite system that consists of several (separate) subsystems, each with internal energy $U_j = U_j(S_j, V_j, N_j)$, is characterised by

$$U_{\mathrm{tot}} = \sum_j U_j(S_j, V_j, N_j) \tag{2.6}$$

While this may seem obvious based on empirical and practical experience, it is nonetheless an important statement which will be employed in the subsequent sections.

Furthermore, it is postulated that a state of thermodynamic equilibrium is one of minimal internal energy constrained by the independent variables, such that

$$U_{\mathrm{eq}} = \min_{S,V,\underline{\boldsymbol{n}}} U_{\mathrm{tot}} \tag{2.7}$$

In many practical situations, holding e.g. the entropy constant may prove to be difficult. Thus, it is desirable to be able to formulate other energy functions

where one or more of the extensive variables are interchanged with the corresponding intensive variables. From a practical perspective, it is usually easier to work with, measure and control intensive variables such as temperature or pressure. [5] Herein lies some of the true power of classical equilibrium thermodynamics – the state variables and the corresponding energy function may be chosen so that it is *the most convenient for the problem at hand.* The mathematical framework to achieve this – the Legendre transform – is presented in Section 2.2.

2.2 Legendre transform

The mathematical transformation known as the *Legendre transform* is an important tool in thermodynamics, as it allows for variable transformation necessary to conveniently describe the problem using the energy function that is most suited. In short, the Legendre transform allows the conversion from one set of independent variables to another *without loss of any information*. The mathematics of the concept may easily be extended to functions of any number of variables. The Legendre transform provides a powerful framework for formulating classical thermodynamics – it ensures consistency, and lends itself to elegant abstraction.

Following (Haug-Warberg, 2006*b*), the formal definition of the *Legendre transform*, f_i, of the function f is taken to be

$$f_i(\xi_i, x_j, x_k, \ldots, x_n) \triangleq f(x_i, x_j, x_k, \ldots, x_n) - \left(\frac{\partial f}{\partial x_i}\right)_{x_j, x_k, \ldots, x_n} x_i \tag{2.8}$$

$$f_i(\xi_i, x_j, x_k, \ldots, x_n) = f(x_i, x_j, x_k, \ldots, x_n) - \xi_i x_i \tag{2.9}$$

where

$$\xi_i \triangleq \left(\frac{\partial f}{\partial x_i}\right)_{x_j, x_k, \ldots, x_n} \tag{2.10}$$

[5] Indeed, the Gibbs free energy– $G(T, p, \underline{\boldsymbol{n}})$, as will be shown in Section 2.2 – is regarded as the classical state function of chemical thermodynamics due to the fact that T and p are frequently the variables under our control in a laboratory setting (Atkins and de Paula, 2010; Dill and Bromberg, 2010). From a theoretical point of view, it may be argued that the Helmholtz free energy may be a better choice in many cases as the equation of state (EOS) employed are often given on pressure-explicit form, $p = p(T, V, \underline{\boldsymbol{n}})$, and thus the $(T, V, \underline{\boldsymbol{n}})$ are the most natural state variables. This will be further discussed in

If needed, it is possible to perform several transformations, obtaining several new transformed functions. The only information needed to define an arbitrary Legendre transform is the knowledge of the function f and its corresponding (partial) first derivatives, as can be seen from eq. (2.8). It is important to note that repeated Legendre transformations using the same variable will lead back to the original function. Thus, no information is lost in the transformation process. Essentially, the Legendre transform exploits the fact that a curve may either be represented as a set of points (x, y), or as a set of slopes of tangent lines α and their intersection with the y-axis, β, as illustrated by Løvfall (2008).

By applying the concept of the Legendre transformation to the internal energy $U(S, V, \underline{\boldsymbol{n}})$ postulated in Section 2.1, several new thermodynamic potentials may be defined. Each of these will have their own set of canonical variables from the above definitions and the transformation defined in eq. (2.8)

Enthalpy:
$$H(S, p, \underline{\boldsymbol{n}}) \triangleq U - \left(\frac{\partial U}{\partial V}\right)_{S,\underline{\boldsymbol{n}}} V = U + pV \tag{2.11a}$$

Helmholtz free energy:
$$A(T, V, \underline{\boldsymbol{n}}) \triangleq U - \left(\frac{\partial U}{\partial S}\right)_{V,\underline{\boldsymbol{n}}} S = U - TS \tag{2.11b}$$

Gibbs free energy:
$$\begin{aligned} G(T, p, \underline{\boldsymbol{n}}) &\triangleq U - \left(\frac{\partial U}{\partial V}\right)_{S,\underline{\boldsymbol{n}}} V - \left(\frac{\partial U}{\partial S}\right)_{V,\underline{\boldsymbol{n}}} S \\ &= U + pV - TS = H - TS \end{aligned} \tag{2.11c}$$

Here, the most used thermodynamic potentials are defined in terms of their respective Legendre transform from the internal energy, U. Thus, when facing a particular problem, the thermodynamics may be transformed to *fit the problem* – working in the *canonical variables* for the particular case. The fact that the partial first derivatives of the fundamental equation are *intensive variables of physical significance* – e.g. $\left(\frac{\partial U}{\partial S}\right)_{V,\underline{\boldsymbol{n}}} = T$ – the concept of the Legendre transform is particularly appealing in the context of thermodynamics.

It should be noted theconcept of a Legendre transform is not restricted to using internal energy as a starting point. As an example, the latter may be expressed

as a function of the Helmholtz free energy as follows

$$U = A - \left(\frac{\partial A}{\partial T}\right)_{V,\underline{n}} T \tag{2.12}$$

$$U = A - TA_T \tag{2.13}$$

where A_T denotes the partial derivative of Helmholtz free energy with respect to (absolute) temperature. Thus, given that $A(T, V, \underline{n})$ is known, U may be calculated.[6] As will be further discussed in Chapter 4 and later in the current chapter, the Helmholtz free energy– corresponding to the independent variables $(T, V, \underline{n})$, as shown in eq. (2.11b) – is a convenient state function for describing the gas phase, and will be employed in the current work. On the other hand, the Gibbs free energy– corresponding to the independent variables $(T, p, \underline{n})$, as shown in eq. (2.11c) – is often the most suitable state function for the description of condensed phases, e.g. liquids and solids, and has historically been the state function of choice in chemical engineering. However, Helmholtz free energy models have been used more frequently to describe both gas and liquid phases due to progress in the development of suitable EOS in the later years. As such, it is argued that the classical choice of using Gibbs free energy models in chemical engineering should be reconsidered in light of this (Pereira et al., 2014).

As a side note, performing a Legendre transform on U with respect to each of the extensive variables S, V and $\underline{n}$ yields the zero potential

$$\text{Zero potential} \quad O(T, p, \underline{\mu}) = U - \left(\frac{\partial U}{\partial V}\right)_{S,\underline{n}} - \left(\frac{\partial U}{\partial S}\right)_{V,\underline{n}} - \left(\frac{\partial U}{\partial \underline{n}}\right)_{S,V} \tag{2.14}$$

$$= U - TS + pV - \sum_{i=1}^{m} \mu_i \, \mathrm{d}N_i = 0 \tag{2.15}$$

From a total differential of the latter equation, the *Gibbs-Duhem equation* is ob-

[6] The approach may be taken one step further; differentiation of eq. (2.12) with respect to X yield $U_X = A_X - T_X A_T - T A_{TX}$, where $X \in \{T, V, \underline{n}\}$. This is a useful way of quickly finding the partial derivatives of U in Helmholtz free energy coordinates. E.g. taking $X = T$, one quickly finds $U_T = \cancel{A_T} - \cancel{A_T} - T A_{TT} = -T A_{TT}$.

tained

$$
\begin{aligned}
0 &= \cancel{T\,\mathrm{d}S} - \cancel{p\,\mathrm{d}V} + \sum_{i=1}^{m} \cancel{\mu_i}\,\mathrm{d}N_i - \cancel{T\,\mathrm{d}S} - S\,\mathrm{d}T + \cancel{p\,\mathrm{d}V} + V\,\mathrm{d}p \\
&\quad - \sum_{i=1}^{m} \cancel{\mu_i}\,\mathrm{d}N_i - \sum_{i=1}^{m} N_i\,\mathrm{d}\mu_i \\
0 &= -S\,\mathrm{d}T + V\,\mathrm{d}p - \sum_{i=1}^{m} N_i\,\mathrm{d}\mu_i
\end{aligned}
\tag{2.16}
$$

This equation plays an important part in consistency checking in thermodynamics, as it provides a relationship between the $2 + m$ intensive variables of an m component system. In other words, the Gibbs-Duhem equation dictates that only $1 + m$ of the intensive variables are independent. This restriction will provide an important relationship in the discussion of the thermodynamic driving force for mass transfer

The same relationship may be derived by combining eq. (2.1) and the *Euler integrated form* of the internal energy. The latter concept is the topic of Section 2.3.

2.3 Euler integration and Euler homogeneous functions

The concept of *Euler homogeneity* is closely related to the thermodynamic concept of *intensive* and *extensive* variables – the latter are Euler homogeneous of order zero and one, respectively. When this is established, *Euler integration* may be used to go from the (total) differential form to the Euler integrated form of a thermodynamic potential.

Euler homogeneous functions are explored with mathematical rigour in (Haug-Warberg, 2006*b*, chap. 4). Below, the approach of (Callen, 1985, chap. 3) is followed, with focus on the practical implications in the context of thermodynamics.

Using λ as a dimensionless parameter and employing vector notation, a function

is said to be Euler homogeneous of order k if the following holds true

$$F = f(\underline{\boldsymbol{X}}, \underline{\boldsymbol{\xi}}) \tag{2.17}$$

$$F = \lambda^k f(\underline{\boldsymbol{x}}, \underline{\boldsymbol{\xi}}) \tag{2.18}$$

$$\underline{\boldsymbol{X}} = \lambda \underline{\boldsymbol{x}} \tag{2.19}$$

Using the fact that the thermodynamic energy functions are known to be *extensive functions* , and thus Euler homogeneous of first order, it is possible to write the following for the internal energy

$$U(\lambda S, \lambda V, \lambda \underline{\boldsymbol{n}}) = \lambda U(S, V, \underline{\boldsymbol{n}}) \tag{2.20}$$

Differentiation with respect to λ yields

$$\begin{aligned} \frac{\partial U(\lambda S, \lambda V, \lambda \underline{\boldsymbol{n}})}{\partial \lambda S} \frac{\partial \lambda S}{\partial \lambda} + \frac{\partial U(\lambda S, \lambda V, \lambda \underline{\boldsymbol{n}})}{\partial \lambda V} \frac{\partial \lambda V}{\partial \lambda} \\ + \sum_{i=1}^{m} \frac{\partial U(\lambda S, \lambda V, \lambda \underline{\boldsymbol{n}})}{\partial \lambda N_i} \frac{\partial \lambda N_i}{\partial \lambda} = U(S, V, \underline{\boldsymbol{n}}) \end{aligned} \tag{2.21}$$

Note that the variables that are held constant in each partial derivative are omitted for clarity. By simplifying eq. (2.21) using eq. (2.20) and eq. (2.5), the equation may be rewritten as

$$U(S, V, \underline{\boldsymbol{n}}) = \frac{\partial U(S, V, \underline{\boldsymbol{n}})}{\partial S} S + \frac{\partial U(S, V, \underline{\boldsymbol{n}})}{\partial V} V + \sum_{i=1}^{m} \frac{\partial U(S, V, \underline{\boldsymbol{n}})}{\partial N_i} N_i \tag{2.22}$$

$$U(S, V, \underline{\boldsymbol{n}}) = TS - pV + \sum_{i=1}^{m} \mu_i N_i \tag{2.23}$$

The latter is referred to as the *Euler integrated form* of the internal energy. By applying the Legendre transform discussed in Section 2.2, equivalent expressions may be derived for the enthalpy (H), Gibbs free energy (G) and Helmholtz free energy (A). As the Euler integrated form of the Helmholtz free energy will prove to be crucial in Chapter 4, the explicit expression is shown in eq. (2.24) below. Using the definition of A as the Legendre transform of U with respect to S – as shown in eq. (2.11b) – along with eq. (2.23) above, it follows that

$$A(T, V, \underline{\boldsymbol{n}}) = U - TS = -pV + \sum_{i=1}^{m} \mu_i N_i \tag{2.24}$$

From eq. (2.24) it is evident that if $p = p(T, V, \underline{\boldsymbol{n}})$ and $\mu = \mu(T, V, \underline{\boldsymbol{n}})$ are known, the Helmholtz free energy may be calculated for a given state $(T, V, \underline{\boldsymbol{n}})$. This idea forms the backbone of the thermodynamic model utilized in Chapter 4.

Euler integration and consistency checking

The concept of Euler homogeneous functions provides an additional useful feature – it allows for *consistency checking* of the implemented thermodynamic model. As stated in Section 2.3, any thermodynamic potential is an Euler homogeneous function of 1st order, and may be written on Euler integrated form as

$$P(\underline{\boldsymbol{x}}_{\text{ext}}, \underline{\boldsymbol{x}}_{\text{int}}) = \left(\frac{\partial P}{\partial \underline{\boldsymbol{x}}_{\text{ext}}^{\top}} \right) \underline{\boldsymbol{x}}_{\text{ext}} \tag{2.25}$$

where P is a generalised thermodynamic potential, $\underline{\boldsymbol{x}}_{\text{ext}}$ represents the (canonical) extensive variables and $\underline{\boldsymbol{x}}_{\text{int}}$ represents the (canonical) intensive variables. Following (Siepmann, 2006), differentiating eq. (2.25) with respect to the extensive variables yield

$$\frac{\partial P(\underline{\boldsymbol{x}}_{\text{ext}}, \underline{\boldsymbol{x}}_{\text{int}})}{\partial \underline{\boldsymbol{x}}_{\text{ext}}} = \left(\frac{\partial^2 P}{\partial \underline{\boldsymbol{x}}_{\text{ext}} \partial \underline{\boldsymbol{x}}_{\text{ext}}^{\top}} \right) \underline{\boldsymbol{x}}_{\text{ext}} + \frac{\partial P}{\partial \underline{\boldsymbol{x}}_{\text{ext}}} \tag{2.26}$$

Thus, eq. (2.27) must be fulfilled

$$\left(\frac{\partial^2 P}{\partial \underline{\boldsymbol{x}}_{\text{ext}} \partial \underline{\boldsymbol{x}}_{\text{ext}}^{\top}} \right) \underline{\boldsymbol{x}}_{\text{ext}} = 0 \tag{2.27}$$

This may be used as a check that e.g. the Hessian[7] of a thermodynamic potential with only extensive variables such as U is correct, by calculating $\underline{\underline{\boldsymbol{U}}}_{\underline{\boldsymbol{X}}\underline{\boldsymbol{X}}} \cdot \underline{\boldsymbol{X}} \stackrel{?}{=} 0$, where $\underline{\boldsymbol{X}} = [S, V, \underline{\boldsymbol{n}}]^{\top}$.[8] For potentials that are functions of both intensive and

[7] The Hessian of a scalar-valued function f is a square matrix of second-order partial derivatives, $\underline{\underline{\boldsymbol{H}}}^{\top} = \nabla^2 f(\underline{\boldsymbol{x}})$. The Hessian is central in thermodynamics in several respects, among others when the mapping between coordinate sets are concerned. See (Thomas Jr. et al., 2009; Nocedal and Wright, 1999) for a more thorough mathematical description of the Hessian and it's central place in e.g. optimization problems

[8] In order to provide a concise notation, P_X designates the partial derivative of P with respect to X, holding other state variables constant. In a similar fashion, $P_{X_1 X_2}$ designates the second derivative of P with respect to X_1 and X_2, holding other state variables constant. Note that X_1 and X_2 may be the same variable. Using vector notation, $\underline{\boldsymbol{P}}_{\underline{\boldsymbol{X}}}$ and $\underline{\underline{\boldsymbol{P}}}_{\underline{\boldsymbol{X}}\underline{\boldsymbol{X}}}$ designates the gradient and Hessian of P with respect to $\underline{\boldsymbol{X}}$, respectively.

extensive variables, such as Helmholtz free energy, the part of the Hessian with respect to the extensive variables must still fulfil eq. (2.27). As such, $\underline{\underline{\boldsymbol{A}}}_{\boldsymbol{XX}} \cdot \underline{\boldsymbol{X}} \stackrel{?}{=} 0$ should evaluate to zero when $\underline{\boldsymbol{X}} = [V, \underline{\boldsymbol{n}}]^\top$ and $\underline{\underline{\boldsymbol{A}}}_{XX}^\top$ is a sub-matrix of the Hessian of A containing the derivatives with respect to V and $\underline{\boldsymbol{n}}$.

In terms of consistency checking, the above property allows the verification of the thermodynamic model implementation in the sense that if the model is not consistent – either by mistake or by design – the requirement of eq. (2.27) will not hold.

While the main topic of the current work is to study *irreversible phenomena*, the concept of *thermodynamic equilibrium* remains important also in this context – e.g. as a possible set of *driving forces* for such processes. The purpose of Section 2.4 is to explore the general criterion for such an equilibrium state.

2.4 Thermodynamic equilibrium

From the pragmatic perspective of the experimentalist, it may be stated that a thermodynamic system is in equilibrium when none of its thermodynamic properties are changing with time at any measurable rate (Reiss, 1996).[9] The purpose of Section 2.4 is to show that a state of thermodynamic equilibrium between two subsystems may be more precisely characterised by *equality of the intensive variables of the respective subsystems*[10] , using phase equilibrium between gas and liquid as an illustrative example.

In general, the equilibrium state of a given system corresponds to a minimum of the thermodynamic potential that uses the system's independent variables as

[9] Note that it is essential that such a definition must account for both changes in the system and the surroundings – otherwise, it would be impossible to distinguish the time-invariant state of true thermodynamic equilibrium from the time-invariant *steady-state* that is a limiting case of non-equilibrium systems. While the distinction between the two may seem small at first glance, the difference is of large importance in subsequent chapters.

[10] It should be noted that true thermodynamic equilibrium – however practically unattainable – is a time and space invariant state. Put differently, classical thermodynamics is not concerned with the coordinates of regular space and time at all – a statement such that "the temperature varies with time" has no place in equilibrium thermodynamics. In contrast, the intensive variables of non-equilibrium systems are in general both time and space variant, e.g. $T = T(t, \underline{x})$, the latter representing the space coordinates.

its canonical variables.[11] In the case of internal energy, a phase equilibrium may thus be characterised as

$$U_{\text{tot,eq}} = \min_{S,V,\underline{\boldsymbol{n}}} U_{\text{tot}} = \min_{S,V,\underline{\boldsymbol{n}}} \left(U^{\text{liq}} + U^{\text{gas}} \right) \tag{2.28}$$

Assuming that the system is closed and isolated – i.e. that there are no flows of mass, energy or momentum across the boundary – the following constraints apply[12]

$$S^{\text{liq}} + S^{\text{gas}} = S_{\text{tot}} \tag{2.29a}$$
$$V^{\text{liq}} + V^{\text{gas}} = V_{\text{tot}} \tag{2.29b}$$
$$\underline{\boldsymbol{n}}^{\text{liq}} + \underline{\boldsymbol{n}}^{\text{gas}} = \underline{\boldsymbol{n}}_{\text{tot}} \tag{2.29c}$$

Here, the superscripts $^{\text{gas}}$ and $^{\text{liq}}$ are used to distinguish the two phases, as this corresponds to the physical interpretation of the problem. Note, however, that this is arbitrary. This minimisation of the internal energy is the same as finding the entropy, volume and composition distribution that gives a zero total differential in the potential

$$\mathrm{d}(U_{\text{tot}}) = \mathrm{d}(U^{\text{liq}} + U^{\text{gas}}) = 0 \tag{2.30}$$

Substituting in the derivatives of U with respect to S, V and $\underline{\boldsymbol{n}}$ from Section 2.1,

[11] From statistical thermodynamics, a state of equilibrium is typically characterised by $S_{\text{eq}} = \max_{U,V,\underline{\boldsymbol{n}}} S_{\text{tot}}$ (Hill, 1960; Dill and Bromberg, 2010). As argued by e.g. (Callen, 1985), the choice of characterising an equilibrium state as a state of maximum entropy or minimum energy is – from a theoretical point of view – equivalent. In practical terms, minimizing an energy function is frequently easier to achieve in practise, as the state variables are usually variables that are easier to control, such as $G(T, p, \underline{\boldsymbol{n}})$ discussed earlier.

[12] It is important to note the distinction between the system described here and the actual model system of Chapter 4. The former allow a redistribution of volume – in the words of the chosen example, the gas-liquid interface is allowed to move. In the implemented model system, the volumes are specifically *fixed*. Thus, the *equality of pressure in each subsystem will not in general be the equilibrium criterion.* However, by invoking the assumption of *mechanical equilibrium* – as discussed in Chapter 4 – a non-thermodynamic constraint will impose the equality of pressure *at all times*, including at the state of equilibrium.

so that the total differential may be written as

$$\left(\left(\frac{\partial U}{\partial S}\right)^{\text{liq}}_{V,\underline{\boldsymbol{n}}} \mathrm{d}S^{\text{liq}} + \left(\frac{\partial U}{\partial V}\right)^{\text{liq}}_{S,\underline{\boldsymbol{n}}} \mathrm{d}V^{\text{liq}} + \left(\frac{\partial U}{\partial \underline{\boldsymbol{n}}}\right)^{\text{liq}}_{S,V} \mathrm{d}\underline{\boldsymbol{n}}^{\text{liq}}\right)$$
$$+\left(\left(\frac{\partial U}{\partial S}\right)^{\text{gas}}_{V,\underline{\boldsymbol{n}}} \mathrm{d}S^{\text{gas}} + \left(\frac{\partial U}{\partial V}\right)^{\text{gas}}_{S,\underline{\boldsymbol{n}}} \mathrm{d}V^{\text{gas}} + \left(\frac{\partial U}{\partial \underline{\boldsymbol{n}}}\right)^{\text{gas}}_{S,V} \mathrm{d}\underline{\boldsymbol{n}}^{\text{gas}}\right) = 0 \tag{2.31a}$$

$$(T^{\text{liq}}\,\mathrm{d}S^{\text{liq}} - p^{\text{liq}}\,\mathrm{d}V^{\text{liq}} + \underline{\boldsymbol{\mu}}^{\text{liq}}\,\mathrm{d}\underline{\boldsymbol{n}}^{\text{liq}})$$
$$+(T^{\text{gas}}\,\mathrm{d}S^{\text{gas}} - p^{\text{gas}}\,\mathrm{d}V^{\text{gas}} + \underline{\boldsymbol{\mu}}^{\text{gas}}\,\mathrm{d}\underline{\boldsymbol{n}}^{\text{gas}}) = 0 \tag{2.31b}$$

$$(-T^{\text{liq}}\,\mathrm{d}S^{\text{gas}} + p^{\text{liq}}\,\mathrm{d}V^{\text{gas}} - \underline{\boldsymbol{\mu}}^{\text{liq}}\,\mathrm{d}\underline{\boldsymbol{n}}^{\text{gas}})$$
$$+(T^{\text{gas}}\,\mathrm{d}S^{\text{gas}} - p^{\text{gas}}\,\mathrm{d}V^{\text{gas}} + \underline{\boldsymbol{\mu}}^{\text{gas}}\,\mathrm{d}\underline{\boldsymbol{n}}^{\text{gas}}) = 0 \tag{2.31c}$$

$$[T^{\text{gas}} - T^{\text{liq}}]\,\mathrm{d}S^{\text{gas}} - [p^{\text{gas}} - p^{\text{liq}}]\,\mathrm{d}V^{\text{gas}} + [\underline{\boldsymbol{\mu}}^{\text{gas}} - \underline{\boldsymbol{\mu}}^{\text{liq}}]\,\mathrm{d}\underline{\boldsymbol{n}}^{\text{gas}} = 0 \tag{2.31d}$$

where the relations $\mathrm{d}S^{\text{liq}} = -\mathrm{d}S^{\text{gas}}$, $\mathrm{d}V^{\text{liq}} = -\mathrm{d}V^{\text{gas}}$ and $\mathrm{d}\underline{\boldsymbol{n}}^{\text{liq}} = -\mathrm{d}\underline{\boldsymbol{n}}^{\text{gas}}$ from the differentiation of the total balances in eq. (2.29) are used. In order for eq. (2.31) to hold for any arbitrary choice of $\mathrm{d}S^{\text{gas}}$, $\mathrm{d}V^{\text{gas}}$ and $\mathrm{d}\underline{\boldsymbol{n}}^{\text{gas}}$, it must be true that

$$(T^{\text{gas}} - T^{\text{liq}}) = 0 \quad \Longrightarrow \quad T^{\text{gas}} = T^{\text{liq}} \tag{2.32a}$$

$$-(p^{\text{gas}} - p^{\text{liq}}) = 0 \quad \Longrightarrow \quad p^{\text{gas}} = p^{\text{liq}} \tag{2.32b}$$

$$(\underline{\boldsymbol{\mu}}^{\text{gas}} - \underline{\boldsymbol{\mu}}^{\text{liq}}) = 0 \quad \Longrightarrow \quad \underline{\boldsymbol{\mu}}^{\text{gas}} = \underline{\boldsymbol{\mu}}^{\text{liq}} \tag{2.32c}$$

Thus, it is shown that the *intensive variables* – that is, $(T, p, \underline{\boldsymbol{\mu}})$ – of the gas and liquid phase must be the same at equilibrium conditions. In fact, it may be shown that this is a general observation that holds for any number of components and phases.

As such, it may be natural to take the *deviation* from T_{eq}, p_{eq} and $\underline{\boldsymbol{\mu}}_{\text{eq}}$ of the intensive variables as driving forces for irreversible phenomena – such as heat, momentum and mass transfer. With a few alterations – accounting for the fact that $S(U, V, \underline{\boldsymbol{n}})$ is taken as the starting point – this is indeed proposed in the non-equilibrium thermodynamics (NET) framework, to be further discussed in Section 3.2.

2.5 Choice of thermodynamic coordinates

The choice of thermodynamic coordinates for modelling is a non-trivial matter. The true power – from the perspective of the master – and a source of frequent confusion – from the perspective of the inexperienced student – lies in the many possible choices of thermodynamic coordinates.

The concept of *state variables* is central to thermodynamics. Simply put, the state variables of a certain model are the variables that need to be known in order to determine all other properties of interest. In other words, if the state variables of the system are known, the state of the system is uniquely defined and any other quantity may be derived. The choice of state variables for any given case is closely tied to the choice of thermodynamic model used. For example, given a pressure-explicit EOS on the form $p = p(T, V, \underline{\boldsymbol{n}})$, it is natural to take the variable set $(T, V, \underline{\boldsymbol{n}})$ as the state variables.

As briefly mentioned in Section 2.1, the *canonical variables* of any thermodynamic state function are those natural to that function, as defined by the Legendre transform outlined in Section 2.2. Thus, the canonical variables of Helmholtz free energy are $(T, V, \underline{\boldsymbol{n}})$, while the canonical variables for Gibbs free energy are $(T, p, \underline{\boldsymbol{n}})$. While using non-canonical thermodynamic functions is possible, it may be argued that employing canonical variables for thermodynamic modelling is beneficial (Siepmann, 2006). This way, a suitable Legendre transform may provide an alternative thermodynamic potential of which the natural variables may be better suited to describe the problem at hand. It is frequently desired that the constrained or controlled variables of the problem correspond to the free variables of the chosen potential, as discussed by Berglihn (2010). Thus, if the problem is constrained in $(T, p, \underline{\boldsymbol{n}})$ – as is often the case in a laboratory setting – employing the Gibbs free energy as the chosen state function is likely beneficial with respect to problem structure.

It should be noted that there is a trade-off between exploiting the structure of the problem and adhering to the natural variables of the thermodynamic model describing the system in question. As an example, employing an internal energy description, $U(S, V, \underline{\boldsymbol{n}})$, in the context of the model developed in Chapter 4 will

structurally simplify the calculation of the Jacobian. The same is true in the case of employing the slightly more exotic $V(S, U, \underline{\boldsymbol{n}})$, which would structurally simplify matters further.

However, while there is no theoretical issue with using a canonical potential in non-EOS coordinates by employing a suitable Legendre transform, in practice it must be assessed whether the construction of the mapping Jacobians needed and the extra code and functions it requires has a sufficient pay-off in terms of simplifying the problem at hand. In other words, modelling directly in the same thermodynamic coordinates as the thermodynamic model – frequently dictated by the choice of EOS– has the benefit of avoiding such mappings to a large extent unless a framework for automatic calculation of analytical Jacobians is used – as done by Løvfall (2008) – the use of non-EOS coordinates may be (pragmatically) prohibited by the needed calculations.

These difficulties are further illuminated by a brief discussion of *thermodynamic surfaces* versus *thermodynamic manifolds*. Working directly in the state variables of the chosen thermodynamic model – e.g. the ideal gas EOS– provides an *explicit* thermodynamic surface, in this case $A(T, V, N)$. Given a point on this surface, any other thermodynamic property of interest may be derived. The same is not true in the case when non-model state variables are employed. As an example, the use of $U(S, V, \underline{\boldsymbol{n}})$ when the thermodynamic model for the system is given in $(T, V, \underline{\boldsymbol{n}})$, the former potential forms an *implicitly* defined manifold.[13] In order to go from $(S_1, V_1, \underline{\boldsymbol{n}}_1) \rightarrow (S_2, V_2, \underline{\boldsymbol{n}}_2)$, one must go via the Helmholtz free energy surface, thus requiring an iteration on T_2 until the value of U equals that of U_2. While this is certainly possible, it requires either **a)** iteration or **b)** a linearisation (assuming that the manifold is sufficiently smooth in relation to the step size of the linearisation) which in turn requires a Jacobian. Either of these requires extra work from the perspective of the modeller, and while this may pay off in terms of ease of model structure, such a pay-off is not necessarily guaranteed.

[13] In mathematics, a manifold may be seen as a geometrical object with local Euclidean properties. The simplest example is perhaps that of the surface of a sphere – the latter is a manifold, thus not an Euclidean space. However, living on Earth we have no problems with assuming that the *local* surface is indeed a surface in Euclidean $\mathbb{R}^2$ space. It should be noted that while the above description is not in conflict with the distinction between *explicit* surfaces and *implicit* manifolds in a thermodynamic context in the main text, the latter is more practically valuable here.

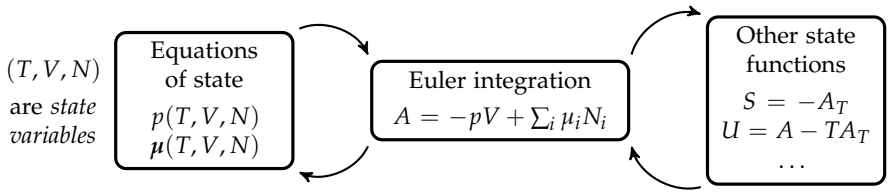

FIGURE 2.1: The relationship between state variables, equation of state and other state functions

The reader is referred to (Berglihn, 2010) for a more in-depth discussion on this topic.

2.5.1 A visual summary

The summary of the relationship between the concepts of EOS, state variables and the corresponding thermodynamic potential, and other state functions and thermodynamic properties is illustrated in Figure 2.1

Given the necessary equations of state and the current (values of the) state variables, a corresponding thermodynamic potential may be calculated from Euler integration, as outlined in Section 2.3. In the case of (T, V, N) coordinates - as in the current model implementation using the ideal gas EOS- the Helmholtz free energy is a suitable choice, given that (T, V, N) are the canonical variables of the latter.

Now, knowing (the value of) the Helmholtz free energy makes the calculation of any state function possible using a suitable Legendre transform, as described in Section 2.2. As an example, the pressure may be re-calculated as A_V, or the enthalpy may be calculated from $H = A - TA_T - VA_V$

Herein lies the true elegance of equilibrium thermodynamics. The choice of thermodynamic model implies a set of natural state variables, and thus a corresponding thermodynamic potential given that one is to work in canonical variables. However, *any desired property may be derived once the potential is known for a given state.*

2.6 Entropy and its role in irreversible processes

Entropy has a central role in the study of irreversible processes. As discussed in Section 2.4, the entropy attains a maximum value at the state of equilibrium. Furthermore, the *entropy production* arising from irreversible processes is positive for all non-equilibrium systems (Sandler, 1989). The role of entropy and the entropy production in the context of the NET framework will be briefly discussed in Chapter 3 – the purpose of the present chapter is to show how the entropy balance may be used for ensuring *model consistency* when modelling irreversible phenomena.

For the purpose of the current work, only a macroscopic entropy balance for a *lumped system*[14] is required. A more detailed microscopic entropy balance may also be derived – the interested reader is referred to (Sandler, 1989, Chap. 3.6) or (Kjelstrup et al., 2010).

The entropy balance may be formulated as

$$\frac{\mathrm{d}S}{\mathrm{d}t} = \hat{S}_{\text{in}} - \hat{S}_{\text{out}} + \sum_j \frac{\hat{Q}_j}{T_j} + \dot{S}_{\text{irr}} \tag{2.33}$$

where $\hat{S}$ is the entropy transported into or out of the control volume across the boundary due to mass flow, $\sum_i \frac{\hat{Q}_j}{T_j}$ represents the entropy gain or loss of the system due to heat flows and $\dot{S}_{\text{irr}}$ represents the internal entropy production of the control volume due to *irreversible processes* – a source term analogous to that of chemical reactions. Note that the sum of heat flows in eq. (2.33) above may be seen as the total net heat flow into the control volume in question, *assuming that the flow is perpendicular to the area of heat transfer.* If the latter assumption does not hold, the sum in eq. (2.33) must be replaced by an integral. Note also that $\hat{S}_{\text{in}} - \hat{S}_{\text{out}} = \sum_j \hat{N}_j \bar{s}_j$, where $\hat{N}_j$ is the jth mass flow to the system, transporting the jth partial molar entropy, $\bar{s}_j$.[15]

[14] In this context, a lumped system refers to a system that is uniform and homogeneous. Put differently, the system is assumed to be well-mixed – no significant internal gradients are present. While the state of the system may vary with time, it is assumed to be *space invariant*.

[15] Note that the latter applies to multicomponent systems. For flows of pure components – e.g. from a single-component reservoir, as further discussed in Chapter 4 – the molar entropy s_j should be used in place of the partial molar entropy $\bar{s}_j$

It is important to realise that while the balance equations for mass, energy and momentum – to be discussed in Chapter 4 – all arise as a result of *conservation laws*[16] of the same quantities. The entropy balance, on the other hand, is not derived from a conservation law – the entropy is not a conserved quantity.

As discussed in Section 2.4, the entropy attains its maximum at the time-invariant state that is thermodynamic equilibrium. This implies that the left-hand side of eq. (2.33) – $\frac{\mathrm{d}S}{\mathrm{d}t}$ – is zero. Also, there can be no fluxes across the system boundaries at equilibrium, thus eq. (2.33) implies that the entropy production must vanish at the equilibrium state

$$(\dot{S}_{\mathrm{irr}})_{\mathrm{eq}} = 0 \tag{2.34}$$

For all non-equilibrium states, the entropy production must be positive according to the second law of thermodynamics (Kjelstrup et al., 2010).

The entropy balance provides *an additional balance* – that is, in addition to the mass, energy and momentum balances commonly applied in chemical engineering practice. Thus, it allows us to study, analyse and solve problems that may not be solved by the three former balances alone. The entropy balance extends our toolbox – sometimes, this extra tool is not particularly useful, but at other times it is an absolute necessity in order to solve the problem at hand.

The entropy balance may be employed for consistency checking of irreversible models in two important ways. First, as discussed by (Kondepudi, 2008), the *integration of the local entropy production at the steady-state must yield the flux of entropy across the boundaries*. In the context of the macroscopic, lumped entropy balance of eq. (2.33), this is equal to the statement that

$$(\dot{S}_{\mathrm{irr}})^{\mathrm{ss}} = (\hat{S}_{\mathrm{in}})^{\mathrm{ss}} - (\hat{S}_{\mathrm{out}})^{\mathrm{ss}} + (\sum_j \frac{\hat{Q}_j}{T_j})^{\mathrm{ss}} \tag{2.35}$$

[16] From the work of Emily Noether it is argued that such conservation laws are in turn a result of underlying symmetries in the Universe we live in (Susskind and Hrabovsky, 2014; Bird et al., 2007). In short, Noether's theorem proves a deep link between the *symmetries* of a variational problem and the conservation laws for the associated variational equations. A detailed discussion of the consequences of Noether's brilliant formulation – "one of the most amazing and useful theorems in physics" (Hanc et al., 2004) – is far beyond the scope of this work. The interested reader is referred to this paper, or the historical overview provided by (Schwarzbach and Kosmann-Schwarzbach, 2010) – the latter containing English translations of Noether's original work.

where the ^{ss} superscript signifies the steady-state. From eq. (2.35), it is clear that for any model treating irreversible phenomena at steady-state *the internal entropy production due to irreversible phenomena must equal the influx of entropy to the system stemming from the processes that maintain the system at a steady-state*. In other words, eq. (2.35) may also be seen as two alternative routes for evaluation the entropy production of a steady-state system – either by a detailed description of the internal irreversible phenomena or by regarding the internals of the system as a black box and only considering the flows of entropy into and out of the system. The practical implications of the above for the current modelling will be treated in Chapter 4.

Furthermore, it is shown by van der Ham (2011) that while eq. (2.35) provides a powerful consistency check for the modelling, it may also be employed to determine certain properties needed for calculation of irreversible phenomena such as mass transport. In (van der Ham, 2011, Chap. 7), such an approach is used to determine the ratio of the vapour and liquid film thickness, using the assumption that the calculated entropy production must be equal using the two approaches outlined above. This may be seen as an interesting strategy for determining properties that are otherwise hard to measure.[17]

It should be pointed out that the above argument does not rely on any particular choice of transport model, as long as the internal entropy production arising from the model may be evaluated. Thus, while the NET framework is frequently employed in this context – assuming that the local entropy production is calculated as a sum of force-flux products, integrated over the system volume in question – the fundamental requirement for consistency given in eq. (2.35) applies regardless of whether this framework is utilized or not. Frequently, employing the NET framework might be beneficial for calculating the local entropy production – but it is not a necessary requirement.

Given that the entropy attains its maximum value at thermodynamic equilib-

[17] It should be emphasised that in (van der Ham, 2011, Chap. 7), a binary nitrogen-oxygen mixture was investigated. Whether or not the argument readily extends to multicomponent mixtures is unclear – but the suspicion is that it will not. In a multicomponent system, it is not in general possible to define a single film thickness ratio – and since the entropy production argument is related to the overall transfer process, it is difficult to imagine that this alone would provide sufficient information.

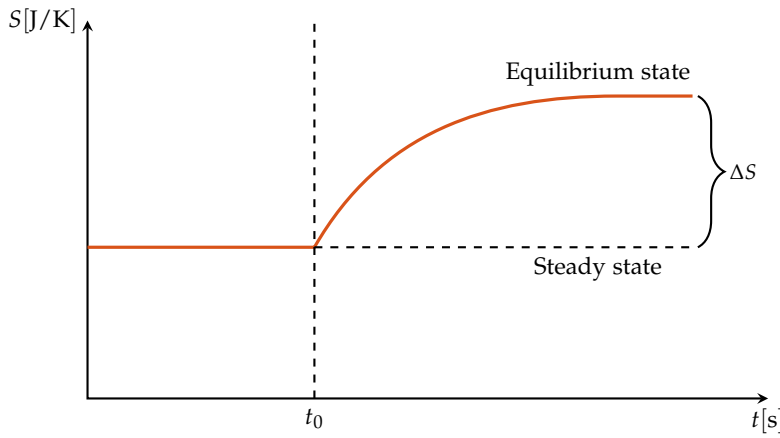

FIGURE 2.2: The difference in entropy, ΔS, between a steady-state and a state of thermodynamic equilibrium. Note that ΔS is positive as defined in eq. (2.36)

rium, any non-equilibrium steady-state must necessarily have a lower value for S, such that

$$\Delta S = (S)_{\text{eq}} - (S)^{\text{ss}} > 0 \tag{2.36}$$

As defined in eq. (2.36), ΔS is a positive quantity that designates how far the steady-state system is from that of equilibrium. This is illustrated in Figure 2.2, where a transition from a steady-state to the state of thermodynamic equilibrium is shown. This concept is further discussed below in terms of entropy production. Imagine that a system is at first maintained at a non-equilibrium, time-invariant steady-state – a state of entropy lower than that of equilibrium – by influx of mass and heat from the surroundings. Such a system is said to be *driven* – if the external constraints that maintain the non-equilibrium situation are removed, *the system will relax to the state of equilibrium given sufficient time.* Thus, if the system is suddenly isolated at $t = t_0$, the internal irreversible processes ensure that the system moves towards equilibrium – *"all spontaneous flows in Nature tend to dissipate the driving forces that cause them"* (Sandler, 1989). This situation is illustrated in Figure 2.3.

If the (time-variant) entropy production is integrated along the relaxation path outlined in Figure 2.3, the difference in entropy between the steady-state and

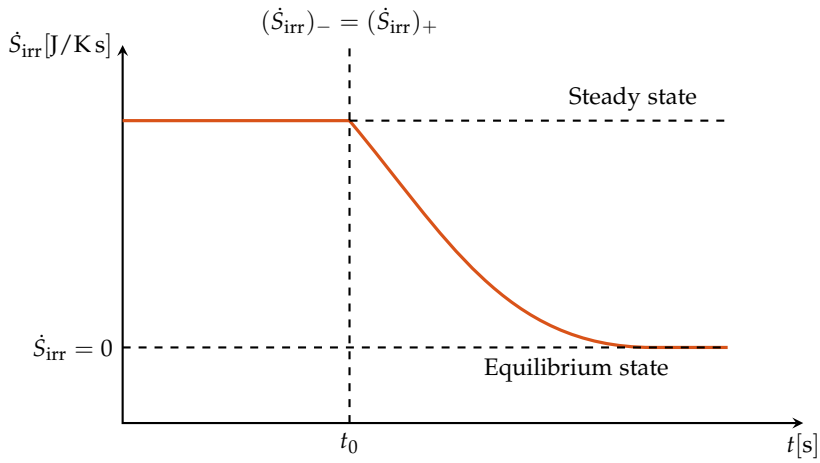

FIGURE 2.3: Illustration of the change in entropy production, $\dot{S}$, for the transition from a steady-state to a state of (thermodynamic) equilibrium. In is postulated that the entropy production should be continuous at t_0, i.e. in the transition from a steady-state situation to a dynamic situation.

the equilibrium state (ΔS) must be obtained (de Koeijer, 2002; Kjelstrup et al., 2010). Stated differently,

$$\Delta S = \int_{t=t_0}^{t=\infty} \dot{S}_{\mathrm{irr}}\,\mathrm{d}t \tag{2.37}$$

The accumulated entropy production over the time interval necessary to reach the state of thermodynamic equilibrium must equal ΔS. This provides an additional consistency check for the modelling of irreversible processes. Note that integration to $t = \infty$ is practically unfeasible. Thus, it is assumed that the following holds approximately

$$\Delta S = \int_{t=t_0}^{t=\infty} \dot{S}_{\mathrm{irr}}\,\mathrm{d}t \approx \int_{t=t_0}^{t\gg t_0} \dot{S}_{\mathrm{irr}}\,\mathrm{d}t \tag{2.38}$$

where the actual value of the upper integration limit, $t \gg t_0$, must be chosen so theentropy production is negligibly small with respect to the desired accuracy of the consistency check.

2.7 The differences and equalities of equilibrium and non-equilibrium systems

The purpose of this section is to shed light on the similarities and differences between equilibrium and non-equilibrium systems. Such an understanding is deemed to be of great importance for the current work.

Classical thermodynamics is *space invariant*. In other words, the system is assumed to be homogeneous and isotropic – no matter where you are or in which direction you look, the properties of the system (e.g. T, V, μ_i) are the same. At the state of equilibrium, a thermodynamic system is also *time invariant* – there is no change in any of the system's properties between the time t and $t + \Delta t$. As such, a thermodynamic system in equilibrium may be fully described in a coordinate system that is fully separate from time and space. E.g. an isolated container with pure H_2O - assuming that the thermodynamic equilibrium is reached, thus that the time passed is much greater than the relaxation time for any relevant internal processes - the state of the system is uniquely specified given only three variables[18] , e.g. (T, p, N_{H_2O}).

In contrast, a non-equilibrium system is in general neither space nor time invariant. One or more of the properties of the system – e.g. the temperature T – will vary in space. More precisely stated, there will be a continuous change throughout space for one or more of the scalar fields describing the system state. This notion is analogous to that of a local equilibrium invoked in the context of NET, as further discussed in Chapter 3. Often, the anisotropy is negligible for fluid phases – gas and liquids do seldom display directional variations in the basic properties. In other words, long-range interactions are seldom of great importance[19] The same assumption may not necessarily be applied to the solid state.

[18] It follows from *Gibbs' phase law* – see e.g. (Callen, 1985) – that any simple system, single-phase system may be described by $F = 2 + C$ variables, where C is the number of components in the system

[19] This may be justified due to the frequent interactions – e.g. in terms of collisions – of the molecules composing the fluid. The inherit randomness of such interactions seldom allow directional variations to arise, although exceptions - such as *liquid crystals* - exist (Atkins and de Paula, 2010)

For an isolated system – a system with no interactions with the surroundings, i.e. no transport of heat, mass or momentum across the boundary – the system will proceed towards an equilibrium state. The rate of relaxation towards equilibrium may vary, but for the case where $t \to \infty$ the equilibrium state will always be attained.

For a non-equilibrium system, the concept of a *steady state* occurs when the system is *time invariant* due to the boundary conditions – the net flux of any conserved quantity across the boundaries is zero.

As pointed out by e.g. (Denbigh, 1951), the concept of a time-invariant equilibrium state in classical thermodynamics and the treatment of reversible processes is – in a sense – analogous to the time-invariant steady-state of non-equilibrium thermodynamics and the treatment of irreversible phenomena such as mass and heat transfer.

Chapter 3

Transport phenomena

The study of irreversible processes – rate processes such as mass and heat transport or chemical kinetics – is a vast field. The common reality for the chemical engineer – that of a non-isothermal, multi-component, reactive multi-phase system – seems to be far from common and consistent description. As discussed by (Bird, 2004), such systems are generally still considered to be "extremely difficult problems". This is not to diminish the science of transport phenomena – only to emphasise that a full understanding of the reality of such phenomena is not yet attained. In light of the inherent complexity of such systems, it may be doubted that a full understanding is ever attainable.

The purpose of this chapter is to given an overview of the theory related to irreversible phenomena, with emphasis on the treatment of mass and heat transfer. Chemical kinetics and momentum transport is beyond the scope of the current work – as such, *mechanical equilibrium* is assumed and a *non-reactive* gas mixture is modelled. These assumptions are further discussed in Chapter 4. The interested reader is directed to (Bird et al., 2007) for an introduction to the former, and (Chorkendorff and Niemantsverdriet, 2007; Fogler, 2005) for an introductory treatment of the latter. The common engineering approach will be contrasted with that of irreversible thermodynamics, and a discussion of the respective benefits and limitations follow. As a thermodynamically consistent treatment of diffusive mass transfer seem to be more difficult to obtain than a thermodynamically consistent treatment of diffusive heat transfer. While both will be presented, the discussion of the different formulations of the driving forces for

mass transfer will dominate.

It should be explicitly emphasised that the focus of the current chapter is *diffusive transport phenomena* as opposed to *bulk transport*. The latter describe how mass and energy are transported by a bulk flow - such a transport is called *advection*. This term is often confused with *convection* – to be precise, the latter is the sum of advection and diffusion (Bird et al., 2007).

3.1 Classical approach to mass and heat transfer: Fick's and Fourier's laws

In this section, a brief presentation of the classical treatment of diffusive mass and heat transfer – using Fick's and Fourier's laws, respectively – is given. In the case of the former, it is – usually implicitly – assumed that the conditions are isothermal. While this is not true in the current context, it is interesting to observe what such a naive formulation yields in terms of tracing the constant entropy production manifold. This will be further discussed in Section 3.3.

Following (Geankoplis, 2003), the classical formulation of Fick's law for diffusive mass transport in a binary system of A and B is

$$J_A = -CD_{AB}\frac{\mathrm{d}x_A}{\mathrm{d}z} \tag{3.1}$$

$$J_A = -D_{AB}\frac{\mathrm{d}C_A}{\mathrm{d}z} \tag{3.2}$$

where J is the diffusive component mass flux of A, and x is the mole fraction of A. The latter formulation is the one most commonly used, where the concentration gradient is assumed to act as the driving force for diffusive mass transfer. While the transition from eq. (3.1) to eq. (3.2) is only strictly valid in the case of constant total concentration C, this formulation is frequently employed as long as the variation is relatively small (Geankoplis, 2003).

At this point, it should be noted that there is often more convenient to work with the *total diffusive component mass flux* instead of the aforementioned diffusive component mass flux used in eq. (3.1). The two variables are related through

$$\hat{N} = A_{\mathrm{char}}J \tag{3.3}$$

where A_{char} is the characteristic contact area relevant for the diffusive mass transfer. Assuming that the *gradient* in eq. (3.2) may be adequately treated as a *difference*, and by introducing the characteristic diffusion length l_{char}, it follows that

$$\hat{N} = -(D_{\text{tot}})_{AB}\Delta C_A \tag{3.4}$$

where $(D_{\text{tot}})_{AB} = D_{AB}\frac{A_{\text{char}}}{l_{\text{char}}}$ is the total diffusion coefficient. This is the form of Fick's law that is used in the context of the current model, as further discussed in Chapter 4. At this point, it should be noted that for equimolar counterdiffusion of an ideal gas, it may be shown that $D_{AB} = D_{BA}$ – in other words, that diffusivity coefficient for A diffusion into B is identical to that of B diffusing into A (Geankoplis, 2003; Haug-Warberg, 2015*b*). This notion is also employed in Chapter 4.

Similarly, the classical treatment of conductive[1] heat transfer is that of using Fourier's law. The mathematical nature of this equation is similar to that of eq. (3.2)

$$q = -k\frac{\mathrm{d}T}{\mathrm{d}z} \tag{3.5}$$

where q is the heat flux. From eq. (3.5), it is evident that the driving force for conductive heat transfer is that of the temperature gradient. By using a similar approach as the one yielding eq. (3.4), one may obtain

$$\hat{Q} = A_{\text{char}}q \tag{3.6}$$

$$\hat{Q} = -k_{\text{tot}}\Delta T \tag{3.7}$$

where $(k_{\text{tot}} = k\frac{A_{\text{char}}}{l_{\text{char}}}$ and the temperature gradient is approximated by a temperature difference as the driving force for heat transfer. The formulation of eq. (3.7) is the one employed in Chapter 4.

3.2 Non-equilibrium thermodynamics

The purpose of this section is to give a brief overview of non-equilibrium thermodynamics, and its relation to the description and modelling of irreversible

[1] As conductive heat transfer is by nature diffusive – as opposed to convective (bulk) heat transfer or heat transfer by radiation – the terms are used interchangeably.

phenomena. While this approach is not rigorously employed in the current work, many notions and concepts from non-equilibrium thermodynamics (NET) are of interest in the current context.

The NET framework is mainly concerned with *coupled transport processes* – simultaneous heat and mass transfer being one such example. In such cases, the transport phenomena are in general not independent – that is, mass transfer will induce heat flux and vice versa. While it is frequently argued that such cross-effects are small in most practical applications, e.g. by Denbigh (1959), they are known to exist – that is, they have been frequently verified experimentally for many different systems since the notions of such couplings where first put forth in the 1850s[2]. Scholars working within the field of NET– e.g. Kjelstrup et al. (2010) – strongly argues that such coupling effects should in general not be ignored. Thus, the NET framework seek to provide a consistent way of modelling such phenomena – in the cases where such *cross-couplings* are of interest, they are accounted for, and in the cases where such effects are small they will simply be quantitatively insignificant without requiring any change in the framework itself. In contrast, the classical approach to mass and heat transfer in the chemical engineering literature – e.g. (Geankoplis, 2003) – seldom mentions or accounts for such coupling effects.

From a theoretical point of view, the effects of cross-coupling are restricted by what is known as *Curie's principle*[3] One important consequence of this principle

[2] Lord Kelvin proposed relations describing *thermoelectric effects* – the coupling of simultaneous heat fluxes and electric fluxes – in 1854 on the basis of experimental observations (Callen, 1985)

[3] There is a fundamental restriction to the direct coupling of rate phenomena in isotropic systems: namely that *processes whose tensorial character differ by an odd integer may not couple* (Glasser, 1965) This is a consequence of the more fundamental restriction that *the fluxes and thermodynamic forces of different tensorial order do not couple in an isotropic system*. The latter is a result of the spatial symmetry properties of matter (de Groot and Mazur, 1984, Chap. VI). As explained by (Kjelstrup et al., 2010), former of the above statements is true due to the fact that tensorial phenomena (e.g. the shear pressure tensor in the momentum balance) may be decomposed into a scalar contribution (tensorial order 0) and a tensorial contribution (tensorial order 2). As such, coupling between chemical reactions and viscous phenomena is - in theory - possible. In practise, the most important consequence of the above statements is that *scalar phenomena* (tensorial order 0, e.g. chemical reactions) do not directly couple with *vectorial* phenomena (tensorial order 1, e.g. mass and heat transfer). Intuitively, this may seem plausible: a chemical reaction - producing a scalar reaction field - does not directly alter the vector field representing mass and heat transfer in an isotropic system. However, the *driving forces* for the latter phenomena - e.g. the scalar field of T for the process of diffusive heat transfer - may indeed by affected by chemical reactions of (due to the effect of heat of reaction). Thus, indirect coupling is still possible.

is that vectorial transport phenomena such as mass and heat transfer do not directly couple with the scalar phenomena of (irreversible) chemical reactions. In light of this, choosing to model a non-reactive mixture should not fundamentally change the nature or structure of the problem. This valuable a valuable notion in the context of Chapter 4.

3.2.1 Transport phenomena in non-equilibrium thermodynamics

In the context of NET, transport phenomena are generally described by the relations between *fluxes* and their response to the *thermodynamic forces* – sometimes called *affinities* – that drive the process towards the equilibrium state (Callen, 1985). At equilibrium, the driving forces cease to exist – thus, the same is true for the fluxes.

Following Denbigh (1959), a general procedure for treating irreversible processes such as transport phenomena in the NET framework is presented. To simplify the discussion, a discrete system is treated. It is assumed that the thermodynamic driving forces satisfy the following relation for the production of entropy

$$\frac{\mathrm{d}S}{\mathrm{d}t} = \sum J_i X_i \tag{3.8}$$

where J_i may be seen as the flux corresponding to the driving force X_i. Furthermore, it is assumed that the fluxes J_i may be expressed – to the desired accuracy – as linear functions of the forces X_i such that

$$J_i = \sum_{k=1}^{n} L_{ik} X_k \tag{3.9}$$

with n being the number of fluxes in the system of interest and L_{ik} being the *phenomenological coefficients* that relate the flux J_i to each of the driving forces X_k. As may be seen from eq. (3.9), each flux is dependent on *all* driving forces as long as $L_{ik} \neq 0$. Note that if the cross-coupling coefficients are zero – or if they may be neglected for the system in question without much error – the framework reduces to that of no coupling between the irreversible processes.

An important result due to Onsager (1931*a*,*b*) – the *Onsager reciprocal relations* – is given below. Onsagers pioneering discovery exploits the concept of microscopic

reversibility, yielding the seemingly simple relation that

$$L_{ik} = L_{ki} \tag{3.10}$$

In other words, the cross-coefficients must be equal – e.g. the phenomenological constant that determines the (diffusive) mass flux due to a temperature gradient (known as the *thermal diffusion* or *Soret effect*) must be equal to the one that determines the heat flux due to a concentration gradient (known as the *Dufour effect*). Thus, the Onsager relation determines an important symmetry of the linear effects dictated by eq. (3.9).

As discussed by (Kondepudi, 2008, p. 330), the assumption of *local equilibrium* is central to irreversible thermodynamics. The assumption is essentially that the equilibrium thermodynamic relations are valid for small subvolumes. The intensive variables are thus functions of both time and space

$$T = T(\underline{\boldsymbol{x}}, t) \tag{3.11}$$

$$p = p(\underline{\boldsymbol{x}}, t) \tag{3.12}$$

$$\mu = \mu(\underline{\boldsymbol{x}}, t) \tag{3.13}$$

Furthermore, the relations of classical equilibrium thermodynamics – such as eq. (2.5) – are assumed to hold locally. According to (Kondepudi and Prigogine, 1998), this notion of a local equilibrium holds for systems of characteristic length of more than 1 µm.[4]

3.2.2 The driving force for heat transfer

Using the NET framework to treat the process of conductive heat transfer for a discrete system, the driving force for this irreversible process is seen as $\Delta(\frac{1}{T})$ rather than ΔT as in eq. (3.7). The purpose of this short outline is exemplify that

[4] The concept of local equilibrium is closely tied to that of the Maxwellian velocity distribution. It is argued by Kondepudi (2008) – on the basis of molecular dynamic simulations – that the characteristic time scale for phenomena that significantly perturbs the Maxwellian distribution must be $\sim 1 \times 10^{-8}$ s. Thus, only very fast processes – such as very fast chemical reactions – may ruin the validity of the assumption of local equilibrium. The interested reader is referred to (Prigogine, 1949) for the original paper arguing that the local equilibrium assumption is valid using the Chapman-Enskog kinetic theory.

these two formulations for the heat transfer driving force are identical – thus introducing the notion that many of the seemingly different driving forces for irreversible phenomena may be related upon closer inspection.

Following Kjelstrup et al. (2010), it may be shown that when the driving forces for mass transfer are zero, the conductive heat transfer is given by

$$J_q^{'} = l_{qq}\nabla(\frac{1}{T}) \quad \Longrightarrow \quad J_q^{'} \approx -l_{qq}(\frac{\Delta T}{T^2}) \tag{3.14}$$

where the gradient is approximated by the difference. Furthermore, the NET notion of $J_q^{'}$ must equal that of q – the conductive heat transfer predicted by the NET approach must equal that of eq. (3.5) – so that

$$k = (\frac{1}{T^2})l_{qq} \tag{3.15}$$

In other words, the only distinction between the Fourier's law and the equations of NET is the proportionality constant used.[5] As such, it is hard to argue that one is better than the other – it seems that eq. (3.5) and eq. (3.14) differ only in choice of k versus l_{qq}.

3.3 Driving force formulations for mass transfer

The main purpose of this section is to outline and contrast some of the commonly employed driving forces for diffusive mass transfer, in addition to postulating some fundamental requirements for these driving forces that must apply also in the non-isothermal case.

As stated in eq. (3.4), the diffusive mass transfer using Fick's law is frequently argued as being proportional to

$$J_A \propto \Delta C_A \tag{3.16}$$

Note that the implicit assumption of constant total concentration is often not explicitly stated. If one accounts for the latter, the following is obtained

$$J_A \propto \Delta x_A \tag{3.17}$$

[5] This is true for the limiting case of heat transfer only – i.e. no other irreversible phenomena occurring simultaneously. If such coupling is introduced, the predictions of Fourier's law and that of the NET is likely to differ. However, the relation between the coefficients should remain the same.

If one is to use a – seemingly – slightly more sophisticated approach, one might argue that the difference in chemical potential should be employed as a driving force for mass transfer

$$J_A \propto \Delta\mu_A \tag{3.18}$$

This notion is attractive in the sense that it obeys classical thermodynamics – $\mu_{A,1} = \mu_{A,2}$ at equilibrium, thus the driving force disappears. The same is in general not true for eq. (3.16) or eq. (3.17) – for non-ideal solutions, equal component concentrations is not the equilibrium criterion.

In the non-isothermal case, one quicly realises that both using eq. (3.16) and eq. (3.18) leads to the non-physical situation of which the predicted diffusive mass transfer is a direct function of the temperature difference, $J \propto \Delta T$.[6] As argued by Atkins and de Paula (2010), from the microscopic view the diffusion process is inherently one of statistical nature. Thus, particles tend to diffuse as a result of non-uniform particle density in space – "Nature abhors a wrinkle" – and any non-uniform distribution will tend to level out in the absence of constraints. As such, it is postulated that the *physically sensible* driving force in the non-isothermal case is that of eq. (3.17).

In addition to the aforementioned issue of temperature dependence, the chemical potential is in *general dependent on the choice of reference state*. As this is an arbitrary choice made by the modeller, it cannot fundamentally impact the diffusive mass transfer occuring in Nature.

Lastly, it should be noted that the diffusive mass flux of a component A should be proportional to the particle density of the same component – either explicitly or implicitly in terms of the driving force. The argument is physically simple – if there are no particles present to diffuse, no diffusion should occur.

As such, one must take care in order to avoid these issues. To counteract this,

[6] The pure pragmatic might argue that based on a time-scale analysis, the irreversible heat transport phenomena will in certain cases be sufficiently fast as to dampen out any temperature gradients – thus yielding quasi-isothermal mass transport conditions. However, this does not seem to be a general argument of sufficient validity, and one should take care if such arguments are employed in the modelling process.

one[7] might propose that the mass transfer should be governed by

$$J_A \propto \Delta \left(\frac{\mu_A - \mu_A^{\text{ref}}}{RT} \right) \tag{3.19}$$

This expression is analogous to the one governing rates in chemical kinetics. The analogy is seen as a strong point in favour of eq. (3.19).

Another possible solution is to employ

$$J_A \propto \Delta(C_A RT) \tag{3.20}$$

which reduces to that of

$$J_A \propto \Delta p_A \tag{3.21}$$

in the case of the ideal gas, using that $\frac{N_A RT}{V} = p_A$. One should note that the diffusion coefficient – often measured with a Fickian model approach – must be adjusted in order to employ these formulations.

Lastly, it is shown by Haug-Warberg (2015*a*) that a thermodynamic driving force that is consistent with the criterion discussed above yields

$$J_A \propto R \left(\mathrm{d} \ln(a_i) \right)_{T,p} \tag{3.22}$$

Here, a_i is the activity of component i. The derivation is based on a backwards reasoning, answering the question "What must the thermodynamic driving force look like in order to give a predicted diffusive mass flux that is equal to that of eq. (3.17) for the limiting case of an ideal gas?". In this limiting case, the activity of component i is x_i, so that a difference form of eq. (3.22) reduces to

$$J_A \propto R \ln \left(\frac{x_{i,2}}{x_{i,1}} \right) \tag{3.23}$$

This notion is exploited in Section 6.5, where it is shown that the manifold of constant entropy and the manifold of constant entropy production may be related through the transformation of ellipses.

Some authors argue strongly that the only true treatment of transport phenomena should be based on experiments. Thus, theoretically based frameworks such

[7] This analogy to chemical kinetics was suggested by the author's co-supervisor, dr.ing. Volker Siepmann.

as NET are often seen as having little practical value. As an example, Cussler (2009) argue strongly against both NET and more elaborate theories for diffusive mass transfer such as the Maxwell-Stefan (M-S) approach of Krishna and Taylor (1993). Mass transfer is best viewed as a Fickian diffusion process, and any other theories are seen as unnecessary complications.

While complicated mathematical theories may serve to obscure the underlying physical principles, there is not necessarily any inherent conflict between seeking fundamental principles and ending up with models for irreversible phenomena that illuminate the underlying physical principles. While fit between theory and experiment is not necessarily ensured, having a general framework that is based on correct physical insight is greatly preferred to empirical correlations as black-box models. As famously stated by John von Neumann: "With four parameters I can fit an elephant, and with five I can make him wriggle his trunk."[8] A sufficiently complex model with sufficiently many fitted parameters may always *describe* the physical reality to a high degree of accuracy. The main question is whether the same model will allow for *predictions* of hitherto unmeasured and unfitted experiments. A sound framework based on the correct principles and physical insight may – at the very least – provide a correct qualitative picture of the phenomenon in question. Thus, such frameworks may be of greater value to the engineer who is constantly asked to make predictions about problems or experiments that have not yet been conducted, as opposed to relying on black-box models with little or no rooting in physical principles.

[8] Attributed to JOHN VON NEUMANN by ENRICO FERMI, as stated in *Nature*, **427**, 297 (22 January 2004)

Chapter 4

Model development

> Remember that all models are wrong; the practical question is how wrong do they have to be to not be useful.
>
> G. BOX and N. DRAPER[1]

The purpose of the present chapter is to describe the model system being studied, with emphasis on its equation structure and underlying assumptions. Attention is given to the difference between the case of the closed system being perturbed from equilibrium and that of the open system being maintained at steady-state through the use of external reservoirs. The former yields a constant entropy manifold upon solution using the methods of Chapter 5, while the latter yields a constant entropy production manifold upon solution with the same methods. The underlying aim is to use a relatively simple model to illuminate and investigate the different driving force formulations for mass and heat transfer.

As stated in Chapter 1, it is not the ambition to use the models developed in this chapter to realistically represent any real system of industrial or practical interest. Rather, an *idealised case* is studied in order to shed light on the effects of different transport formulations and the possible correlations of reversible and irreversible phenomena. It is deemed that such relations are more apparent when any non-essential complexities are stripped away. The main aim is to

[1] Chapter 3 in *"Response Surfaces, Mixtures, and Ridge Analyses"*, (Box and Draper, 2007)

describe the *principles* at work, not the detailed behaviour. The idea is that using simplified models without unnecessary complications will give maximum insight for minimum effort.[2]

4.1 Model overview

The model to be investigated is illustrated in Figure 4.1. The system consists of two connected compartments, each filled with a binary (two-component) gas mixture.[3] The gases are assumed to be governed by the ideal gas equation of state (EOS)

$$p = p(T, V, \underline{\boldsymbol{n}}) = \frac{NRT}{V} \tag{4.1}$$

where p is the pressure, T is the (absolute) temperature and V is the volume. Furthermore, $\underline{\boldsymbol{n}}$ is the mole vector while N is the total mole number. R is the universal gas constant.

As discussed in Chapter 2, the use of Helmholtz free energy as the thermodynamic potential to describe the system is natural when a pressure-explicit EOS is given for a gas-system. As such, $(T, V, \underline{\boldsymbol{n}})$ are taken as the thermodynamic state variables – such that $A(T, V, \underline{\boldsymbol{n}})$ is used to describe each individual subsystem.[4]

For the closed system shown in Figure 4.1, the equilibrium state is that characterised by equality in the intensive variables $(T, p, \underline{\boldsymbol{\mu}})$, as discussed in Section 2.4. Thus, a perturbation in one or more of these variables will – as the general rule –

[2] The latter philosophy - "Maximum insight for the minimum effort" - is attributed to Associate Professor Tore Haug-Warberg (Haug-Warberg, 2006*b*)

[3] While the same two components are used in both compartments in each simulation, different species are available in order to investigate the effect of e.g. differences in c_p on the resulting mass and heat transfer, and thus the resulting manifolds.

[4] Since the ideal gas law given in eq. (4.1) may be equally stated on a *volume explicit form*, $V = V(T, p, \underline{\boldsymbol{n}}) = \frac{NRT}{p}$, the Gibbs free energy formulation might seem equally justified. While this is true for the limiting EOS that is the ideal gas law, most other EOS describing gas phase behaviour – e.g. Redlich-Kwong (RK), Peng-Robinson (PR), Soave-Redlich-Kwong (SRK)– are given on *pressure explicit form*. Thus, using a Helmholtz free energy model to describe the gas phase is – for the sake of modularity, i.e. being able to alter the chosen EOS without modifying the structure of the model – preferred.

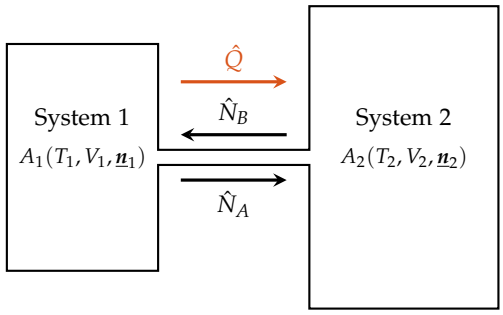

FIGURE 4.1: Illustration of the model system: a connected, two-compartment system using an Helmholtz free energy model with the ideal gas law as EOS

result in a non-equilibrium system, giving rise to mass, momentum and energy fluxes between the two subsystems until a new equilibrium is attained.[5]

4.1.1 Model assumptions

For the model implemented in this work, the assumption of *mechanical equilibrium* is invoked, such that $p_1 = p_2$ at all times.[6] Such an argument is frequently used in the chemical engineering literature – see e.g. (Krishnamurthy and Taylor, 1985*a*) – due to the fact that the explicit treatment of the momentum balance and momentum transport inherently lead to a more complex mathematical treatment due to the tensorial character of the latter phenomena. On the basis of a time-scale analysis, it may be argued that since the pressure equilibration is usually a fast process compared to those of thermal, chemical and diffusive processes, mechanical equilibrium may be seen as instantaneous on the time-scales of interest. This assumption is often taken as valid for normal engineering applications – no substantial error is expected to be introduced as a result. A

[5] This is true for a *closed system*: when $t \to \infty$, a new equilibrium will be reached. For an *open system*, the external influxes of mass, heat and momentum may keep the system at a time-invariant *steady state*.

[6] Note that this is *not* to say that the pressure is invariant with the state of the system or time, *only that any such variation must be equal in each subsystem*. As shall be seen in Chapter 6, the pressure does indeed vary as the manifold is traced out in both the constant entropy and constant entropy production case – although not substantially.

rigorous discussion in support of this is given by de Groot and Mazur (1984, Chap. 5, §2).

As such, the relationship $p_1 = p_2$ effectively substitutes the momentum balance – thus, no explicit treatment of the momentum balance or (irreversible) momentum transfer is permitted.[7] However, the connection between the two compartments permit a redistribution of both mass and energy. The resulting simultaneous mass and heat transfer is the main focus of the current work.

Each of the subsystem in Figure 4.1 are assumed to be *lumped* and *well-mixed* – that is, each subsystem is homogeneous, with no spatial variation in the state variables. The connection between the two subsystems is not modelled as a separate volume – it has no capacity. As such, the nature of the connection between the two subsystem is *discrete* – thus, any *gradients* are approximated by the corresponding *differences*. In the general case, a non-equilibrium system is both time and space invariant, and should be modelled as a continuous system. However, such a model will in general result in a mathematical treatment involving partial differential equations (PDEs). Avoiding such complexity is the main rationale behind the choice of the system as lumped.

A further assumption is made regarding the *direct coupling* of mass and heat transport phenomena – namely that such couplings are assumed to be small, and thus negligible. There is certainly an *indirect coupling* in the sense that a diffusive mass flux will result in a net transport of energy between the compartments, but the *Soret effect* (thermal diffusion) and *Dufour effect* are not accounted for. While these effects may be substantial in certain situations, they are generally assumed to be small in most practical situations (Bird et al., 2007; Denbigh, 1959).

In addition, reacting mixtures are not treated – neither equilibrium reactions nor rate-limited reactions governed by chemical kinetics are studies in the proposed models. The reason for making this restriction is straightforward: while such reactive systems would definitively be of great interest, it makes for a more complicated model system that is beyond the scope of the current work. From a

[7] While a fully general non-equilibrium model should take the momentum balance and the momentum transfer into explicit consideration, the resulting model will drastically more complex to solve and investigate. For the purpose of the current work, this assumption is deemed an appropriate simplification in order to make the study of mass and heat transfer more accessible.

theoretical point of view, the *Curie principle* briefly outlined in Section 3.2 asserts that chemical reaction – being scalar phenomena – would in any case *not directly couple to the vectorial phenomena of mass and heat transfer*. As such, excluding the explicit treatment of chemical reactions should not substantially affect the nature of the irreversible phenomena studied.[8]

4.1.2 Modelling the components

The gas phase components implemented, along with the key parameters for the thermodynamic modelling of these, are shown in Table 4.1. Note that the components are labelled as polyatomic, diatomic and monoatomic, respectively. This is done in order to emphasise that focus is on the characteristic behaviour of the components of a certain class (e.g. diatomic) rather than specific behaviour of e.g. N_2.

TABLE 4.1: Key thermodynamic parameters of the gas phase components. The values of $\Delta_f h^\circ$ and s° are taken from (Linstrom and Mallard, n.d.)

Component	c_p	$\Delta_f h^\circ$	s°
	$\mathrm{J\,K^{-1}\,mol^{-1}}$	$\mathrm{J\,mol^{-1}}$	$\mathrm{J\,K^{-1}\,mol^{-1}}$
Polyatomic (SF_6)	$\frac{23}{2}R$	-1220.47	291.52
Diatomic (N_2)	$\frac{7}{2}R$	0.00	191.61
Monoatomic (Ar)	$\frac{5}{2}R$	0.00	154.84

As shown in eq. (2.24), the Helmholtz free energy may be calculated given that $p = p(T, V, \underline{\boldsymbol{n}})$ and $\underline{\boldsymbol{\mu}} = \underline{\boldsymbol{\mu}}(T, V, \underline{\boldsymbol{n}})$ are known. The former is found directly from eq. (4.1) in the case of an ideal gas – the latter may be found from

$$\underline{\boldsymbol{\mu}}^{\mathrm{ig}}(T, V, \underline{\boldsymbol{n}}) = \underline{\boldsymbol{h}}^{\mathrm{ig}} - T\underline{\boldsymbol{s}}^{\mathrm{ig}} \tag{4.2}$$

[8] In this context, it should be explicitly repeated that while no *direct coupling* between the scalar phenomena of chemical reactions and the vectorial phenomena of mass and heat transfer may occur, *indirect coupling* is still possible. Indeed, any reaction will in general affect both the composition and temperature of the reacting mixture, thus influencing the driving force of mass and heat transfer – to a smaller or larger extent, depending on the rate of reaction and heat of reaction, among other factors.

where $\underline{\boldsymbol{s}}^{\mathrm{ig}}$ is the ideal gas molar entropy vector and $\underline{\boldsymbol{h}}^{\mathrm{ig}}$ is the ideal gas molar enthalpy vector

$$\underline{\boldsymbol{h}}^{\mathrm{ig}}(T) = \Delta_f \underline{\boldsymbol{h}}^{\mathrm{ig}}(T_{\mathrm{ref}}) + \int_{T_{\mathrm{ref}}}^{T} \underline{\boldsymbol{c}}_p(\tau)\,\mathrm{d}\tau \tag{4.3}$$

where $\underline{\boldsymbol{c}}_p$ is the molar heat capacity as defined in the second column of Table 4.1, and $\Delta_f \underline{\boldsymbol{h}}^{\mathrm{ig}}$ is the standard molar enthalpy of formation found in the third column of the same table.

The former, $\underline{\boldsymbol{s}}^{\mathrm{ig}}$, is found as

$$\underline{\boldsymbol{s}}^{\mathrm{ig}}(T, V, \underline{\boldsymbol{n}}) = \underline{\boldsymbol{s}}^{\mathrm{ig}}(T_{\mathrm{ref}}, p_{\mathrm{ref}}) + \int_{T_{\mathrm{ref}}}^{T} \frac{\underline{\boldsymbol{c}}_p(\tau)}{\tau}\,\mathrm{d}\tau - R \ln\left(\frac{\underline{\boldsymbol{n}} RT}{V p_{\mathrm{ref}}}\right) \tag{4.4}$$

where $\underline{\boldsymbol{s}}^{\mathrm{ig}}(T_{\mathrm{ref}}, p_{\mathrm{ref}})$ is the reference entropy found in the fourth column of Table 4.1.

Using the above definitions, the Euler integrated form of the Helmholtz free energy for an ideal gas is found as

$$\begin{aligned} A^{\mathrm{ig}}(T, V, \underline{\boldsymbol{n}}) &= -p^{\mathrm{ig}} V + \underline{\boldsymbol{n}}^{\top} \underline{\boldsymbol{\mu}}^{\mathrm{ig}} \\ &= -NRT + \underline{\boldsymbol{n}}^{\top} (\underline{\boldsymbol{h}}^{\mathrm{ig}} - T\underline{\boldsymbol{s}}^{\mathrm{ig}}) \end{aligned} \tag{4.5}$$

All other ideal gas properties of interest may be found from eq. (4.5) and its derivatives. This expression is the core of the thermodynamic model object implemented in PYTHON.

The ideal gas heat capacities for the components given in Table 4.1 are taken to be multiples of R. Following (Saad, 1997), the specific molar heat capacity at constant volume of an ideal gas may be found from

$$c_V = \frac{1}{2} f R \tag{4.6}$$

where f is the fully developed degrees of freedom of the molecules that constitute the gas.[9] Thus, using the fact that $c_p = c_V + R$, the specific molar heat

[9] This is a result of the *equipartition theorem*, or *principle for the partition of energy*, which states that each degree of freedom will contribute $\frac{1}{2} k_{\mathrm{B}} T$ to the total energy (Dill and Bromberg, 2010). Here, k_{B} is Boltzmann's constant and T is (absolute) temperature. For macroscopic systems, using $R = k_{\mathrm{B}} N_A$ is frequently more convenient, and eq. (4.6) follows

capacity of an ideal gas at constant pressure may be found as

$$c_p = \left(1 + \frac{1}{2}f\right) R \tag{4.7}$$

For monoatomic gases, only the translational degrees of freedom contribute to the heat capacity. Thus, $f = 3$, and $c_p = \frac{5}{2}R$. This compares favourably to the empirical evidence for monoatomic gases such as helium or argon at room temperature. Furthermore, in diatomic gases, two additional rotational degrees of freedom contribute to the heat capacity. As such, $f = 5$, and $c_p = \frac{7}{2}R$.

In the case of more complicated, polyatomic molecules such as SF_6, it is harder to predict the exact heat capacity following the above argument without detailed knowledge of its symmetry and consequent vibrational modes. Thus, the heat capacity is chosen to correspond well with that from (Aylward and Findlay, 2008) – while being kept a multiple of R.

For the purpose of this work, using the ideal gas heat capacities described above is deemed sufficiently accurate. The main objective is to investigate the irreversible phenomena of heat and mass transfer – an accurate thermodynamic description is not the goal. For more accurate values of the ideal gas heat capacity, the Shomate equation employed by NIST Chemistry Webbook (Linstrom and Mallard, n.d.) or the Aly-Lee equation described in e.g. (Gmehling et al., 2012) may be employed. In general, the central philosophy of the way the thermodynamic model is implemented – due to Associate Professor Tore Haug-Warberg – is that the model itself may be substituted *without changing the structure of the rest of the code.*

4.2 Closed system: constant entropy manifold

In this section, the case of a closed system perturbed from its equilibrium state will be outlined. This is illustrated in Figure 4.2 The aim is to formulate the constraint equations such that a *constant entropy manifold* may be allowing mass and energy to be redistributed between the subsystems. Note that no transport equations or irreversible terms are introduced – in this case, the system is purely thermodynamic, only being perturbed from its initial state of equilibrium. Put

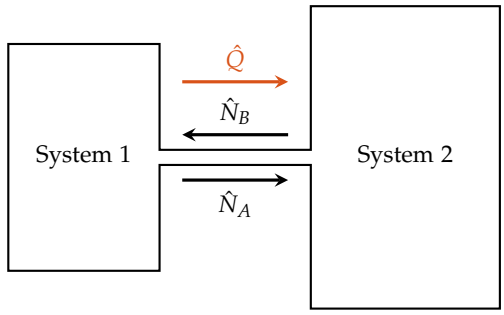

FIGURE 4.2: Illustration of the closed, two-compartment system used to investigate the entropy contour.

differently, the manifold of constant entropy that is defined is that of the system's state at $t = t_0$, before any irreversible transport phenomena take the system back towards the equilibrium state.

Assuming that the system is both isolated and closed – i.e. that there is no flow of mass or energy across the system boundaries – the macroscopic balance equation for mass and energy may be written as

$$U_1 + U_2 = U_{\text{tot}} \tag{4.8}$$

$$N_{A,1} + N_{A,2} = N_{A,\text{tot}} \tag{4.9}$$

$$N_{B,1} + N_{B,2} = N_{B,\text{tot}} \tag{4.10}$$

stating that the sum of component mass and internal energy remains the same for the aggregate system, no matter how mass and energy is redistributed between the two subsystems.

Furthermore, the volumes of the two subsystems are kept constant – the subsystems may be seen as rigid containers. Thus,

$$V_1 = V_1^0 \tag{4.11}$$

$$V_2 = V_2^0 \tag{4.12}$$

where V_1^0 and V_2^0 are the initial (and constant) volumes of subsystem 1 and 2, respectively. Thus, any change in volume is not possible.

Next, the assumption of mechanical equilibrium discussed in Section 4.1 imposes an additional constraint on the system

$$p_1 - p_2 = 0 \tag{4.13}$$

where the equation is formulated implicitly in order to match the structure of the rest of the constraints.

Lastly, the solution of interest is one of constant entropy – the aim is to trace out a constant entropy manifold by varying the distribution of mass and energy between the subsystems. Stated differently, the aim is to describe a curve that is perturbed from equilibrium with a constant deviation in entropy, $\Delta S = \text{const.}$ Thus, the following constraint applies

$$S_1 + S_2 = S_{\text{init}} \tag{4.14}$$

stating that the total entropy of the subsystems is constant along the manifold to be traced, and equal to the initial total entropy of the perturbed composite system, S_{init}.

In other words, the projection of the manifold in the Cartesian $\mathbb{R}^2$ plane of mass and energy deviation should depict a contour curve around the origin, with the origin being the equilibrium state of the compound system.

With the scaled[10] deviation of temperature and (component) chemical potential between the subsystems as the (x, y) coordinates, a contour such as the one depicted in Figure 4.3 is expected. Some elliptic contour enclosing the origin is predicted – the *eccentricity* of the ellipse depending on the relative contributions of mass and energy redistribution on the resulting entropy deviation from equilibrium, ΔS.

As discussed in Chapter 2, the state of equilibrium is characterised by a maximum in the total entropy given the constraints. Thus, any non-equilibrium

[10] The deviation in the chemical potential of component i, $\Delta\mu_i$, and the deviation in temperature, ΔT, is scaled by the equilibrium values $\mu_{i,\text{eq}}$ and T_{eq}, respectively. The reason for such a scaling is to avoid the fact that different units of measure for the two quantities could distort the physical insight arising from the produced curves – i.e. that expected deviations in temperature and chemical potential in absolute terms is expected to be of different orders of magnitude if the appropriate scaling is not used.

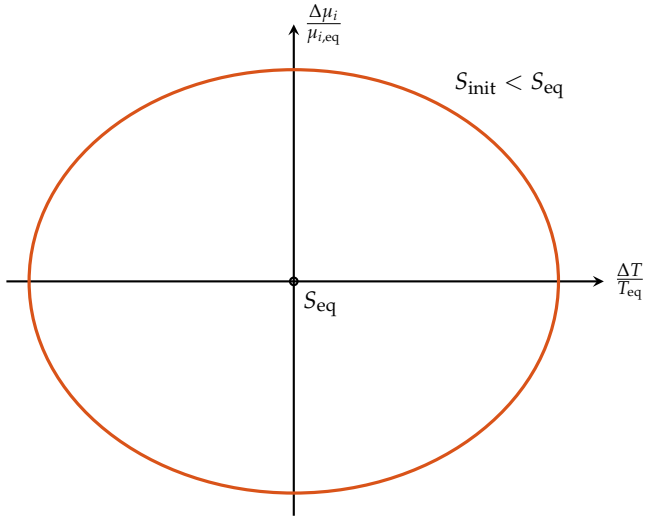

FIGURE 4.3: Illustration of the general form of the expected entropy contour for the closed, two-compartment system

state must by necessity of this criterion have a lower total entropy, as shown in Figure 4.3.

In summary, eqs. (4.8) to (4.14) yield 7 equations constraining the system. With 8 state variables being independent – $(T_1, V_1, N_{A,1}, N_{B,1})$ and $(T_2, V_2, N_{A,2}, N_{B,2})$ – there is a single degree of freedom (DOF) left. Thus, a manifold of constant entropy may be traced out using the methods outlined in Chapter 5.

4.3 Open system: constant entropy production manifold

In order to investigate the time-invariant steady-state, an open system is modelled by adding thermal and component reservoirs to the closed system in Figure 4.2. The four reservoirs for mass influx are modelled as single-component thermodynamic systems, while an explicit model for the two thermal reservoirs is not needed. These reservoirs ensure that the new open system – both subsystem 1 and subsystem 2 – are maintained at a steady-state by continuous supply of heat and mass. This new, extended system is illustrated in Figure 4.4.

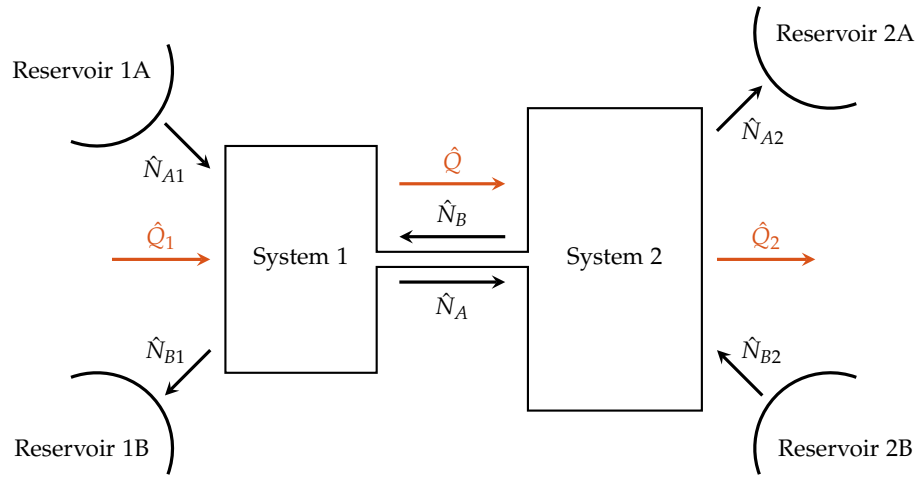

FIGURE 4.4: Illustration of the open, two-compartment system with reservoirs used to investigate the constant entropy production contour.

The purpose of the extended model is to investigate the constant entropy production manifold that arise from the constraint equations – analogous to the constant entropy manifold depicted in Figure 4.3. The idea is that, if these two manifolds are correlated, it may provide interesting insight into the nature of irreversible phenomena and how they should be described in a modelling context.

In order to describe the steady-state situation, new constraint equations and new state variables are introduced. It should be noted that not all these variables are true thermodynamic state variables – rather, some are variables tied to the irreversible transport problem itself. Both the constraint equations and variables will be further discussed after the additional assumptions necessary to describe the open system are listed in Subsection 4.3.1.

4.3.1 Additional assumptions

Compared with the closed system described in Section 4.2, a few additional assumptions are needed for the modelling of the open system shown in Figure 4.4.

First, the connection between subsystem 1 and subsystem 2 is assumed to be maintained at a steady-state in the same way as the rest of the system. Furthermore, this connection is assumed to have zero capacity – it is not explicitly modelled using a thermodynamic model such as for the subsystems or reservoirs.

Second, the component reservoirs are assumed to be in thermal and chemical equilibrium with the respective subsystem at all times. While this may seem like an unrealistic assumption, the reservoirs should be seen as *controlled variables* – in an actual experiment, the properties of these reservoirs would be adjusted to maintain the steady-state.

Third, it is assumed that all the internal entropy production happens at the connection between the two systems. This corresponds to the assumption of a well-mixed, lumped volume that must be seen as a quasi-equilibrium system – the model is created in such a way that the ratio of transported mass and heat to that of the mass and energy capacities of the two subsystems is small. As such, assuming that each subsystem is in quasi-equilibrium is justified.

Fourth, since equilibrium is assumed between the subsystems and the component reservoirs, no entropy is produced by the process of mass transport from the reservoir to the subsystem. While entropy is certainly *transported* across the subsystem boundary, no entropy *production* is taking place during this process. Such a situation might be practically realised e.g. through the use of a suitable membrane.

4.3.2 Open system: mass balance

In order to investigate the extended, open system depicted in Figure 4.4, the steady-state mass balance equations are needed. These are given below. For a more thorough derivation of these equations based on the microscopic equations of change, see (Bird, 1957; Bird et al., 2007).

Mass balance, system 1 (component A)

$$\begin{aligned}\frac{\mathrm{d}N_{A1}}{\mathrm{d}t} &= (\hat{N}_{A1})^{\mathrm{rsvr}} - \hat{N}_A \\ 0 &= (\hat{N}_{A1})^{\mathrm{rsvr}} - \hat{N}_A\end{aligned} \tag{4.15}$$

Mass balance, system 1 (component B)

$$\begin{aligned}\frac{\mathrm{d}N_{B1}}{\mathrm{d}t} &= (\hat{N}_{B1})^{\mathrm{rsvr}} - \hat{N}_B \\ 0 &= (\hat{N}_{B1})^{\mathrm{rsvr}} - \hat{N}_B\end{aligned} \tag{4.16}$$

Mass balance, system 2 (component A)

$$\begin{aligned}\frac{\mathrm{d}N_{A2}}{\mathrm{d}t} &= -(\hat{N}_{A2})^{\mathrm{rsvr}} + \hat{N}_A \\ 0 &= -(\hat{N}_{A2})^{\mathrm{rsvr}} + \hat{N}_A\end{aligned} \tag{4.17}$$

Mass balance, system 2 (component B)

$$\begin{aligned}\frac{\mathrm{d}N_{B2}}{\mathrm{d}t} &= -(\hat{N}_{B2})^{\mathrm{rsvr}} + \hat{N}_B \\ 0 &= -(\hat{N}_{B2})^{\mathrm{rsvr}} + \hat{N}_B\end{aligned} \tag{4.18}$$

where $(\hat{N}_{ij})^{\mathrm{rsvr}}$ is the total component mass flux of i between subsystem j and the corresponding reservoir, and $\hat{N}_i$ is the total component mass flux of i between the two subsystems due to diffusion. Furthermore, $\hat{N}_i$ is taken as positive if there is a net flow of component i from subsystem 1 to subsystem 2. Note that the steady-state mass balances of eqs. (4.15) to (4.18) in effect dictates that the flow of mass from the reservoirs is equivalent to the internal mass transfer between subsystem 1 and subsystem 2 – in other words, the reservoirs act to maintain the steady-state condition of the subsystems in terms of mole numbers of each individual component.

4.3.3 Open system: energy balance

Due to the non-isothermal nature of the problem, the energy balances prove to be slightly more complicated than the mass balances of Subsection 4.3.2. While

no separate mass balance was needed for the zero-capacity connection between subsystem 1 and 2, an explicit steady-state energy balance for this connection must be given in order to account for the *difference in partial molar enthalpy of the mass flows*.[11] This idea will be further elaborated.

The steady-state macroscopic energy balances given below may – analogous to the mass balances in Subsection 4.3.2 – be derivation based on the microscopic equations of change. The interested reader is again referred to (Bird, 1957; Bird et al., 2007).

Energy balance, system 1:

$$\frac{\mathrm{d}U_1}{\mathrm{d}t} = \hat{Q}_1 - \hat{Q} - \hat{Q}^\dagger + \hat{N}_{A1}(h_{A1})^{\mathrm{rsvr}} + \hat{N}_{B1}(h_{B1})^{\mathrm{rsvr}} - \hat{N}_A\bar{h}_{A1} - \hat{N}_B\bar{h}_{B1} \tag{4.19}$$

$$0 = \hat{Q}_1 - \hat{Q} - \hat{Q}^\dagger + \hat{N}_{A1}(h_{A1})^{\mathrm{rsvr}} + \hat{N}_{B1}(h_{B1})^{\mathrm{rsvr}} - \hat{N}_A\bar{h}_{A1} - \hat{N}_B\bar{h}_{B1} \tag{4.20}$$

Energy balance, system 2:

$$\frac{\mathrm{d}U_2}{\mathrm{d}t} = -\hat{Q}_2 + \hat{Q} - \hat{N}_{A2}(h_{A2})^{\mathrm{rsvr}} - \hat{N}_{B2}(h_{B2})^{\mathrm{rsvr}} + \hat{N}_A\bar{h}_{A2} + \hat{N}_B\bar{h}_{B2} \tag{4.21}$$

$$0 = -\hat{Q}_2 + \hat{Q} - \hat{N}_{A2}(h_{A2})^{\mathrm{rsvr}} - \hat{N}_{B2}(h_{B2})^{\mathrm{rsvr}} + \hat{N}_A\bar{h}_{A2} + \hat{N}_B\bar{h}_{B2} \tag{4.22}$$

Energy balance, connection:

$$\frac{\mathrm{d}U_{\mathrm{con}}}{\mathrm{d}t} = \hat{Q} - \hat{Q} + \hat{Q}^\dagger + \hat{N}_A\bar{h}_{A2} - \hat{N}_A\bar{h}_{A1} + \hat{N}_B\bar{h}_{B2} - \hat{N}_B\bar{h}_{B2} \tag{4.23}$$

$$0 = \hat{Q}^\dagger + \hat{N}_A(\bar{h}_{A2} - \bar{h}_{A1}) + \hat{N}_B(\bar{h}_{B2} - \bar{h}_{B2}) \tag{4.24}$$

In the eqs. (4.20) to (4.24), $\hat{Q}_j$ is the total heat flux from the thermal reservoir to system j, $\hat{Q}$ signifies the diffusive heat transport between subsystem 1 and 2 and

[11] This issue arises due to the simplification of viewing the transition from subsystem 1 to subsystem 2 as a *discrete change*. Imagine a molecule leaving subsystem 1 with temperature T_1 and entering subsystem 2 with a temperature $T_2 > T_1$, so that $T_2 - T_1 = \Delta T$. A certain amount of energy is needed for the molecule to attain this new state of higher temperature, and *that energy must be taken from somewhere*. In order to ensure that the connection between the subsystems is indeed maintained at steady-state, this energy requirement must be taken into explicit account. In a continuous system, such a situation would not arise – a scalar temperature field $T(t, \underline{x})$ exists everywhere between subsystem 1 and subsystem 2. Rather, the situation is analogous to that of vaporisation from liquid to gas – this is usually viewed as a discrete change of state where an amount of energy equal to $\Delta_{\mathrm{vap}}h$ must be supplied in order for the process to occur.

$\hat{Q}^{\dagger}$ is discrete heat of transfer to be further explained below.[12] The total mass flux notation is the same as the one employed in Subsection 4.3.2 – the same is true for the definition of positive flow direction, which also applies to the heat transfer. Furthermore, $(h_{i,j})^{\text{rsvr}}$ is the molar enthalpy of reservoir j, while $\bar{h}_{i,j}$ is the partial molar enthalpy of component i in subsystem j. These two latter quantities account for the transport of energy that arises due to the diffusive mass transfer.

From eq. (4.24), $\hat{Q}^{\dagger}$ may be seen as the amount of heat that must be added to the channel connecting the two subsystems in order to compensate for the change in partial molar enthalpy for the components between subsystem 1 and subsystem 2 . In a sense, this is the amount of heat that must be added to ensure that the molecules that flow through the channel are maintained at the channel temperature at each point in space.

The introduction of $\hat{Q}^{\dagger}$ is analogous to the non-equilibrium thermodynamics (NET) notion of a difference between an *energy flux* and a *measurable heat flux* (Kjelstrup et al., 2010, Chap. 3)

$$J_q = J_q^{'} + \sum_{j=i}^{n} H_j J_j \tag{4.25}$$

where J_q is the total energy flux, $J_q^{'}$ is the measurable heat flux and the sum signifies the partial molar enthalpies H_j carried by the diffusive component fluxes J_j. Note that the notation of (Kjelstrup et al., 2010) is used in eq. (4.25).

Using the notation from eq. (4.24), it seems that

$$J_q - J_q^{'} = + \sum_{j=i}^{n} H_j J_j \implies \hat{Q}^{\dagger} = J_q - J_q^{'} \tag{4.26}$$

Thus, $\hat{Q}^{\dagger}$ may be seen as a difference between the total energy flow and the actual measurable heat flow. Analogous to the argument made by (Kjelstrup

[12] It is important to explicitly note that $\hat{Q}^{\dagger}$ is *not the same* as the concept of *heat of transfer* – often denoted as Q^{*} – as discussed by extensively by (Denbigh, 1951; Lewis and Randall, 1961). The latter concept seems firmly tied to coupled irreversible phenomena, such as the Soret effect or thermal effusion. While the author was at one point puzzled by the seemingly similar nature of $\hat{Q}^{\dagger}$ and Q^{*} – and while the latter concept is interesting in its own right – it is concluded that the *heat of transfer* has no direct implication for the current work. As such, no further discussion is provided – the interested reader is referred to the above books, both which are excellent.

et al., 2010) regarding the role of $J_q - J_q^{'}$ in a steady-state process, $\hat{Q}^{\dagger}$ may be seen as the difference between the amount of heat $\hat{Q}_1$ entering subsystem 1 and the amount of heat $\hat{Q}_2$ exiting subsystem 2 *in order to maintain the system at steady-state conditions.*

It should be noted that the $\hat{Q}^{\dagger}$ only appears in eq. (4.20), not in eq. (4.22). As such, only subsystem 1 is directly affected by $\hat{Q}^{\dagger}$, which introduced an asymmetry into the equations. While this is not expected to have a large impact on the resulting constant entropy production manifold, the full implications of this assumption is not understood.

Here, the analogy to that of a phase change should by noted.[13] Imagine a bucket filled with water (H_2O), where the latter is allowed to evaporate. This is – by nature – an endothermic process, so that heat must be supplied *from somewhere*. In other words, either the liquid phase of H_2O in the bucket, the gas/vapour phase of H_2O and air or *both the liquid and the gas/vapour phase* must be cooled by the process. The fact that thermal equilibrium between the two phases will be rapidly instilled in reality does not subtract from the fact that when modelling – or observing – such a system, one has to make an assumption as to *where the necessary thermal energy for the evaporation comes from.* In reality, one might argue that the rapid dynamic equilibrium between local evaporation and re-condensation will ensure that no single phase is the source of the necessary thermal energy. When modelling discrete systems, such an assumption is not possible. While the above will introduce a certain asymmetry in the system,

4.3.4 Open system: additional constraints

The constraints on subsystem volume, total internal energy and total component mole numbers – as stated by eqs. (4.8) to (4.12) in Section 4.2 – also apply to the open system. The same is true for the criterion of mechanical equilibrium of eq. (4.13).

Constant entropy production:
In place of the constrain on entropy, eq. (4.14), a constraint on the entropy

[13] Due credit is given to dr.ing. Volker Siepmann form pointing out this analogy, which helps put the rather abstract notion of $\hat{Q}^{\dagger}$ into a more understandable perspective.

production is given for the open system at steady-state

$$\dot{S}_{\text{irr}} = (\dot{S}_{\text{irr}})_{\text{init}} \tag{4.27}$$

$$\implies 0 = -\frac{\hat{Q}_1}{T_1} + \frac{\hat{Q}_2}{T_2} - \hat{N}_{A1}(s_{A1})^{\text{rsvr}} + \hat{N}_{A2}(s_{A2})^{\text{rsvr}} - \hat{N}_{B1}(s_{B1})^{\text{rsvr}} + \hat{N}_{B2}(s_{B2})^{\text{rsvr}} - (\dot{S}_{\text{irr}})_{\text{init}} \tag{4.28}$$

where the notation from Subsection 4.3.2 and Subsection 4.3.3 is employed, both in terms of symbols and positive flow direction. Furthermore, $(s_{i,j})^{\text{rsvr}}$ is the molar entropy of component A in the pure-component reservoir connected to subsystem j. In eq. (4.27), the steady-state entropy production is calculated from the reservoir flows alone – *thus no explicit reference is made to the internal irreversible phenomenon of mass and heat transfer.* As pointed out in Section 2.6, $\bar{s}$ may alternatively be calculated directly from looking at the internal irreversible processes. The implications of this are further discussed in Subsection 4.3.5.

Transport equations:
In order to separate the *problem structure* from the *model implementation*, the equations governing the diffusive heat and component mass transfer are taken as implicit constraints – rather than being taken as explicit terms in the mass, energy and entropy production equations. This simplifies the implementation of different transport equations, which is exploited in the PYTHON implementation.

Note that all the transport equations are necessarily implemented on a difference form, due to the discrete nature of the model. The equations utilized are listed below:

- **Heat transfer:**
  - Fourier's law, given in eq. (3.7)
- **Mass transfer:**
  - Fick's law, given in eq. (3.4)
  - $\Delta\mu_i$
  - $\Delta(C_i RT)$

The reader is referred to Chapter 3 for a more thorough review of the virtues and deficiencies of the different formulations. Note that the transport laws implemented are not claimed to be physically correct – e.g. Fick's law for a non-isothermal case leads to a strong, non-physical coupling between the diffusive mass transfer and the temperature, as discussed in Chapter 3. Rather, the implications of the different formulations on the resulting constant entropy production manifold is the desired outcome.

In order to evaluate the total diffusive fluxes of component mass and heat, characteristic values for the constant area and diffusion length are introduces. As discussed in Chapter 3, A_{char} is a characteristic contact area and l_{char} is a characteristic diffusion distance. The values of these quantities are chosen so that the resulting D_{tot} produces a characteristic relaxation time of the diffusive mass transfer that is deemed physically sensible. A similar approach is taken with the heat transfer coefficient.

In addition, a simplifying assumption is made regarding the relationship between D and k, namely that the magnitude of the latter is $\approx 1 \times 10^3$ times that of the former in SI units. A summary of these assumptions is given in Table 4.2.

TABLE 4.2: Transport coefficients used in the model implementation

Transport property	**Value**
k	$0.025\,\mathrm{W\,K^{-1}\,m^{-1}}$
D	$2.5 \times 10^{-5}\,\mathrm{m^2\,s^{-1}}$
A_{char}	$0.02\,\mathrm{m^2}$
l_{char}	$1 \times 10^{-3}\,\mathrm{m}$

Using the total heat transfer coefficient and total diffusion coefficient in the mass and heat transport calculations allows the diffusive flows of component mass and heat to be calculated.

Thermal and chemical equilibrium with pure-component reservoirs:
As stated in Subsection 4.3.1, the pure-component reservoirs depicted in Figure 4.4 are assumed to be in chemical and thermal equilibrium with the respect-

ive subsystems. Additionally, a unit reservoir volume is considered – thus, a constraint on the reservoir volume results.

As such, the following equations must be fulfilled for each of the four reservoirs

$$T_j - (T_{i,j})^{\text{rsvr}} = 0 \tag{4.29}$$

$$(V_{i,j})^{\text{rsvr}} - (V^0_{i,j})^{\text{rsvr}} = 0 \tag{4.30}$$

$$\mu_{i,j} - (\mu_{i,j})^{\text{rsvr}} = 0 \tag{4.31}$$

Thus, an additional 12 constraints for the open system are added. All in all, this makes 29 constraint equations in total – yielding a single degree of freedom for the 30 state variables[14] shown in Table 4.3. Note that the latter show the state variables collected in natural groups – thinking in terms of such groups simplify the PYTHON implementation of the model. A complementary overview of the constraint equations and variables may be found in the discussion of the Jacobian structure – see Appendix C.2.

TABLE 4.3: An overview of the state variables of the open system

Group	**Variables**
System 1	T_1, V_1, $N_{A,1}$, $N_{B,1}$: (4)
System 2	T_2, V_2, $N_{A,2}$, $N_{B,2}$: (4)
Reservoir 1A	$(T_{A,1})^{\text{rsvr}}$, $(V_{A,1})^{\text{rsvr}}$, $(N_{A,1})^{\text{rsvr}}$: (3)
Reservoir 2A	$(T_{A,2})^{\text{rsvr}}$, $(V_{A,2})^{\text{rsvr}}$, $(N_{A,2})^{\text{rsvr}}$: (3)
Reservoir 1B	$(T_{B,1})^{\text{rsvr}}$, $(V_{B,1})^{\text{rsvr}}$, $(N_{B,1})^{\text{rsvr}}$: (3)
Reservoir 2B	$(T_{B,2})^{\text{rsvr}}$, $(V_{B,2})^{\text{rsvr}}$, $(N_{B,2})^{\text{rsvr}}$: (3)
Heat transport	$\hat{Q}$, $\hat{Q}_1$, $\hat{Q}_2$, $\hat{Q}^\dagger$: (4)
Mass transport	$\hat{N}_A$, $\hat{N}_{A,1}$, $\hat{N}_{A,2}$,$\hat{N}_B$, $\hat{N}_{B,1}$, $\hat{N}_{B,2}$: (6)
Total:	**30**

[14] It is once again emphasised that the use of the term *state variable* here is not restricted to that of true thermodynamic state variables – also the transport variables are accounted for. This is evident from Table 4.3. The majority of the latter variables may be seen as *controlled* – the modelling may be seen as a computer version of a lab experiment where these variables are adjusted in order to maintain a steady-state.

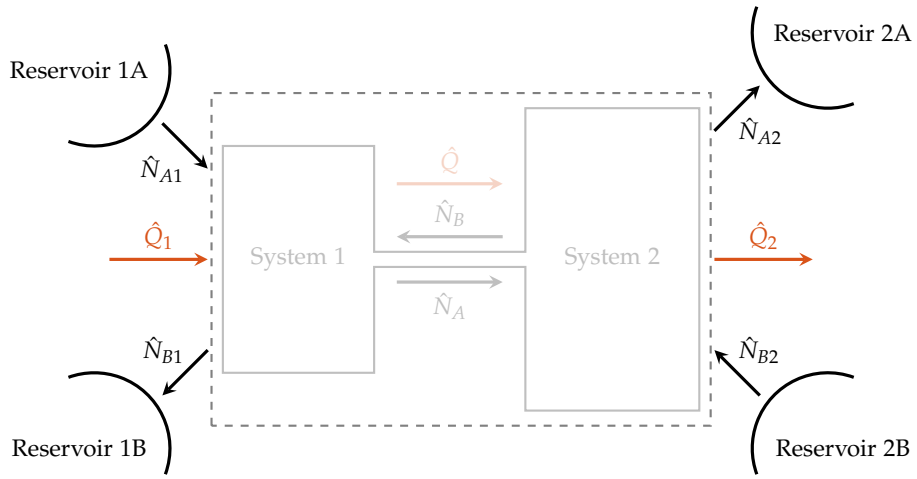

FIGURE 4.5: Illustration of the external entropy flows arising from the mass and heat transfer between the subsystems and the respective reservoirs. No account is made of the internal workings of the system – it is seen as a black-box in the context of the entropy balance,

4.3.5 Two roads to $\dot{S}_{\text{irr}}$: a powerful consistency check

As previously stated, the subsystems themselves are assumed to be well-mixed – the entropy production in these are negligible compared to that of the connecting bridge where the irreversible transport processes occur. The states of subsystem 1 and 2 pass through a succession of equilibrium states – this is a *quasi-static process* (Sandler, 1989, p. 87).

In Figure 4.5, the emphasis is on the flows of mass and heat from the reservoirs to the system. These flows result in entropy transport between the reservoirs and the system, and may be calculated as a sum of contributions from the mass and heat fluxes, as shown in eq. (4.27). Here, the resulting entropy production – $\dot{S}_{\text{irr}}$ – is calculated without assuming anything about the inner workings of the systems or the transport laws. This may be viewed as a *black-box* entropy balance; simply accounting for all fluxes of heat and mass into the system is sufficient.

On the other hand, if the inner workings of the system are known, the entropy production from the irreversible phenomena occurring may be calculated. In

this case, only the system is studied – the transport between subsystem 1 to subsystem 2 is the only relevant piece of information. This is illustrated in Figure 4.6. None of the flows between the system and the reservoirs are considered – as long as the state of the compartments are known, and thus that the mass and heat transfer between them can be calculated, there is no need to know the fluxes to and from the system.

Exploiting an approach proposed by Siepmann (2015), the time derivative of total differential of the internal energy for one of the subsystems is found from eq. (2.1)

$$\frac{\mathrm{d}U_j}{\mathrm{d}t} = T_j \frac{\mathrm{d}S_j}{\mathrm{d}t} + \underline{\boldsymbol{\mu}}_j^\top \frac{\mathrm{d}\underline{\boldsymbol{n}}_j}{\mathrm{d}t} \tag{4.32}$$

This is combined with the energy balance for the same subsystem

$$\frac{\mathrm{d}U_j}{\mathrm{d}t} = \underline{\bar{\boldsymbol{h}}}_j^\top \frac{\mathrm{d}\underline{\boldsymbol{n}}_j}{\mathrm{d}t} + \hat{Q} \tag{4.33}$$

Combining eq. (4.32) and eq. (4.33), and using that $(\underline{\bar{\boldsymbol{h}}}_j - \underline{\boldsymbol{\mu}}_j) = \underline{\bar{\boldsymbol{s}}}_j$, the following is obtained

$$T_j \frac{\mathrm{d}S_j}{\mathrm{d}t} = \hat{Q} + T_j \underline{\bar{\boldsymbol{s}}}_j^\top \frac{\mathrm{d}\underline{\boldsymbol{n}}_j}{\mathrm{d}t} \tag{4.34}$$

$$\frac{\mathrm{d}S_j}{\mathrm{d}t} = \frac{\hat{Q}}{T_j} + \underline{\bar{\boldsymbol{s}}}_j^\top \frac{\mathrm{d}\underline{\boldsymbol{n}}_j}{\mathrm{d}t} \tag{4.35}$$

where eq. (4.35) is obtained by dividing through with T_j in eq. (4.34). It may be argued that the final result in eq. (4.35) make intuitive sense – the change of entropy in a subsystem that is not connected to any external flows may be calculated from the (net) internal entropy flow due to diffusive heat transport and the (net) internal entropy flow as transported by mass diffusion. Note that $\hat{Q}$ and $\frac{\mathrm{d}\underline{\boldsymbol{n}}_j}{\mathrm{d}t}$ must be calculated from the chosen transport equations as the total heat flux and total mass flux, respectively.

The main point is that these two approaches *describe the same entropy production*. Thus, the two approaches must result in the same value for the entropy production. This may serve as a consistency check for the modelling, as discussed in Section 2.6.

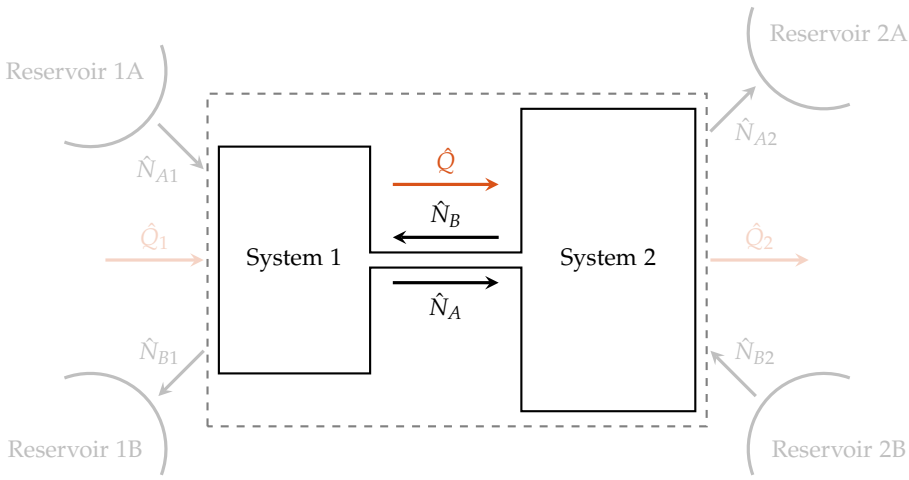

FIGURE 4.6: Illustration of the internal entropy production that is a result of the irreversible processes – mass and heat transfer – occurring within the system. There is no need to account for the fact that there may or may not be external flows between the system and the reservoirs.

Chapter 5

Numerical methods for manifold tracing

> One approach is to think of the computer as an employee with certain strengths, like speed and precision, and particular weaknesses, like lack of empathy and inability to grasp the big picture.
>
> ALLEN DOWNEY[1]

The purpose of the current chapter is to present the numerical method used for the tracing of manifolds of constant entropy and constant entropy production, as this is seen as a central part of the current work. In order to achieve this, an outline of the general manifold tracing problem is first provided, followed by a presentation of the generalised predictor-corrector method for manifold tracing that is implemented – the latter being done in PYTHON. The main ideas of this numerical solution strategy are discussed, using both pseudocode and flowchart to illuminate the overall structure of the approach.

[1] "Think Python - How to Think Like a Computer Scientist", (Downey, 2012)

5.1 The general manifold tracing problem

In order to provide an easy-to-grasp analogue to the multi-dimensional manifold tracing problem, the (simple) problem of tracing out a circle centred at the origin in the Cartesian (x, y) plane is presented.[2] Such a circle may be defined as all points that satisfy the implicit equation

$$F(x, y) = x^2 + y^2 - R^2 = 0 \tag{5.1}$$

where R is the radius of the circle (a parameter) and $F : \mathbb{R}^2 \mapsto \mathbb{R}^1$. Thus, eq. (5.1) may be seen as a (non-linear) system of equations with a single degree of freedom (DOF). The points (x, y) that fulfil eq. (5.1) constitute a curve C in $\mathbb{R}^1$ – the circle.[3]

The multi-dimensional problem of tracing the manifolds of constant entropy and constant entropy production may be seen as that of computing the set of solutions to a system of non-linear equations defined by the constraints presented in Chapter 4. In other words, the aim is to trace out the curve C in $\mathbb{R}^{N-1}$ defined by

$$\boldsymbol{F}(\underline{\boldsymbol{X}}) = \underline{\boldsymbol{0}} \tag{5.2}$$

where $\boldsymbol{F}$ is the general vector-valued function describing the constraints of the model, such that $\boldsymbol{F} : \mathbb{R}^N \mapsto \mathbb{R}^{N-1}$. In the case of constant entropy, $\boldsymbol{F} : \mathbb{R}^8 \mapsto \mathbb{R}^7$, with $\underline{\boldsymbol{X}} \in \mathbb{R}^8$. Similarly, for the case of constant entropy production, $\boldsymbol{F} : \mathbb{R}^{30} \mapsto \mathbb{R}^{29}$, with $\underline{\boldsymbol{X}} \in \mathbb{R}^{30}$. In both cases, there is a single DOF– thus describing a curve in $\mathbb{R}^{N-1}$.

Following (Brendsdal, 1999), this curve may alternatively be defined by differentiating eq. (5.2)

$$\dot{\boldsymbol{F}} = \nabla_{\underline{\boldsymbol{X}}} \boldsymbol{F}(\underline{\boldsymbol{X}}) \dot{\underline{\boldsymbol{X}}} = 0 \tag{5.3}$$

[2] The similarity between the circle in $\mathbb{R}^1$ and the constant entropy manifold in $\mathbb{R}^7$ and constant entropy production manifold in $\mathbb{R}^{29}$ is exploited later to provide an *a priori* metric for the predictor vector used in the general manifold tracing algorithm. The details regarding this strategy are outlined in Appendix A.

[3] It is so common to view the circle as a curve in the Cartesian (x, y) space that it may be counter-intuitive that a circle *with a given radius* is indeed a curve in $\mathbb{R}^1$. The easiest way to realise that this must be true is by looking at the same circle in polar coordinates (ϕ, r). Here, it is evident that if r is taken to be a (constant) parameter, the circle is defined by $\phi \in \mathbb{R}^1$ alone.

This is equivalent to the statement that the tangent of the curve C – that is, the manifold to be traced – is in the nullspace of the gradient of $\boldsymbol{F}$. The latter corresponds to the 29×30 Jacobian matrix that is obtained by differentiating the constrain equations from Chapter 4 with respect to all the independent variables. Thus, by considering the curve C as the solution to the differential equation that is eq. (5.3), the manifold may be traced out by employing a predictor-corrector method. Here, the vector spanning the nullspace of the Jacobian, $\underline{\boldsymbol{p}}$ (with dimensions 30×1), is used as a starting point for computing the necessary predictor steps. A corrector step is needed to ensure that the constraints of the problem – given as eq. (5.2) – are fulfilled along the entire manifold to within the *a priori* given tolerance. This corrector is implemented using the Newton-Raphson (N-R) method, to be further discussed in Section 5.2 and Section 5.4 below.

5.1.1 The relation to numerical continuation methods

The author did not realise until after the method was implemented that this procedure – and the manifold tracing problem that it solves – may in fact be seen as a particular implementation of the more general methods of *numerical continuation*, as described in e.g. (Allgower and Georg, 2003). The latter is an area of mathematics concerned with solving non-linear systems of equations of the type

$$\boldsymbol{F}(\underline{\boldsymbol{x}}) = 0 \tag{5.4}$$

where no good approximation $\underline{\boldsymbol{x_0}}$ to the zero point is known. For such problems, applying a regular N-R-approach – as described in e.g. (Kreyszig, 2010) and further discussed in Subsection 5.4.1 – will often fail to converge. The N-R method is known to be sensitive with respect to the given initial values, and one can not hope to obtain a converged solution if the initial guess is far from the actual solution. The numerical continuation methods propose to remedy this issue by instead tracing out an implicitly defined curve C from a (known) starting point to an end-point that corresponds to the solution of eq. (5.4). While a more detailed description of numerical continuation methods is beyond the scope of the current work, it is interesting to note that the central problem tackled

is essentially a manifold tracing problem – parallel to the ones that are solved in the current work, but with a different end goal.

According to (Allgower and Georg, 2003), some of the key items that must be "carefully developed" when applying predictor-corrector methods to numerical continuation problems are

- An effective step size adaptation
- An efficient implementation of the corrector step
- handling or approximating special points on the curve such as turning points

That the above points are crucial to the manifold tracing problem was realised by hard-won experience – through the process of implementing the predictor-corrector method that is the main topic of Section 5.2 – rather than by examining the theory of numerical continuation. It is likely that the method implemented in this work would be improved by utilizing some or several of the techniques and concepts found in the numerical continuation literature. Due to time constraints and the fact that the current algorithm adequately traces out the desired manifolds, any such improvement has not been attempted.

5.2 The predictor-corrector method

The purpose of Section 5.2 is to present and discuss the predictor-corrector implemented to solve the manifold tracing problem. The particular workings of the predictor step computation and the N-R corrector step computation is discussed in Section 5.3 and Section 5.4, respectively. Thus, the topic of the current section is the main algorithm. Note that details are omitted for clarity.

The main goal of the predictor-corrector algorithm is to trace out the manifolds of constant entropy and constant entropy production, as discussed in Section 5.1. In order to achieve this goal, a variable step-length predictor-corrector method is implemented

Predictor: The predictor method consists of an Euler-type integration, following the tangent of C the predictor step.

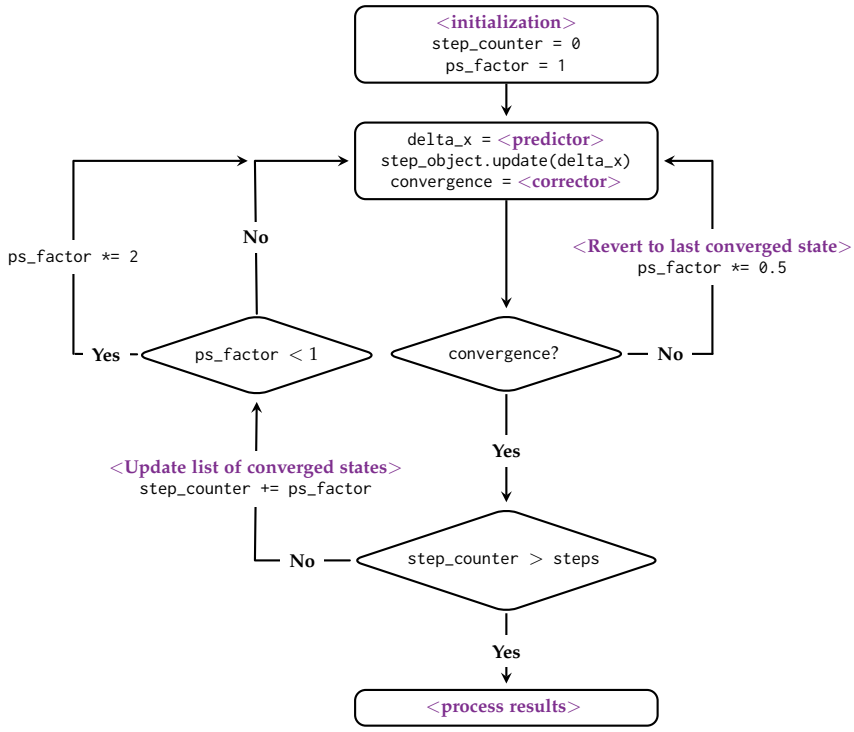

FIGURE 5.1: Flowchart for the variable step-length predictor-corrector method. Note that `step_counter` is a floating point number here; this is done in order to account for steps smaller than the nominal length of 1 that arises due to the variable step-length strategy

Corrector: The corrector method used a N-R-type corrector, demanding that the corrector step is orthogonal to that of the predictor, $\left(\Delta x_{\text{predictor}}\right)^T \mathrm{d}x_{\text{corrector}} = 0$. This condition augments the Jacobian matrix stemming from the constraints described in Chapter 4. As such, a square $N \times N$ Jacobian for the corrector is obtained, as needed by the N-R method.

The flowchart describing the overall algorithm is given in Figure 5.1. This is a graphical representation of the pseudocode given in Algorithm 1 – both emphasise on outlining the principles of the method rather than the implementation details.

The main idea of the predictor-corrector method shown in Figure 5.1 and Al-

gorithm 1 is to ensure that the predictor step is sufficiently small so that the corrector converges quickly – i.e. that the step size of each predictor step is sufficiently small so that the *integration stays close to the manifold at all times*. This is necessary in order to secure convergence at all points along the manifold.

The two main work-horses of the method – `<predictor>`, the calculation of the predictor step at line 9 – and `<corrector>`, the N-R corrector method at line 11 – are outlined in Section 5.2 and Section 5.4, respectively. Here, the `< . . . >` notation is used to indicate that actually calling either the predictor or the corrector needs both function input (i.e. variables such as number of predictor steps and corrector tolerance) and a slightly more complicated syntax. However, for the purpose of outlining the general workings of the method, it is judged that such details provide no further insight – only clutter. Thus, they are not shown.

If the corrector does not converge during the maximum allowed corrector steps (currently `maxiter`$= 7$[4]), the state object is reverted back to the last converged state and the step size is halved – and the predictor step is repeated with a smaller step size. From Algorithm 1 it seems that such halving may – in theory – produce an infinite loop if the method for some reason hits a singularity. In practice, this is avoided by forcing the user to approve further step size reduction after a certain threshold (currently 5 step size reductions, i.e. a step size scaling factor of $\frac{1}{2^5} = 32$). Such intervention from the user is seldom needed – the step size reduction is not needed for most points along the manifold, and even at the turning points where convergence is most tricky, the method usually converges after a few step size reductions.

Note that the method tries to go back to full step size – this is ensured by increasing the scaling factor at line 17. Thus, any step size reduction due to particular points along the manifold that are difficult to converge will quickly be reverted back to the full step size as soon as possible. Note that the predictor has its own, intrinsic argument for both predictor scaling and predictor direction

[4] While this choice is admittedly somehow arbitrary, it is chosen in order to ensure a sufficiently strict criterion on the step-size reduction. In other words, by choosing a (relatively) small number for `maxiter`, the algorithm is forced to reduce the step-size at difficult pints along the manifold. This in turn ensures that the condition number κ of the Jacobian is kept within reasonable bounds.

based on an *a priori* argument regarding the change of angle using a suitable polar coordinate mapping. This is further discussed in Appendix A.

Algorithm 1 Variable step-length predictor-corrector method

```
# Given external values:
#     steps:          The total number of steps to trace out the manifold
#     state_object:   Object holding the current state

step_count = 0
ps_factor  = 0

while step_counter < steps:
    delta_x     = <predictor>
    state_object.update(delta_x)
    convergence = <corrector>

    if convergence:
        <Add current state to list of converged states>
        step_counter  += ps_factor
        if ps_factor < 1:
            ps_factor *= 2
    else:
        <Revert back to copy of last converged state>
        ps_factor *= 0.5
```

5.3 Computing the predictor step

As discussed in Section 5.1, the predictor step is taken to be the $X \times 1$ vector spanning the nullspace of the Jacobian matrix of the constraint equations, where $X \in \{8, 30\}$, depending on whether it is the constant entropy manifold or the constant entropy production manifold that is to be traced. The Jacobian is calculated analytically from the constraint equations. For the constant entropy manifold, the Jacobian is relatively dense – on the other hand, the Jacobian is much more sparse in the case of the constant entropy production manifold; most of the elements are zero.[5] As the respective Jacobians are an integral part of both the

[5] In the case of constant entropy, of the $7 \times 8 = 56$ elements of $\underline{\underline{J}}$, there are 30 non-zero elements (54% of all possible). In the case of constant entropy production, of the $29 \times 30 = 870$ elements of $\underline{\underline{J}}$, there are 127 non-zero elements (15% of all possible). Note that the above numbers refer to the

predictor in Section 5.3 and corrector in Section 5.4, a more detailed discussion of their structure is deemed appropriate – this may be found in Appendix C.

The nullspace – and more importantly, the vector spanning the nullspace – of $\underline{\underline{J}}(\underline{\boldsymbol{X}})$ is calculated using Gauss elimination.[6] The reader is referred to e.g. (Kreyszig, 2010) or (Süli and Mayers, 2003) for details on the latter.

When the nullspace vector is calculated, it is subsequently scaled by **1)** the intrinsic scaling argument given in Appendix A on line 11 and **2)** by the scaling factor from the main algorithm stemming from the variable step-size strategy on line 14. The actual scaling of the nullspace vector elements is performed inside the **for**-loop on line 14. The scaled nullspace vector is returned as the predictor.

Algorithm 2 Computing the predictor step

```
1  # Given external values:
2  #     steps:          The total number of steps to trace out the manifold
3  #     ps_factor:      Predictor step scaling factor from main algorithm
4
5  jacobian        = self.jacobian
6  nullspace_vector = null(jacobian)
7  phi_dot         = self.calculate_phi_dot
8
9  # Direction and intrinsic scaling from phi dot argument
10 direction       = sign(phi_dot)
11 step_scaling    = (2*pi/steps)*(1/abs(phi_dot))
12
13 # Multiply by scaling factor from main algorithm
14 step_scaling    *= ps_factor
15
16 # Initialize predictor vector
17 delta_x         = []
18
19 for i in nullspace_vector:
20     delta_x[i] = direction*step_scaling*i
21
22 return delta_x
```

The reason for introducing a scaling strategy is based on the fact that the Jacobian

elements that are non-zero from an analytical point of view: one or several of the analytical elements may evaluate to zero at the given state.

[6] The PYTHON module that performs this Gauss elimination and subsequent nullspace vector extraction is written by Associate Professor Tore Haug-Warberg, and is used with kind permission.

of the constraints – from which the nullspace, and subsequently the nullspace vector – is extracted is not normed in any way. As such, the resulting nullspace vector length – an thus the predictor step of a method not employing any scaling – would vary (greatly) along the manifold. This is not the desired behaviour. While it is difficult to visualize the full 30×1 nullspace vector, a useful proxy is the projection of the nullspace vector into the $\mathbb{R}^2$ Cartesian plane of the driving forces for mass and heat transfer. It is postulated that if the method manages to restrict the step size in this projection – i.e. that the arc length traced out by the method in each step is approximately constant – a smooth tracing of the hypersurface that is the manifold is possible.

The fact that there are two separate scaling strategies is important. The scaling based on the intrinsic $\dot{\phi}$ argument in **1)** above is sufficient in itself when the manifold to be traced has a circle-like shape when projected down into $\mathbb{R}^2$ Cartesian plane of the driving forces for mass and heat transfer in the case of the constant entropy production. In such a projection, requiring that the arc length traced out with each predictor step is uniform is *approximately the same as requiring a uniform change in angle*, that is $\dot{\phi} = \text{const}$. In brief, if it is possible to calculate the sign and magnitude of $\dot{\phi}$ at each step along the manifold, both the magnitude and direction of the predictor vector may be appropriately scaled *in the limiting case of a circular projection*. However, the method works fairly well as long as the *eccentricity of the ellipse* – that is, the projection of the manifold in $\mathbb{R}^2$ – is not large. The details of the argument will be further explained in Appendix A.

While true for some transport law formulations it turned out that this argument was not sufficient when the projections were sufficiently *eccentric* – i.e. that the resulting ellipse has an *eccentricity* approaching unity, $e \to 1$. The eccentricity of a true circle is zero, and while none of the projected manifolds depict a true circle, the degree of eccentricity determined whether or not the intrinsic $\dot{\phi}$ argument worked alone. See (Thomas Jr. et al., 2009) for a discussion on eccentricity.

Thus, an additional scaling argument is needed. A pragmatic approach is taken – the requirement that the corrector converges is taken as a criterion, halving the predictor step if convergence is not possible. Note that this scaling is *superpositioned* on the intrinsic $\dot{\phi}$ argument – the latter is always in effect, while the

former is applied only when necessary (as judged by lack of quick convergence). In practice, this seems like a well-functioning strategy.

5.4 The Newton-Raphson corrector method

The purpose of Section 5.4 is to explain the mathematics behind and implementation of the N-R corrector employed as a part of the general predictor-corrector strategy outlined in Section 5.2. The former is presented in Subsection 5.4.1, where thegeneral N-R iteration scheme for solving systems of (non-linear) equations is discussed. The latter is outlined in Subsection 5.4.2, where the simplified algorithm for the corrector method is outlined in Algorithm 3.

5.4.1 Mathematics of the Newton-Raphson method

The N-R method is an iterative numerical method for finding an approximate solution to the root(s) of a (system of) non-linear equation(s), as described in standard texts on engineering mathematics and numerical methods, e.g. (Kreyszig, 2010).

The method may be derived from a Taylor series expansion for a multi-variable function as shown in eq. (5.5), ignoring 2nd order and higher terms. The left-hand side of eq. (5.5) is taken as zero, as this is the sought-after solution

$$\boldsymbol{F}(\underline{\boldsymbol{x}}_0 + \Delta\underline{\boldsymbol{x}}) \approx \boldsymbol{F}(\underline{\boldsymbol{x}}_0) + \underline{\underline{\boldsymbol{J}}}(\underline{\boldsymbol{x}}_0)\Delta\underline{\boldsymbol{x}} \tag{5.5}$$

$$0 \approx \boldsymbol{F}(\underline{\boldsymbol{x}}_0) + \underline{\underline{\boldsymbol{J}}}(\underline{\boldsymbol{x}}_0)\Delta\underline{\boldsymbol{x}}$$

$$\implies \quad \Delta\underline{\boldsymbol{x}} \approx -\underline{\underline{\boldsymbol{J}}}(\underline{\boldsymbol{x}}_0)^{-1}\boldsymbol{F}(\underline{\boldsymbol{x}}_0) \tag{5.6}$$

where $\underline{\underline{\boldsymbol{J}}}(\underline{\boldsymbol{x}})^{-1}$ is the inverse of the Jacobian matrix of $\boldsymbol{F}(\underline{\boldsymbol{x}})$, the latter being

defined as

$$\underline{\underline{J}}(\underline{x}) = \begin{bmatrix} \left(\frac{\partial f_1}{\partial x_1}\right)_{x_{i\neq 1}} & \left(\frac{\partial f_1}{\partial x_2}\right)_{x_{i\neq 2}} & \cdots & \left(\frac{\partial f}{\partial x_n}\right)_{x_{i\neq n}} \\ \left(\frac{\partial f_2}{\partial x_1}\right)_{x_{i\neq 1}} & \left(\frac{\partial f_2}{\partial x_2}\right)_{x_{i\neq 2}} & \cdots & \left(\frac{\partial f_2}{\partial x_n}\right)_{x_{i\neq n}} \\ \vdots & \vdots & \ddots & \vdots \\ \left(\frac{\partial f_n}{\partial x_1}\right)_{x_{i\neq 1}} & \left(\frac{\partial f_n}{\partial x_2}\right)_{x_{i\neq 2}} & \cdots & \left(\frac{\partial f_n}{\partial x_n}\right)_{x_{i\neq n}} \end{bmatrix} \tag{5.7}$$

Usually, it is preferred to solve the system of linear equations written as

$$\underline{\underline{J}}(\underline{x}_k)(\underline{x}_{k+1} - \underline{x}_k) = -f(\underline{x}_k) \tag{5.8}$$

rather than performing the actual inversion of the Jacobian matrix. The N-R method is iterative, such that $\underline{x}_{k+1}$ is used as a starting point in the subsequent iteration loop, finding the approximate solution $\underline{x}_{k+2}$. The iteration is continued until the approximate roots are sufficiently close to zero, usually governed by a combination of an *a priori* absolute tolerance and a criterion on the size of the $\Delta\underline{x} = (\underline{x}_{k+1} - \underline{x}_k)$ step – the method is allowed to continue as long as the norm of this vector is decreasing. The details of the tolerance criterion implemented are further discussed in Subsection 5.4.2.

It is well-known that the N-R method is a second-order method, which may be shown by analysis of the neglected higher-order terms in the Taylor series of eq. (5.5) (Kreyszig, 2010, Chap. 19.2). As such, the precision of the approximation is doubled at every iteration sufficiently close to the solution. This means that the number of iterations needed for the N-R method to converge is often small. It should be noted that the method is – in general – sensitive with respect to the initial guess. In other words, the first approximation to the solution must be sufficiently close to the actual solution. In the case of employing the N-R method as the corrector in the manifold tracing strategy, this problem may be mitigated by taking sufficiently small predictor steps to ensure that the tracing is always close to the converged manifold.

5.4.2 Outline of the corrector algorithm

It is argued in (Press et al., 2007) that the N-R method is the only elementary method for root finding that is applicable for multidimensional problems. It is emphasised that the N-R method works "very well" given that the initial guess is close to the actual solution. For the manifold tracing problem – using a variable step-length predictor – such proximity is ensured. Additionally, the N-R method shines when an analytical Jacobian is attainable. In the context of thermodynamics, this is usually possible.

Furthermore, it is claimed that "(...) there are no good, general methods for solving systems of more than one non-linear equation." (Press et al., 2007) It is argued that *a priori insight* about the system at hand is crucial to be able to solve it efficiently. In the context of physical problem solving – such as the case in the current work – such insight is usually attainable. While this in itself is not sufficient in order to ensure convergence, it certainly does help the chances for success.

One of the main benefits of using the N-R method over ready-made methods such as the well-known `fsolve()` function in MATLAB is that the N-R method is both *transparent* and *unforgiving*. The former implies that the modeller actually have a fair idea of what the method actually does to find the solution. The latter – while seemingly counter-intuitive – is the fact that since the N-R method is expected to converge fast if everything is as it should be, catching errors is actually made easier. If the method converges, but does so very slowly, it is often an indication that e.g. the Jacobian is wrong. Receiving such feedback is frequently very helpful.

The pseudocode for the implemented N-R method is shown in Algorithm 3. The computation of the solution to the system of equations described by eq. (5.8) on line 20 is the key to the method. Here, the system of non-linear equations is linearised through the use of the Jacobian. The state object is updated by the N-R step, `dx`, on line 23, and a new residual us calculated on line 24. Then, the norm of both the residual and the N-R step is evaluated at line 26. The method is deemed to have converged if **a)** the former norm is below an *a priori* given tolerance (`tolerance` $= 1 \times 10^{-12}$ is used) and **b)** the latter norm is larger than

Algorithm 3 Newton-Raphson corrector method

```
# Given external values:
#     delta_x:            The predictor step
#     state_object:       Object holding the current state
#     tolerance = 1e − 12:  Absolute tolerance
#     maxiter = 7:        Maximum number of allowed iterations

itercounter     = 0
convergence     = False
last_dx_norm    = ∞

current_res = state_obj.residual()

while not convergence and itercounter < maxiter:
    itercounter += 1
    # Augmenting the Jacobian with predictor step
    # Ensures N × N square Jacobian, as needed
    current_jac  = state_obj.jacobian(delta_x)

    # Solving system of linearised equations
    dx = solve(current_jac, current_res)

    # Update state, re-evaluate residual
    state_obj.update(dx)
    current_res = state_obj.residual()

    if norm(current_res < tolerance) and norm(dx < last_dx_norm):
        convergence = True

    # No convergence? Update dx norm
    last_dx_norm = norm(dx)

return convergence
```

that of the last N-R step. Thus, the method is allowed to iterate to a solution that is *as accurate as possible* – within the given maximum number of allowed iterations (`maxiter` $= 7$).

If the method converges, the **`while`**-loop terminates and the method returns `True`. The `state_object` now holds the converged state of the system, so there is no *explicit* return of any values. Using such an object-oriented programming (OOP) approach is natural in PYTHON, and is – if implemented with care – a strong tool for providing proper *abstraction* of the code.

If the convergence check at line 26 returns false, the norm of the current N-R step is stored and the method continues. The Jacobian and residual are re-evaluated using the new object state, and a new system of linear equations is solved. As such, the method continues until convergence – or until the maximum number of allowed iterations is reached. If the latter limit is reached without convergence, a `convergence = False` flag is returned to the main algorithm described in Section 5.2, and the step size is subsequently reduced in order to attempt to find an initial point for the N-R corrector that is closer to the converged solution – thus securing convergence.

Chapter 6

Results and discussion

> The purpose of computing is insight, not numbers.
>
> RICHARD HAMMING[1]

The purpose of the current chapter is to present and discuss the results from tracing the manifolds of constant entropy and constant entropy production. This includes verification of the internal entropy production matches that calculated from the external flows, that the integration of the entropy production from a perturbed state back to that of equilibrium yields the original perturbation in S.

6.1 Overview of the cases

The purpose of the current section is to provide the reader with an overview of the cases examined and discussed in the current chapter. These are outlined in Table 6.1 below. It is emphasised that N_2 and Ar should be seen as representative diatomic and monoatomic components, respectively.

While the original intention was to provide the reader with an extensive set of cases to be contrasted, time constraints disallowed such an attempt. Thus, the base cases are studies – in addition to the integration of the entropy production discussed in Section 6.4 and the notion of a deep relationship between the

[1] Preface to and motto of *"Numerical Methods for Scientists and Engineers"*, (Hamming, 1973)

TABLE 6.1: Overview of the cases discussed in the current chapter

Case	Components	Initial ΔT	System
Case 0	N_2,Ar	0.5 K	Closed system
Case 1	N_2,Ar	0.5 K	Open system
Integration	N_2,Ar	1 K	Closed system
Ellipses	N_2,Ar	1 K	Open & closed system

constant entropy manifold and the constant entropy production manifold as outlined in Section 6.5

6.2 Case 0: Constant entropy manifold

The purpose of this section is to establish a familiarity with the base case for the constant entropy manifold by studying the behaviour of a chosen set of variables along the manifold. The idea is that this makes it easier to appreciate the differences between this base case and those resulting from varying e.g. the composition or initial perturbations of T.[2]

The constant entropy manifold visualised in $(\Delta T_{\text{red}}, \Delta(C_A)_{\text{red}})$ coordinates in $\mathbb{R}^2$ are shown in Figure 6.1. The initial perturbation corresponding to $\Delta T = 0.5\,\text{K}$ is shown as a triangle. It is noted that the contour forms that of an ellipse around the origin, as expected.

Furthermore, the temperature and mass profiles along the constant entropy manifold are shown in Figure 6.2. As expected, these are inversely correlated – the deviation from the equilibrium temperature is at a maximum when the deviation from equilibrium composition is zero, and vice versa. This behaviour is apparent from the constraint equations – in order to fulfil these, the mass and energy redistribution along the constant entropy manifold must balance, so to speak.

[2] As noted in the Section 6.1, time constraints disallowed the study of more cases than the base case. However, the argument still stands – establishing familiarity with the base case will make further investigations easier.

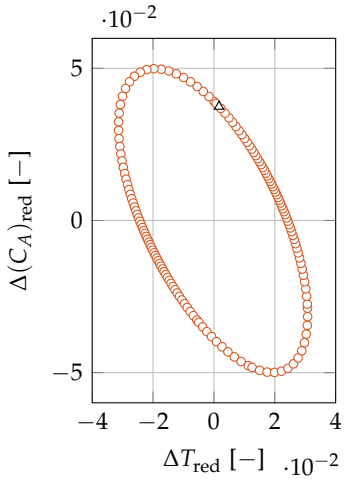

FIGURE 6.1: Case 0: Constant entropy manifold given in $(\Delta T_{\text{red}}, \Delta(C_A)_{\text{red}})$ coordinates. The initial point corresponding to $\Delta T = 0.5\,\text{K}$ is designated by triangle.

It is seen from Figure 6.2 that the maximum temperature deviation from that of equilibrium for subsystem 1 along the manifold is twice that of subsystem 2. This corresponds well with the fact that the initial mole number in subsystem 2 is twice that of subsystem 1 – 15 mol and 7.5 mol, respectively.[3]

The pressure profile along the constant entropy manifold is given in Figure 6.3. It is evident that the mechanical equilibrium of eq. (4.13) is fulfilled at all points along the manifold. Note also that the overall change in pressure is small, with a maximum of a few Pa from that of equilibrium.[4] This notion of a small overall change in pressure along the manifold will be exploited when the entropy production of the closed system is integrated from a perturbed state to that of equilibrium, as further discussed in Section 6.4.

The initial entropy production $(\dot{S}_{\text{irr}})_{\text{init}}$ along the constant entropy manifold is

[3] The fact that the components have different heat capacity – $\frac{5}{2}R$ and $\frac{7}{2}R$ for the monoatomic (Ar) and diatomic (N_2) gas component, respectively – is hard to discern from Figure 6.2 alone. This is largely due to the fact that the change in composition along the manifold is relatively small.

[4] At first glance, it may seem counter-intuitive to have a pressure variation in a system at mechanical equilibrium. However, as briefly discussed in Chapter 4, the fact that $p_1 = p_2 = p$ along the manifold does put any restrictions on the actual magnitude of the pressure – only thatisequal in the two subsystems at all times.

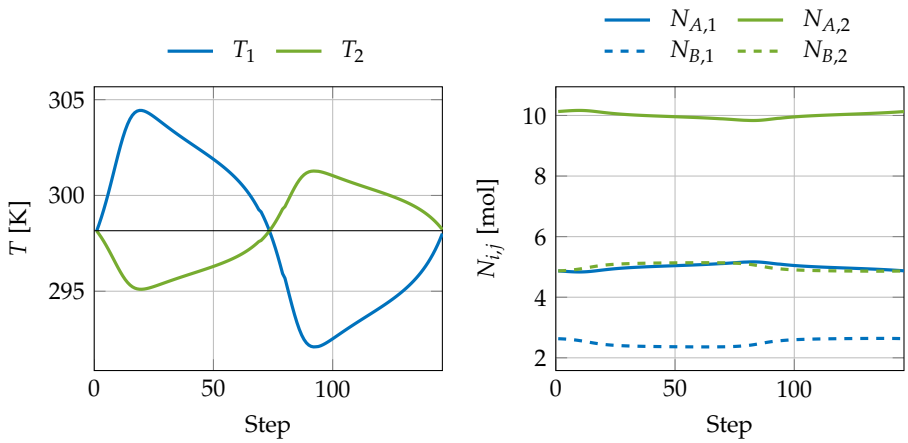

FIGURE 6.2: Case 0: Temperature and component mass profiles along the constant entropy manifold.

shown in Figure 6.4. This is calculated using Fick's law for the mass transport. In the same figure, the characteristic time constant $\tau = \frac{\Delta S}{(\dot{S}_{\text{irr}})_{\text{init}}}$ is presented. As is evident from this definition, the τ is inversely proportional to $(\dot{S}_{\text{irr}})_{\text{init}}$. This is the observed behaviour in Figure 6.4.

6.3 Case 1: constant entropy production manifold

As was the case with Section 6.2, the purpose of this section is to establish a familiarity with the base case for the constant entropy production manifold. It is deemed important to have an idea of how the different variables comprising the system behave in this base case, so that characteristic changes of model behaviour when exploring e.g different transport law formulations may be better appreciated.[5]

The constant entropy manifold from case 1 of Table 6.1 is shown in Figure 6.5 Here, the naive formulations of Fick's and Fourier's laws are used for mass

[5] As noted in Section 6.1, time constraints disallowed the study of more cases than the base case. However, the argument still stands – establishing familiarity with the base case will make further investigations easier.

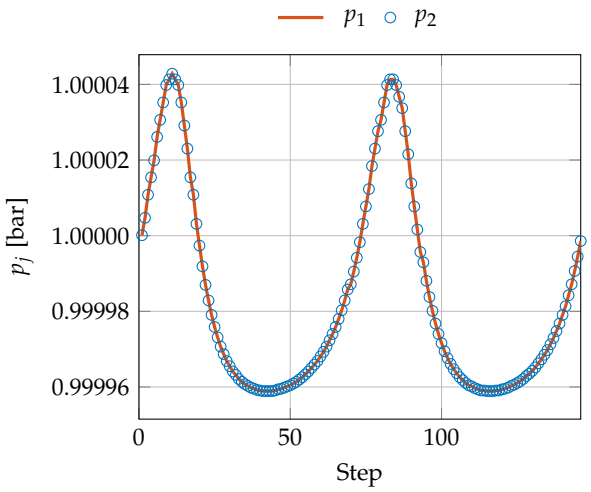

FIGURE 6.3: Case 0: Pressure profile along the constant entropy manifold. Note that $p_1 = p_2$ along the whole manifold – as dictated by the mechanical equilibrium condition of eq. (4.13) – and that the overall change in pressure is small.

transfer and heat transfer, respectively.

Note the close similarity between Figure 6.1 and Figure 6.5. Both are elliptic, centred around the origin. The possible consequences of this similarity is further discussed in Section 6.5

The temperature and component mass profiles of the constant entropy manifold are displayed in Figure 6.6. While these profiles in some ways are similar to the ones displayed in Figure 6.2, there are distinct differences. The temperature and component mass profiles closely match the profiles of mass and heat transfer shown in Figure 6.7, as must be expected. It is noted that the point of zero total heat flow corresponds to the point where $\Delta T = 0$, as it should.

The mass and heat transfer – both internal and external – is shown in Figure 6.7. The notation used is that of Chapter 4. Note that in the case of mass transfer – displayed to the right of Figure 6.7 – the external transport exactly match the internal transport in order to maintain the system at steady-state. On the other hand, $\hat{Q}^{\dagger}$ will necessarily ensure that $\hat{Q}_1 \neq \hat{Q}_2$, as discussed in Subsection 4.3.3.

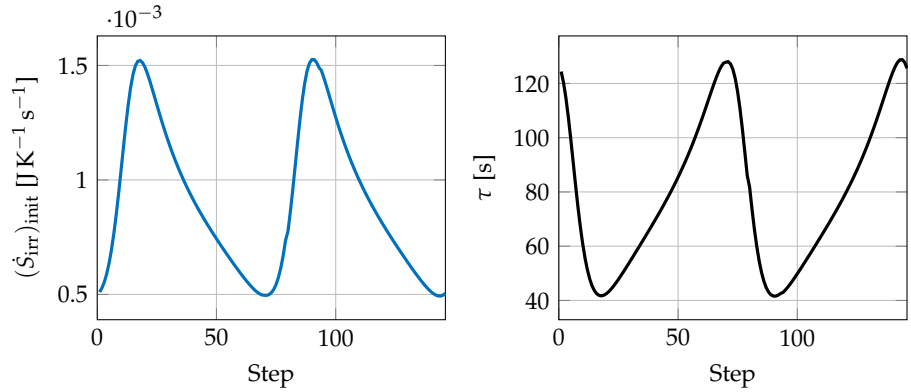

FIGURE 6.4: Case 0: The initial entropy production and characteristic time constant along the constant entropy manifold.

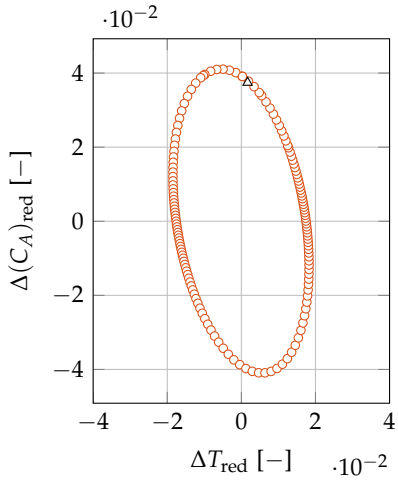

FIGURE 6.5: Case 1: Constant entropy production manifold given in $(\Delta T_{\text{red}}, \Delta(C_A)_{\text{red}})$ coordinates. The initial point corresponding to $\Delta T = 0.5\,\text{K}$ is designated by triangle.

However, as is evident from the figure, this effect is small relative to the absolute magnitude of the heat transfer – as expected.

As is expected, the maximum mass transport occurs around the point where $\hat{Q} = 0$. This is a direct consequence of the equation structure for the open system

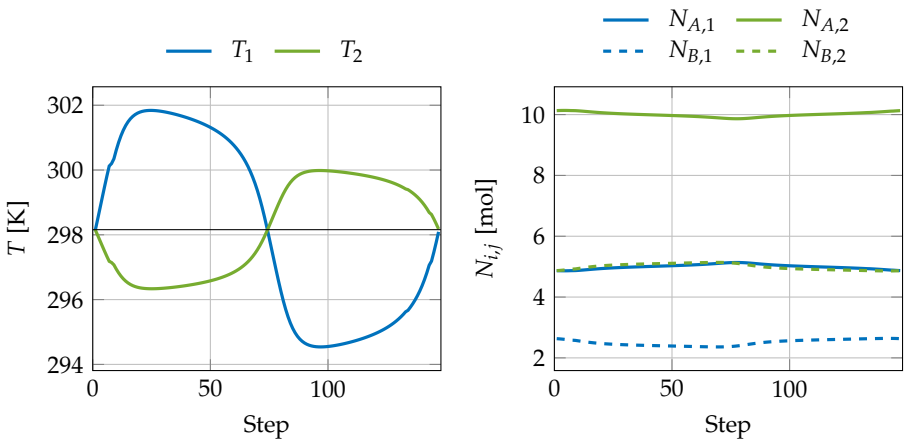

FIGURE 6.6: Case 1: Temperature and component mass profiles along the constant entropy production manifold.

– since a restriction is put on $\dot{S}_{\text{irr}}$ to be constant, the mass and heat transport must vary out of sync along the manifold in order to fulfil this criterion.

In Figure 6.8, the variation of system pressure and reservoir pressures of the open system along the constant entropy production is shown. As is expected, the criterion of mechanical equilibrium is maintained at all times. Furthermore, the change in magnitude of the pressure along the manifold may be seen as negligible for all practical purposes – a maximum deviation of a couple Pa from that of the equilibrium state.

The change in the reservoir pressures displayed to the right of Figure 6.8 reflect the mass transfer occurring between the subsystems. As chemical equilibrium is assumed to be instilled at all times between the reservoirs and their respective subsystems, the pressure of the reservoirs is the necessary degree of freedom (DOF) to ensure that this is fulfilled. In other words: the pressure of the reservoirs will adjust so that $\mu_{i,j} = (\mu_{i,j})^{\text{rsvr}}$.

The error of the entropy production calculated from the external flows ($(\dot{S}_{\text{irr}})_{\text{ext}}$) along the manifold is contrasted with that calculated from the internal irreversible processes ($(\dot{S}_{\text{irr}})_{\text{int}}$) in Figure 6.9. Note that the error here is taken as

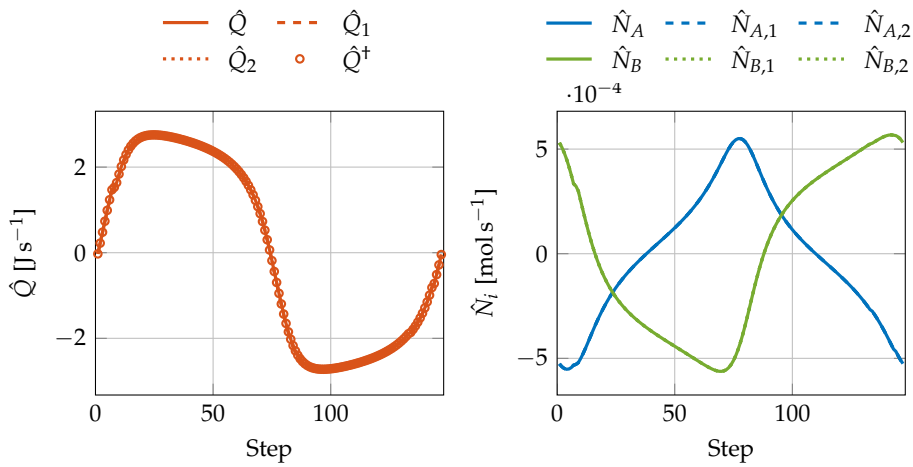

FIGURE 6.7: Case 1: Mass and heat transfer along the constant entropy production manifold. The notation employed is that of Chapter 4. Note that the external flows in essence are identical to the internal transfer – thus, the reservoirs merely act to supply mass and energy (the latter in terms of heat) such that the system is maintained at a steady-state.

the deviation from the entropy production calculated at the initial perturbation point. As such, the value of Figure 6.9 is twofold; first, it shows that the entropy production is indeed constant along the traced manifold – to within the accuracy of the numerical method. Secondly, and perhaps slightly more interesting, is the fact that the entropy production calculated from observing the external flows is indeed identical to the one calculated from explicitly accounting for the internal irreversible processes. The theoretical argument for this is given in Section 2.6 – as such, Figure 6.9 may be seen as a proof-of-concept for this idea.

In Figure 6.10, the number of Newton-Raphson (N-R) iterations needed at each step along the manifold is shown. It is evident that the corrector rapidly converges at each step, as is the desired behaviour based on the discussion in Chapter 5. Furthermore, the condition number for the Jacobian of the system is shown. While there is some variation along the manifold, the condition number never rises to unacceptable values due to the variable step-length method employed, as discussed in Chapter 5.

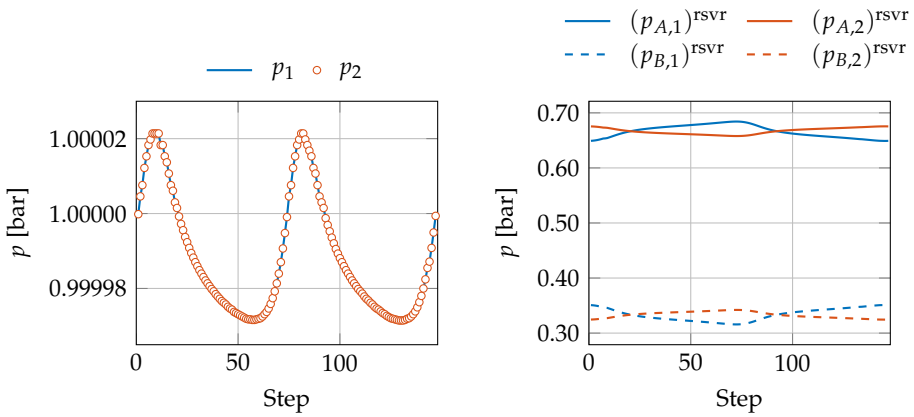

FIGURE 6.8: Case 1: System and reservoir pressure along the constant entropy production manifold. It is observed that as in the case of the constant entropy manifold, the change in pressure is small – and the constraint of mechanical equilibrium is maintained along the manifold. Furthermore, the respective reservoir pressures are observed to correlate well with the mass transfer – the pressure of the reservoirs must necessarily change in order to ensure that chemical equilibrium is instilled at all times between the reservoir and the corresponding subsystem.

6.4 Integrating the entropy production

As discussed in Section 2.6, it is shown that integrating the entropy production along the trajectory from a perturbed state and back to the state of equilibrium should yield the difference in entropy between the equilibrium state and that of the perturbed state. Assuming that it is sufficient to integrate for a finite time $t \gg t_0$, eq. (2.37) state that

$$\Delta S = \left(\frac{\mathrm{d}\dot{S}_{\text{irr}}}{\mathrm{d}t}\right)_{\text{acc}} \approx \int_{t=t_0}^{t\gg t_0} \dot{S}_{\text{irr}}\,\mathrm{d}t \tag{6.1}$$

Here, $\left(\frac{\mathrm{d}\dot{S}_{\text{irr}}}{\mathrm{d}t}\right)_{\text{acc}}$ refers to the accumulated entropy production along the integration path.

In Figure 6.11, the result of such an integration using a simple forward-Euler approach with logarithmic time is shown. Furthermore, the temperature and

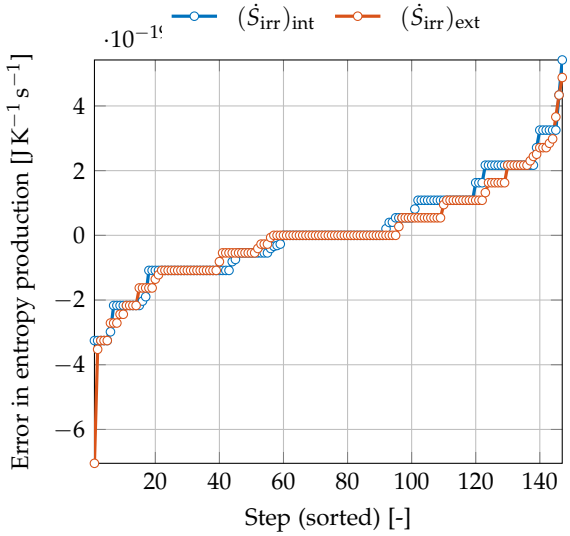

FIGURE 6.9: Case 1: Consistency check on the entropy production by observing the error in $(\dot{S}_{\text{irr}})_{\text{int}}$ and $(\dot{S}_{\text{irr}})_{\text{ext}}$ to that of the initial entropy production. Note the scale on the ordinate axis; the error is negligible for all practical purposes – it is on the order of the numerical method precision – and it is confirmed that $(\dot{S}_{\text{irr}})_{\text{int}} = (\dot{S}_{\text{irr}})_{\text{ext}}$. The latter was argued theoretically in Section 2.6.

pressure profiles for the subsystems along the integration path are shown in Figure 6.12. Fick's and Fourier's laws are used to describe the diffusive mass and heat transport, respectively. Note that the pressure of the subsystems is not controlled during the integration – this will introduce a certain error. However, it is noted that the deviation in pressure during the relaxation process is small; thus, the error is expected to be of similar nature. It seems that the argument given in in eq. (6.1) holds to within the expected error of the integrator. The behaviour depicted in Figure 2.3 is displayed, which may be seen as an experimental verification in favour of the *a priori* argument.

Note that the initial slope of the entropy production trajectory is unexpected. A sharp transition between the steady-state production of the open system and that of the relaxation towards equilibrium for the closed system is predicted – this does not seem to apply to the current modelling experiment. The reason

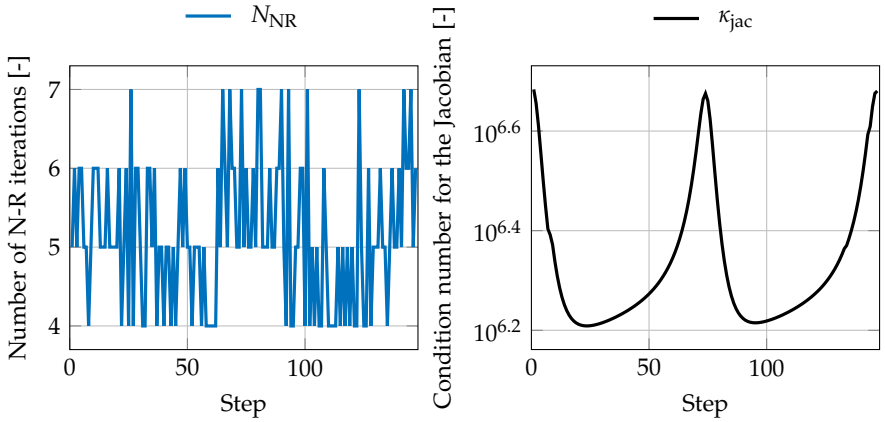

FIGURE 6.10: Case 1: The number of N-R iterations at each point along the constant entropy manifold, along with the condition number for the Jacobian.

for this deviation from expected behaviour is at the present not explainable, and should be further investigated.

6.5 A relationship between $\Delta S = \text{const}$ and $\dot{S}_{\text{irr}} = \text{const}$

In this section, a relationship between the constant entropy manifold and the constant entropy production manifold *in terms of both the respective projections being ellipses in the Cartesian* $\mathbb{R}^2$ *plane when sufficiently close to equilibrium* is explored and discussed. While certainly an intriguing notion, it should be remarked that the full implication of this relationship is not yet understood.

In general, an ellipse may be described as the set of points (x, y) in the Cartesian $\mathbb{R}^2$ plane such that $x = a\cos(\theta)$ and $y = b\sin(\theta + \alpha)$ for $\theta \in [0, 2\pi]$. Here, a correspond to the major axis, b correspond to the minor axis and α is a phase shift governing the angle of the ellipse with respect to the $(x, y$ coordinate system. Thus, three variables (a, b, α) is sufficient to describe a general ellipse. This will be exploited below.

From classical thermodynamics it may be shown that the state of equilibrium is one of maximum entropy, as discussed in Chapter 2. As such, a Taylor expansion

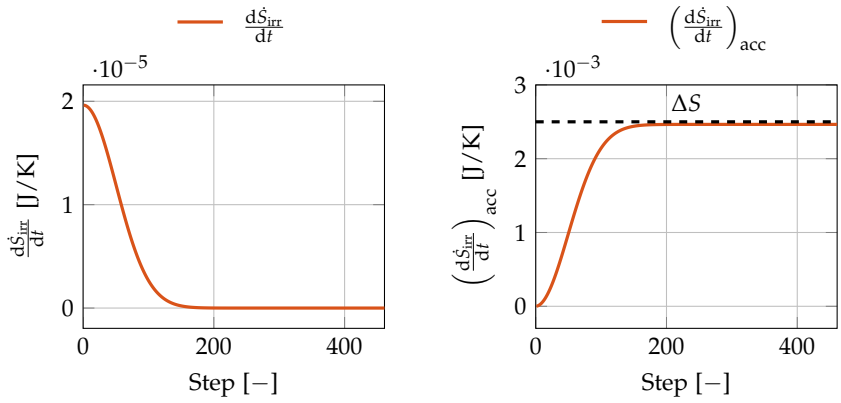

FIGURE 6.11: Integrating the entropy production along the trajectory from a perturbed state and back to the state of equilibrium for the closed system. Fick's and Fourier's laws are used for the mass and heat transfer, respectively. Note that $\left(\frac{d\dot{S}_{irr}}{dt}\right)_{acc} \approx \Delta S$, as expected from Section 2.6.

around the origin yield terms that are of quadratic and higher order, since the first derivatives must by necessity be zero at the extremal (maximum) point. The Hessian of $S$is known to be positive definite, yielding positive eigenvalues. Thus, one would expect such a quadratic function to yield an ellipse-like projection in the Cartesian $\mathbb{R}^2$ plane. This is indeed observed, as is shown in Section 6.2.

Furthermore, by combining eq. (3.8) and eq. (3.9) from Section 3.2, one may show that

$$\dot{S}_{\text{irr}} = \sum_{i,k} X_i L_{ik} X_k \geq 0 \tag{6.2}$$

where X_i, X_k are the thermodynamic driving forces and L_{ik} are the phenomenological coefficients. The inequalities follow from the second law of thermodynamics, stating that the entropy production must be positive at any non-equilibrium state (Kjelstrup et al., 2010). Thus, it is expected that the constant entropy production manifold give an ellipse-like projection in the Cartesian $\mathbb{R}^2$ plane. This is observed behaviour in Section 6.3.

As such, there seems to be a close relationship between the two manifolds. Returning to the earlier argument, an arbitrary ellipse may be transformed into

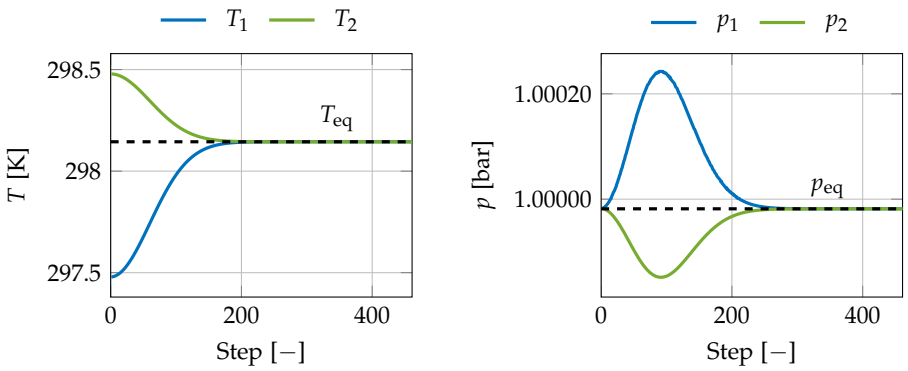

FIGURE 6.12: The temperature and pressure profiles along the integration path from a perturbed state and back to the state of equilibrium for the closed system.

any other manipulating the three variables (a, b, α) alone. Thus, one should be able to *map from the constant entropy manifold to that of constant entropy production using a maximum of three variables* for the case of a binary system.

As a visual proof-of-concept of this behaviour, a general ellipse described with the variables a, b, α is fitted to each of the manifolds of Figure 6.13. Here, the projections of the respective manifolds are shown in the coordinates that are assumed to correspond to the thermodynamic driving forces that give the desired behaviour for the mass and heat transport, as briefly discussed in Section 3.3.[6] This is achieved by a few iterations of trial-and-error, with surprising ease.[7]

The key question that arises is this: is it possible to find uncomplicated transformations between the constant entropy manifold and the manifold of constant entropy production through these ellipses in the general case? If this is so, the applications could prove to be numerous. Before diving too deep into this question,

[6] It should be emphasised that no claim is made from the author to having *proved* that these are the relevant thermodynamic driving forces. A convincing argument is made by Haug-Warberg (2015*a*) in this regard, and the author has used the end result in order to produce the figure given in Figure 6.13. As such, it may be viewed as a *plausible postulate* in the context of the current work.

[7] To the author's slight astonishment, only two to three attempts had to be made in order to fit the general ellipse equation to each of the manifold projections. While the fit is not entirely perfect, as is evident from Figure 6.13, the method works well. That being said, the process could – and should – be automated if this notion of ellipse mapping holds up against further investigation.

others should be investigated:

1. Does this concept easily extend to multicomponent systems – i.e. systems that are non-binary?
2. How close must the manifold projections be to the origin – i.e. how large deviations from equilibrium may be permitted?
3. Is the concept practical – i.e. does a sufficiently simple mapping between the two manifold projections exist in the general case?

That there is a connection between the constant entropy manifold and constant entropy production manifold should perhaps not come as a surprise. Nonetheless, the fact that the projections show such a close relationship through the use of regular ellipses is fascinating. At worst, this concept is of theoretical interest only. At best, it provides a promising approach for describing simultaneous irreversible phenomena using the deviation from equilibrium and a subsequent mapping to the constant entropy manifold. In order to answer the above questions, further investigations must be undertaken.

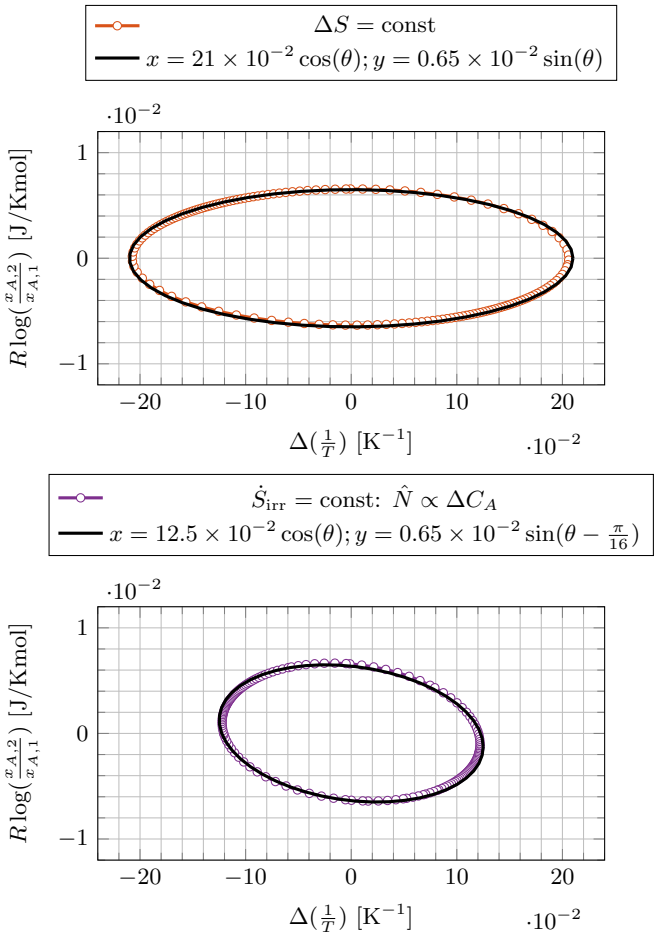

FIGURE 6.13: A relationship between the $\Delta S = \text{const}$ and the $\dot{S}_{\text{irr}} = \text{const}$ manifold projections in $\mathbb{R}^2$ Cartesian coordinates using ellipses. Note that the fit between the ellipses and the manifold projections are relatively accurate. The figure must be seen as a *proof-of-concept* – with a few manual iterations, two general ellipse equations are fitted to their respective manifold.

Chapter 7

Concluding remarks and further work

The purpose of the this chapter is to summarise the most important findings of the current work, and to propose a direction in which this work may be continued. While the concept of relating the manifolds of constant entropy and constant entropy production seem to hold great promise, several aspects of the idea must be clarified in order to judge whether the approach may be put to practical use.

Conclusion

The main purpose of the current work has been to investigate irreversible phenomena in general, with emphasis on simultaneous mass and heat transfer. An entropy production formalism is used in connection with mathematical modelling in order to study these phenomena. A central task has been the development and investigating a model system consisting of two connected subsystems, each containing a binary ideal gas mixture. Mass and heat transfer between the two subsystems is allowed, thus giving rise to irreversible phenomena and entropy production.

First, the case of a closed system perturbed from the equilibrium state is investigated. The equations that constrain this problem give rise to constant entropy manifolds. Next, the subsystems are allowed to exchange mass and energy with external reservoirs, thus maintaining the total system at a steady-state. The con-

straint equations for the system will now give rise to manifolds of constant entropy production. In order to investigate the two situations, a variable step-length predictor-corrector method was developed and employed. Both types of manifolds were successfully traced, and the results were subsequently investigated.

It has become clear that employing the entropy balance in the context of modelling irreversible phenomena is a powerful tool, which may be utilized in addition to the conservation laws of mass, energy and momentum normally applied to chemical engineering problems. Using the entropy balance to ensure modelling consistency is particularly advantageous – the fact that the same entropy production may be calculated in different ways is a powerful principle that should be exploited.

A central purpose of the manifold tracing has been to investigate the – seemingly deep – connection between the manifold of constant entropy and the manifold of constant entropy production. It is shown that the projections of both manifolds to suitable coordinates in the Cartesian $\mathbb{R}^2$ plane may be described as generalised ellipses. This give rise to possibility of a mapping between the two manifolds, thus providing a connection between the deviation from equilibrium entropy on the one hand to that of constant entropy production on the other.

It should be emphasised that the results from the current work are not conclusive as to whether the correlation between the entropy production manifold and manifold of constant entropy may be employed to predict or describe the general behaviour of irreversible processes occurring. Thus, it is not known whether the current work has any direct practical application for the treatment of simultaneous mass and heat transfer. However, the results are seen as a promising, and further investigations are recommended.

Further work

Based on this thesis, it is evident that modelling irreversible phenomena – even employing assumptions such as ideal gas behaviour and binary mixtures – is a

complex endeavour. As such, there are several aspects of the current work which demand further research:

- The current model should be utilized to further investigate the effect of different transport formulations, as well as the effect of more advanced thermodynamic model assumptions. This may shed light on the question of how the connection between the manifolds scale with added complexity.
- The model should be extended so that a two-phase system may be investigated. Such systems are common in the chemical engineering practise – thus, they are seen as a highly attractive target for further work.
- The relationship between the constant entropy production manifold and the manifold of constant entropy should be further investigated. There seems to be a fundamental connection between the two that is yet to be fully understood, and the possible practical implications of this connection should be further investigated.
- Reactive mixtures – both equilibrium reactions and rate-based reactions – should be studied in connection with the simultaneous mass and heat transfer.

Bibliography

Allgower, E. L. and Georg, K. (2003), *Introduction to Numerical Continuation Methods*, Classics in Applied Mathematics, Society for Industrial and Applied Mathematics.

Atkins, P. (2010), *The Laws of Thermodynamics: a Very Short Introduction*, Oxford University Press.

Atkins, P. and de Paula, J. (2010), *Physical Chemistry*, 9 edn, Oxford University Press.

Aylward, G. and Findlay, T. (2008), *SI Chemical Data*, 6 edn, Wiley.

Berglihn, O. T. (2010), Dynamic Simulation on a Thermodynamic Canonical Basis, PhD thesis, Norwegian University of Science and Technology, Faculty of Natural Sciences and Technology, Department of Chemical Engineering.

Bird, R. B. (1957), 'The equations of change and the macroscopic mass, momentum, and energy balances', *Chemical Engineering Science* **6**, 123–131.

Bird, R. B. (2004), 'Five decades of transport phenomena', *AIChE journal* **50**.

Bird, R., Lightfoot, E. and Stewart, W. (2007), *Transport phenomena*, Wiley.

Box, G. E. P. and Draper, N. R. (2007), *"Response Surfaces, Mixtures, and Ridge Analyses"*, Wiley.

Brendsdal, E. (1999), Computation of Phase Equilibria in Fluid Mixtures, PhD thesis, Telemark University College, Faculty of Technology.

Callen, H. B. (1985), *Thermodynamics and an introduction to thermostatistics*, Wiley.

Chatterjee, I. and Joshi, J. (2008), 'Modeling, simulation and optimization: Mono pressure nitric acid process', *Chemical Engineering Journal* **138**, 556–577.

Chorkendorff, I. and Niemantsverdriet, J. (2007), *Concepts of modern catalysis and kinetics*, Wiley.

Cussler, E. L. (2009), *Diffusion: Mass Transfer in Fluid Systems*, 3 edn, Cambridge University Press.

de Groot, S. and Mazur, P. (1984), *Non-equilibrium Thermodynamics*, Dover Publications.

de Koeijer, G. M. (2002), Energy efficient operation of distillation columns and a reactor applying irreversible thermodynamics, PhD thesis, Norwegian University of Science and Technology, Faculty of Natural Sciences and Technology, Department of Chemistry.

Denbigh, K. (1971), *The Principles of Chemical Equilibrium*, 3 edn, Cambridge University Press.

Denbigh, K. G. (1951), *The Thermodynamics of the Steady State*, Methuen & Co, Ltd.

Denbigh, K. G. (1959), 'Nonequilibrium thermodynamics: A survey', *AIChE Journal* **5**, 20–25.

Dill, K. A. and Bromberg, S. (2010), *Molecular Driving Forces: Statistical Thermodynamics in Chemistry and Biology*, 2 edn, Garland Science.

Downey, A. B. (2012), *Think Python - How to Think Like a Computer Scientist*, O'Reilly Media.

Fogler, H. S. (2005), *Elements of chemical reaction engineering*, Prentice-Hall.

Geankoplis, C. (2003), *Transport processes and separation process principles (includes unit operations)*, Prentice Hall.

Glasser, L. (1965), 'The non-equilibrium thermodynamics of chemical processes', *Journal of Chemical Education* **42**, 597–600.

Gmehling, J., Kolbe, B., Kleiber, M. and Rarey, J. (2012), *Chemical Thermodynamics for Process Simulation*, Wiley.

Hamming, R. W. (1973), *Numerical Methods for Scientists and Engineers*, 2 edn, Dover.

Hanc, J., Tuleja, S. and Hancova, M. (2004), 'Symmetries and conservation laws: Consequences of Noether's theorem', *American Journal of Physics* **72**, 428.

Haug-Warberg, T. (2006*a*), 'Cstr thermodynamics', Personal communication.

Haug-Warberg, T. (2006*b*), *Den termodynamiske arbeidsboken*, Kolofon Forlag AS.

Haug-Warberg, T. (2015*a*), 'Consistent thermodynamic driving force for diffusive mass transfer', Personal communication, 15.06.2015.

Haug-Warberg, T. (2015*b*), 'Equimolar counterdiffusion in isothermal, binary ideal gas systems', Personal communication, 22.04.2015.

Haug-Warberg, T. (2015*c*), 'Integrating in a positive mathematical direction', Personal communication, 04.04.2015.

Hill, T. L. (1960), *An Introduction to Statistical Mechanics*, Addison-Wesley.

Jakobsen, H. A. (2008), *Chemical reactor modeling : multiphase reactive flows*, Berlin : Springer.

Kjelstrup, S., Bedeaux, D., Johannessen, E. and Gross, J. (2010), *Non-Equilibrium Thermodynamics for Engineers*, World Scientific.

Kjelstrup, S. and Helbæk, M. (2006), *Fysikalsk kjemi*, 2 edn, Fagbokforlaget.

Kondepudi, D. (2008), *Introduction to Modern Thermodynamics*, Wiley.

Kondepudi, D. and Prigogine, I. (1998), *Modern thermodynamics : from heat engines to dissipative structures*, Wiley.

Kooijman, H. A. and Taylor, R. (1995), 'A nonequilibrium model for dynamic simulation of tray distillation columns', *AIChE Journal* **41**, 1852–1863.

Kreyszig, E. (2010), *Advanced Engineering Mathematics*, John Wiley & Sons.

Krishna, R. and Taylor, R. (1993), *Multicomponent mass transfer*, Wiley.

Krishna, R. and Wesselingh, J. (1990), *Mass transfer*, Ellis Horwood.

Krishnamurthy, R. and Taylor, R. (1985*a*), 'A nonequilibrium stage model of multicomponent separation processes. part i: Model description and method of solution', *AIChE Journal* **31**, 449–456.

Krishnamurthy, R. and Taylor, R. (1985*b*), 'A nonequilibrium stage model of multicomponent separation processes. part ii: Comparison with experiment', *AIChE Journal* **31**, 456–465.

Lewis, G. N. and Randall, M. (1961), *Thermodynamics*, 2 edn, McGraw-Hill. Revised by Kenneth S. Pitzer and Leo Brewer.

Linstrom, P. and Mallard, W., eds (n.d.), NIST *Chemistry WebBook,* NIST *Standard Reference Database Number 69*, National Institute of Standards and Technology. http://webbook.nist.gov, Accessed: 31.05.2015.

Løvfall, B. T. (2008), Computer Realization of Thermodynamic Models Using Algebraic Objects, PhD thesis, Norwegian University of Science and Technology, Faculty of Natural Sciences and Technology, Department of Chemical Engineering.

Nocedal, J. and Wright, S. J. (1999), *Numerical Optimization*, Springer.

Onsager, L. (1931*a*), 'Reciprocal relations in irreversible processes. i.', *Physical Review* **37**, 405–426.

Onsager, L. (1931*b*), 'Reciprocal relations in irreversible processes. ii.', *Physical Review* **38**, 2265–2279.

Pereira, F. E., Galindo, A., Jackson, G. and Adjiman, C. S. (2014), 'On the impact of using volume as an independent variable for the solution of p–t fluid-phase equilibrium with equations of state', *Computers & Chemical Engineering* **71**, 67 – 76.

Pradhan, M. P., Suchak, N. J., Walse, P. R. and Joshi, J. B. (1997), 'Multicomponent gas absorption with multiple reactions: modelling and simulation of nox absorption in nitric acid manufacture', *Chemical Engineering Science* **52**, 4569–4591.

Press, W. H., Teukolsky, S. A., Vetterling, W. T. and Flannery, B. P. (2007), *Numerical Recipes: The Art of Scientific Computing*, 3 edn, Cambridge University Press.

Prigogine, I. (1949), '"Le domaine de validité de la thermodynamique des phénomènes irréversibles"', *Physica* **15**, 272–284.

Redlich, O. (1976), *Thermodynamics: Fundamentals, Applications*, Elsevier Scientific Publishing Company.

Reiss, H. (1996), *Methods of Thermodynamics*, Dover.

Saad, M. A. (1997), *Thermodynamics: Principles and Practise*, Prentice Hall.

Sandler, S. I. (1989), *Chemical and Engineering Thermodynamics*, 2 edn, Wiley.

Schwarzbach, B. E. and Kosmann-Schwarzbach, Y. (2010), *The Noether Theorems: Invariance and Conservation Laws in the Twentieth Century*, Springer.

Siepmann, V. (2006), Process Modelling on a Canonical Basis, PhD thesis, Norwegian University of Science and Technology, Faculty of Natural Sciences and Technology, Department of Chemical Engineering.

Siepmann, V. (2015), 'Rate of entropy production from the time derivative of the total differential of internal energy', Personal communication, 18.05.2015.

Sonerud, K. B. (2014), Rate-based approach to nox absorption modelling using thermodynamic driving forces, Technical report, Norwegian University of Science and Technology, Faculty of Natural Sciences and Technology, Department of Chemical Engineering.

Susskind, L. and Hrabovsky, G. (2014), *Classical Mechanics: The Theoretical Minimum*, Penguin Science, Penguin Books.

Süli, E. and Mayers, D. (2003), *An Introduction to Numerical Analysis*, Cambridge University Press.

Taylor, R., Kooijman, H. and Hung, J.-S. (1994), 'A second generation nonequilibrium model for computer simulation of multicomponent separation processes', *Computers & Chemical Engineering* **18**, 205–217.

Thomas Jr., G. B., Hass, J. and Weir, M. D. (2009), *Calculus 2*, Pearson Custum Publishing. Compiled from: *University Calculus*, (2007).

van der Ham, L. (2011), Improving the Second Law Efficiency of a Cryogenic Air Separation Unit, PhD thesis, Norwegian University of Science and Technology, Faculty of Natural Sciences and Technology, Department of Chemistry.

Weir, M., Hass, J. and Giordano, F. (2005), *Thomas' Calculus*, Thomas Series, Pearson Addison Wesley.

Wesselingh, J. A. (1997), 'Non-Equilibrium Modelling of Distillation', *Chemical Engineering Research and Design* **75**, 529–538.

Zumdahl, S. S. (2009), *Chemical Principles*, 6 edn, Houghton Mifflin Company.

Appendix A

Integrating in a positive mathematical direction

When tracing out the manifolds of constant entropy and constant entropy production using the method outlined in Chapter 5, a it is important to ensure that

1. The manifold is traced in a *continuous direction*. Which direction that is chosen is largely irrelevant – the important point is that *no erratic change of direction during the tracing may be allowed*
2. The predictor step length ensures that the manifold is traced smoothly – in other words, that the *method stays sufficiently close to the manifold at all times.*

Judging the geometric interpretation of the latter criterion is not easy since the constant entropy manifold and constant entropy production manifold are in $\mathbb{R}^7$ and $\mathbb{R}^{29}$, respectively. It is postulated that a useful metric is to ensure that the predictor takes a step which length makes the *arc length* traced in a suitable $\mathbb{R}^2$ projection uniform.[1] The latter projection is assumed to be that of the reduced driving force coordinates, i.e. $(\frac{\Delta C_A}{(C_A)_{\text{eq}}}, \frac{\Delta T}{T_{\text{eq}}}$ using Fick's law for the mass transfer. The rationale is that these coordinates are closely tied to

[1] It should be explicitly stated that while the rationale behind this strategy is neat – especially so because it actually works – it should be seen as a *elegant solution to a practical problem*. In other words, the practical results of using this approach are valuable regardless of the theoretical soundness of the argument.

the irreversible processes that are modelled. For the constant entropy manifold, this argument has no clear tie to the physical interpretation of the model – as no irreversible processes are accounted for – but the $(\frac{\Delta C_A}{(C_A)_{\text{eq}}}, \frac{\Delta T}{T_{\text{eq}}}$ coordinates are used regardless.[2] For the purpose of Appendix A, these driving force coordinates are labelled generically as (x, y), being a projection in the Cartesian $\mathbb{R}^2$ plane.

It is further assumed that for a circular contour in $\mathbb{R}^2$, ensuring that $\dot{\phi} = \text{const}$ is a useful proxy for the arc length argument. For a true circle,

$$\frac{L_{\text{arc}}}{2\pi r} = \frac{\phi}{2\pi} \quad \Longrightarrow \quad L_{\text{arc}} = \phi r \tag{A.1}$$

$$\dot{L}_{\text{arc}} \propto \dot{\phi} \tag{A.2}$$

where L_{arc} is the arc length, ϕ is the angle in polar coordinates and r is the radius in polar coordinates. Thus, the change in arc length is proportional to the change in angle. It should be explicitly noted that while the formal argument is only strictly true for a perfect circle, it is expected to give the (approximate) desired behaviour – $\dot{L_{\text{arc}}} \propto \dot{\phi}$ – for elliptic contours that do not deviate substantially from the circle, thus ensuring a smooth manifold tracing. Now, a way of calculating $\dot{\phi}$ from the change in the driving force coordinates (x, y) is desired. An clever mathematical argument by Haug-Warberg (2015c) for this purpose is explored in Appendix A.1.

A.1 Calculating change in ϕ from change in (x,y)

In the subsequent derivation, the approach of (Haug-Warberg, 2015c) is followed. The main idea is to transform from Cartesian (x, y) to a polar (r, ϕ), and exploiting the fact that this enables the calculation of $\dot{\phi}$ by knowing (x, y) and $(\dot{x}, \dot{y})$ alone.

In general, a mapping from a Cartesian (x, y) to a polar (r, ϕ) coordinate system may be achieved using

$$x = r \cos \phi \tag{A.3}$$

$$y = r \sin \phi \tag{A.4}$$

[2] From a practical point of view, this strategy seems to yield the desired result.

where r is the radius in polar coordinates and ϕ is the angle in polar coordinates.

The former is defined as

$$r = \sqrt{x^2 + y^2} \tag{A.5}$$

The reader is referred to e.g. (Thomas Jr. et al., 2009) for more details on polar coordinates in general.

Differentiation of eq. (A.3) yields

$$\dot{x} = r\cos\phi - r\sin\phi\dot{\phi} \tag{A.6}$$

$$\dot{y} = r\sin\phi + r\cos\phi\dot{\phi} \tag{A.7}$$

Written in matrix notation, and using eq. (A.5) to eliminate r

$$\begin{pmatrix} \dot{x} \\ \dot{y} \end{pmatrix} = \begin{pmatrix} \frac{x}{\sqrt{x^2+y^2}} & -y \\ \frac{y}{\sqrt{x^2+y^2}} & x \end{pmatrix} \begin{pmatrix} \dot{r} \\ \dot{\phi} \end{pmatrix} \tag{A.8}$$

Calculating the inverse of the coefficient matrix (see e.g. (Kreyszig, 2010) for details) in order to write

$$\begin{pmatrix} \dot{r} \\ \dot{\phi} \end{pmatrix} = \frac{1}{\frac{x^2}{\sqrt{x^2+y^2}} + \frac{y^2}{\sqrt{x^2+y^2}}} \begin{pmatrix} x & y \\ \frac{-y}{\sqrt{x^2+y^2}} & \frac{x}{\sqrt{x^2+y^2}} \end{pmatrix} \begin{pmatrix} \dot{x} \\ \dot{y} \end{pmatrix} \tag{A.9}$$

Thus, simplifying $\frac{1}{\frac{x^2}{\sqrt{x^2+y^2}} + \frac{y^2}{\sqrt{x^2+y^2}}} = \frac{1}{\sqrt{x^2+y^2}}$ and multiplying the prefactor into the matrix

$$\begin{pmatrix} \dot{r} \\ \dot{\phi} \end{pmatrix} = \begin{pmatrix} \frac{x}{\sqrt{x^2+y^2}} & \frac{y}{\sqrt{x^2+y^2}} \\ \frac{-y}{x^2+y^2} & \frac{x}{x^2+y^2} \end{pmatrix} \begin{pmatrix} \dot{x} \\ \dot{y} \end{pmatrix} \tag{A.10}$$

Rewriting

$$\begin{pmatrix} \left(\sqrt{x^2+y^2}\right)\dot{r} \\ \left(x^2+y^2\right)\dot{\phi} \end{pmatrix} = \begin{pmatrix} x & y \\ -y & x \end{pmatrix} \begin{pmatrix} \dot{x} \\ \dot{y} \end{pmatrix} \tag{A.11}$$

Now, it is possible to calculate the sign of $\dot{\phi}$ as

$$\text{sign}(\dot{\phi}) = \text{sign}(-y\dot{x} + x\dot{y}) \tag{A.12}$$

and the magnitude of $\dot{\phi}$ as

$$\dot{\phi} = \frac{-y\dot{x} + x\dot{y}}{x^2 + y^2} \tag{A.13}$$

Thus, knowing only the Cartesian coordinates (x, y) and their derivatives $(\dot{x}, \dot{y})$, the derivative of ϕ may be calculated. Note that both the sign and the magnitude of $\dot{\phi}$ is needed – the former avoids erratic change in sign of the predictor, and the latter scales the size of the predictor step. Thus, the above method will always ensure both constant direction and equiangular predictor steps.

The beauty of the $\dot{\phi}$ argument is that it provides an *a priori* condition for the predictor step size. This, in turn, permits defining the number of points on the manifold that are to be calculated – while still ensuring that the complete contour in $\mathbb{R}^2$ is traced out exactly[3] once. From the perspective of the modeller, this is a distinct advantage.

A.2 Visual proof-of-concept

From Figure A.1 it is seen that the argument discussed earlier indeed provides a constant change of angle at each step of the manifold tracing. This is especially visible by looking at the zoomed-in area seen to the right in Figure A.1.

This may be seen as a visual proof-of-concept of the strategy outlined above.

[3] In theory, this would yield an exact metric. In practise, the corrector interferes – more or less, depending on the particular problem – an thus the method overshoots or undershoots slightly. The effects on the corrector are discussed in Appendix A.2 below.

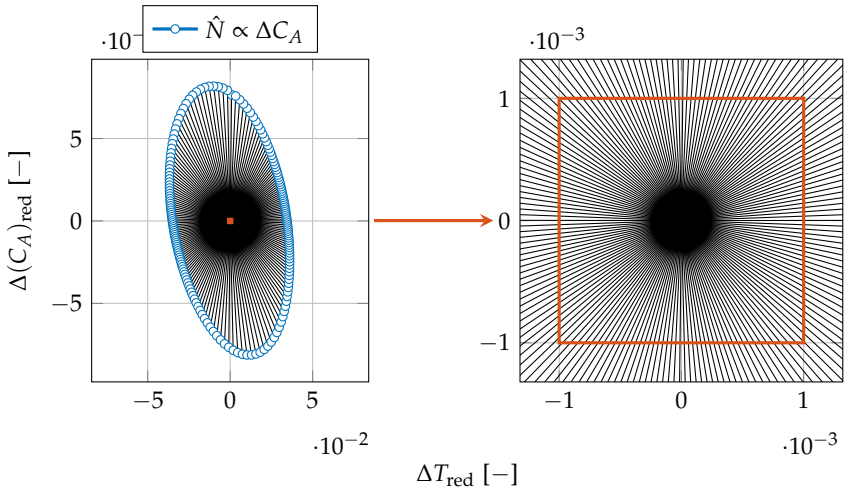

FIGURE A.1: Constant entropy production manifold in $(\Delta(C_A)_{\text{red}}, \Delta T_{\text{red}})$ coordinates, using $\hat{N}_A \propto \Delta C_A$ (Fick's law). By zooming in on a small area surrounding the origin, the fact that $\dot{\phi} = \text{const}$ is clearly visible.

Note, however, that the strategy does not work as well for the tracing of manifold which projection into the chosen $\mathbb{R}^2$ coordinates display an ellipse with eccentricity approaching unity. For such a manifold, the argument demanding constant $\dot{\phi} = \text{const}$ is not a good proxy for the underlying desire of constant arc length of the predictor at each step along the $\mathbb{R}^2$ projection. The predictor steps are (relatively) small in areas close to the origin, and correspondingly (relatively) large in the areas far from the origin – both in the $\mathbb{R}^2$ projection. Large steps imply that the predictor step does not necessarily stay close to the manifold. Thus, the corrector must either **a)** compensate substantially or **b)** will fail to converge, as illustrated in Figure A.2.

While the method successfully traces out the manifold, it is evident that the angle is not constant – a visual clue to the fact that the corrector most compensate substantially due to the (relatively) long predictor taken at certain areas of the manifold.

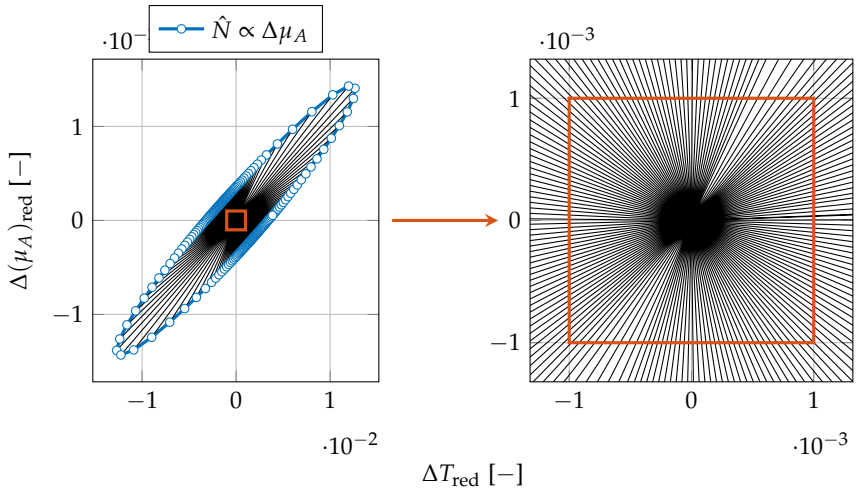

FIGURE A.2: Constant entropy production manifold in $(\Delta(\mu_A)_{\text{red}}, \Delta T_{\text{red}})$ coordinates, using $\hat{N}_A \propto \Delta\mu_A$. By zooming in on a small area surrounding the origin, it is evident that the corrector most compensate substantially in the areas, with the result that $\dot{\phi} \neq$ const at all points along the manifold.

Appendix B

Generating symbolic Hessian using Python

In the current problem formulation, the Helmholtz free energy is used to express the derivatives of the constraint equations directly. However, at an earlier stage is was reasoned that using internal energy, $U(S, V, N)$, would provide a simplified problem structure. The idea was to employ SymPy[1] - a PYTHON library for symbolic mathematics - in order to provide a symbolic nullspace vector, which could in turn be evaluated at the given state. The intention was to avoid any numerical issues when calculating the nullspace vector, as well as providing a better understanding of the nullspace vector elements that would constitute the (unscaled) predictor.

It was found that these benefits were outweighed by the necessity of mapping from $(T, V, N) \mapsto (S, V, N)$, as the former coordinates are those corresponding to the chosen equation of state (EOS) (ideal gas law). This is – in theory – not an issue, but in practise such a mapping requires the construction of additional Jacobians and functions. Also, the symbolic calculations would not scale well as the system was expanded to account for the necessary reservoirs and transport equations. A symbolic nullspace vector may be feasible for a relatively small, purely thermodynamic system, but was deemed to be inadequate for treating the extended problem formulation. Thus, both using (S, V, N) as the chosen state

[1] SymPy is free, lightweight and is written entirely in PYTHON- as such, no external libraries are required. The aim is "(...) to become a full-featured computer algebra system (CAS) while keeping the code as simple as possible in order to be comprehensible and easily extensible." An extensive documentation and example usage is available at http://www.sympy.org/

variables and using SymPy for the nullspace vector calculations was abandoned.

For completeness, an approach to expressing the Hessian of the internal energy in terms of Helmholtz free energy coordinates is outlined below using SymPy for symbolic matrix algebra. The mathematics and thermodynamic argument behind the general approach is discussed by Haug-Warberg (2006*a*).

This short script is shown in PYTHON code B.1. It should be emphasised that while the procedure outlined here will provide a more consistent way of calculating symbolic Hessians of other potentials than that of traditional hand calculations, it is in no way automatic and still requires the user to explicitly state $\frac{\partial x}{\partial y}$, the Jacobian for the mapping from $x \mapsto y$, and $\frac{\partial g}{\partial y}$, the derivative of the gradient of U with respect to y. Thus, the benefit of the approach below is that no matrix inversion is required - an operation that may be both cumbersome and error-prone.

LISTING B.1: hessian_U_SVN_in_TVN.py

```
#########################################################################
# Hessian of U(S,V,N) in terms of A(T,V,N)
#
# Expression the symbolic Hessian of U(S,V,N) in terms of derivatives of
# A(T,V,N), i.e. in Helmholtz coordinates. SymPy - a Python library  for
# symbolic  mathematics  -  is  utilized for the symbolic matrix algebra
#
# Author:     Kjetil Sonerud
# Updated:    2015-03-04 14:09:47
#########################################################################

import sympy as sp

# Define 2nd derivatives of A(T,V,N) as symbols
A_TT, A_TV, A_TN = sp.symbols('A_TT A_TV A_TN')
A_VT, A_VV, A_VN = sp.symbols('A_VT A_VV A_VN')
A_NT, A_NV, A_NN = sp.symbols('A_NT A_NV A_NN')

# x = (S,V,N)
# y = (T,V,N)
# g = dU/dx = (T,-p,mu)

dxdy = sp.Matrix([
                    [-A_TT, -A_TV, -A_TN],
                    [    0,     1,     0],
                    [    0,     0,     1]
                ])

dgdy = sp.Matrix([
                    [1,       0,    0],
                    [A_VT, A_VV, A_VN],
                    [A_NT, A_NV, A_NN]
                ])

# Calculating and printing the symbolic Hessian
H = dgdy*(dxdy**-1)
print H

```

```
39 | # Using SymPy's LaTeX output for ease of use in reports etc.
40 | print sp.latex(H)
```

The result from PYTHON code B.1 is shown in eq. (B.1) below

$$\begin{bmatrix} -\frac{1}{A_{TT}} & -\frac{A_{TV}}{A_{TT}} & -\frac{A_{TN}}{A_{TT}} \\ -\frac{A_{VT}}{A_{TT}} & A_{VV} - \frac{A_{TV}A_{VT}}{A_{TT}} & -\frac{A_{TN}A_{VT}}{A_{TT}} + A_{VN} \\ -\frac{A_{NT}}{A_{TT}} & -\frac{A_{NT}A_{TV}}{A_{TT}} + A_{NV} & A_{NN} - \frac{A_{NT}A_{TN}}{A_{TT}} \end{bmatrix} \tag{B.1}$$

Here, $A_{X_1X_2}$ is the second derivative of Helmholtz free energy with respect to X_1 and X_2, holding other state variables constant with each differentiation. Thus, A_{TT} is shorthand for $\left(\frac{\partial^2 A}{\partial T^2}\right)_{V,\underline{n}}$. Given that $A(T,V,N)$ is known, the separate elements of the above Hessian – or the complete matrix – may be evaluated.

While an equivalent result may be found by treating each element of the Hessian of $U(S,V,N)$ separately, and expressing these in terms of $A(T,V,N)$ by employing suitable *Maxwell relations*[2] and (clever) use of total differentials, the latter approach is found - by hard-won experience - to be much more error-prone. In order to illustrate this alternative approach, finding $U_{SS} \stackrel{?}{=} -A_{TT}^{-1}$ is performed. Starting out with

$$\left(\frac{\partial^2 U}{\partial S^2}\right)_{V,\underline{n}} = \left(\frac{\partial T}{\partial S}\right)_{V,\underline{n}} \tag{B.2}$$

where the definition $\left(\frac{\partial U}{\partial S}\right)_{V,\underline{n}} \triangleq T$ from Section 2.1 is used. Alternatively, from differentiation of eq. (2.11b)

$$S = -\left(\frac{\partial A}{\partial T}\right)_{V,\underline{n}} \quad \Longrightarrow \quad \left(\frac{\partial S}{\partial T}\right)_{V,\underline{n}} = -\left(\frac{\partial^2 A}{\partial T^2}\right)_{V,\underline{n}} = -A_{TT} \tag{B.3}$$

[2] A *Maxwell relation* is a – frequently useful – thermodynamic identity between selected partial derivatives, e.g. $\left(\frac{\partial T}{\partial V}\right)_{S,\underline{n}} = -\left(\frac{\partial p}{\partial S}\right)_{V,\underline{n}}$ (Denbigh, 1971). This may be found from the fact that $\frac{\partial}{\partial V}\left(\frac{\partial U}{\partial S}\right) = \frac{\partial}{\partial S}\left(\frac{\partial U}{\partial V}\right)$ – the state variables that are to be held constant during the differentiation are omitted for clarity. The latter – and Maxwell relations in general – is a result of what is often called the *Mixed Derivative Theorem*: if $f(x,y)$ and its partial derivatives f_x, f_y, f_{xy}, f_{yx} are defined throughout an open region containing a point (a,b) and are all continuous at (a,b), then $f_{xy}(a,b) = f_{yx}(a,b)$. According to (Weir et al., 2005), this result was first published by Leonhard Euler in 1734, in a series of papers he wrote on hydrodynamics.

Thus, combining eq. (B.2) and eq. (B.3), it is found that

$$\left(\frac{\partial^2 U}{\partial S^2}\right)_{V,\underline{\boldsymbol{n}}} = -A_{TT}^{-1} \tag{B.4}$$

as expected from eq. (B.1). Deriving the cross-terms may be done in a similar fashion, but these calculations are more tedious – thus, more prone to human error.

Appendix C

Jacobian structure

> Everyone knows that debugging is twice as hard as writing a program in the first place. So if you're as clever as you can be when you write it, how will you ever debug it?
>
> BRIAN W. KERNIGHAN[1]

The purpose of Appendix C is to visualise and briefly discuss the structure of the Jacobians used as a key part of the manifold tracing strategy of Chapter 5. As both the predictor and the corrector method hinge on the correct implementation – both structurally and numerically – of the Jacobian, a lot of time was spent on both derivation and debugging.[2] First, the Jacobian for the closed system described in Section 4.2 is outlined in Appendix C.1. The resulting Jacobian is the key to tracing the constant entropy manifold. Next, the Jacobian for the open system described in Section 4.3 is outlined in Appendix C.2. The latter is an integral part of the numerical tracing of the constant entropy production manifold.

[1] *"The Elements of Programming Style"*, (McGraw-Hill, 1978)

[2] Through hard-won experience, it was realised that while it is often easy do derive analytical Jacobians for a thermodynamic system of moderate size, the strategy scales badly – the likelihood of human error is large. A single wrong sign may be enough to render the whole Jacobian useless. Even though a more automated approach is beyond the scope of this work, it would be essential if the system structure were to be further scaled. The interested reader is referred to (Løvfall, 2008) for intriguing ideas on this topic in the context of thermodynamics.

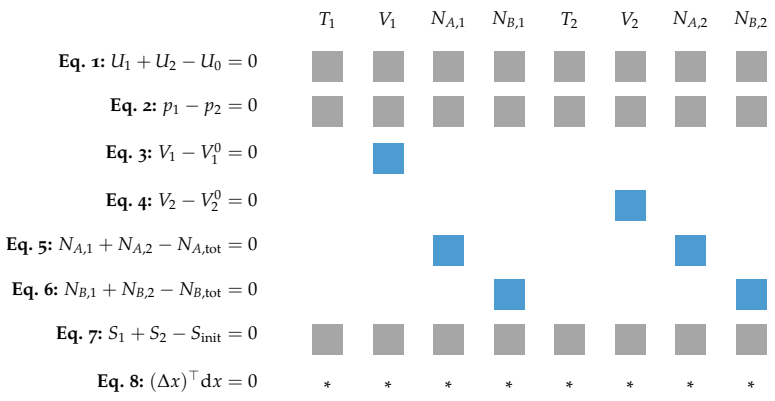

FIGURE C.1: The structure of the Jacobian for the closed system described in Section 4.2. The reader is referred to the main text for an explanation of the sign convention employed.

C.1 Jacobian structure: closed system

The Jacobian for the closed system is a (relatively) dense 8×8 matrix, as visualized in Figure C.1. Here, ■ indicates a positive element with a numeric value of 1. The sign of elements marked as ■ may vary based on the state of the system and the components chosen – no a priori distinction is possible.

Note that the last row – the elements denoted by *** – represent the predictor vector. As discussed in Chapter 5, the predictor vector is used to extend the 7×8 Jacobian that results from the differentiation of the constraint equations with respect to the state variables alone. In addition to ensuring a square Jacobian needed for the Newton-Raphson (N-R) method, the rationale is that it is sensible to require the corrector steps to be orthogonal to that of the predictor. It should be noted that this last row has no connection to the physical model – it is entirely a result of the numerical strategy chosen to solve the manifold tracing problem.

C.2 Jacobian structure: open system

The structure of the Jacobian for the open system is shown in Figure C.2. The convention for the elements are the same as the one employed in Appendix C.1 – ■ denotes a positive element with a numeric value of 1 and ■ denotes that the sign may vary depending on the state of the subsystems and the components chosen for the model. In addition, ■ denotes a negative element with numeric value of -1. It should be noted that all non-starred elements (i.e. ■, ■ and ■) will structurally remain the same *regardless of the implemented thermodynamic model*. Such a distinction is helpful to keep in mind if the model is to be changed – it is duly exploited when implementing new transport models using an object-oriented programming (OOP) approach.If the system structure itself is altered, the Jacobian must evidently be updated accordingly.

As in Appendix C.1, the elements denoted by *** represent the predictor vector. This is a necessary extension of the Jacobian resulting from the constraint equations alone – as discussed in Chapter 5 – yielding a 30×30 square matrix used in the N-R method. Furthermore, the elements denoted by ** signify the thermodynamic state variables of the two subsystems in the two rows that denote the mass transport equations (**Eq. 13** and **Eq. 14**). Whether these elements are zero or non-zero depends on the actual transport equations implemented for the given model – e.g. in the case of Fick's law for transport of component A, both the elements corresponding to V and $N_{B,j}$ are zero.

The elements denoted by * are the derivatives of the partial molar enthalpy with respect to other thermodynamic state variables than T. While these are strictly zero using the current thermodynamic model – i.e. assuming ideal gas, as outlined in Chapter 4 – this is not generally true. Thus, it should be noted that if a new implementation of the thermodynamic model dictates that such derivatives are non-zero, *the Jacobian structure must be updated to reflect this.*[3]

The variables – constituting the columns – and equations – constituting the rows

[3] This should ideally have been implemented as a feature of the ideal gas model, so that e.g. $\frac{\partial \bar{h}_i}{\partial V}$ could be set to zero in this model, not in the Jacobian structure itself. However, this fact was realised too late – thus, the Jacobian corresponding to the open system must be slightly changed if a more complicated thermodynamic model is to be implemented.

– of Figure C.2 are given in TAB1 below. Note that in the case of the equations, there are only 29 physical constraint equations, as discussed earlier. Abbreviations for the energy balances (EBs) and mass balances (MBs) are employed for the purpose of compact notation. For a more thorough description of the constraint equations and variables, see Section 4.3.

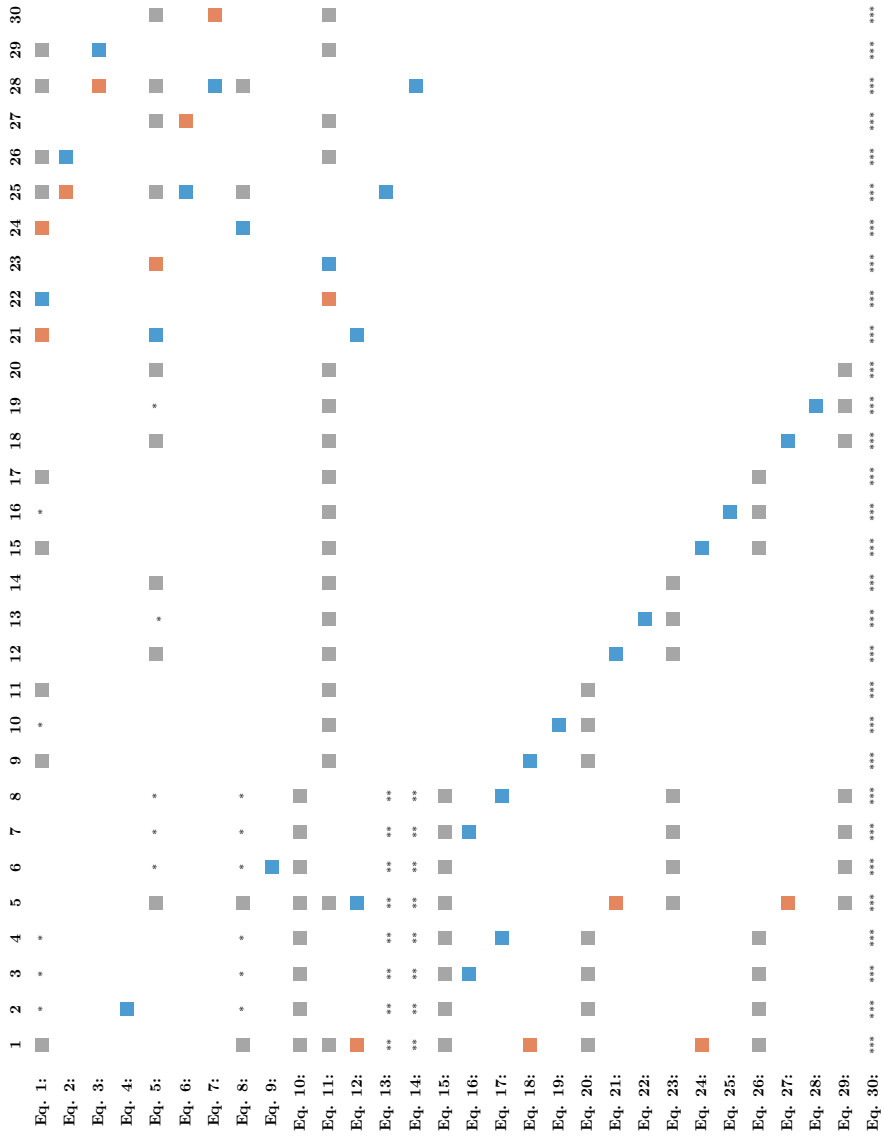

FIGURE C.2: The structure of the Jacobian for the open system described in Section 4.3. The reader is referred to the main text for an explanation of the sign convention employed, and to Table C.1 for the physical interpretation of the variables (columns) and equations (rows).

TABLE C.1: Relating the constraint equations and variables from Section 4.3 to Figure C.2. It is emphasised that there is no link between equation x and variable x other than the fact that they share the same number – as row and column, respectively – in Figure C.2

Row/column number	Constraint equation	Variable
1	EB, system 1	T_1
2	MB, A system 1	V_1
3	MB, B system 1	$N_{A,1}$
4	$V_1 - V_1^0 = 0$	$N_{B,1}$
5	EB, system 2	T_2
6	MB, A system 2	V_2
7	MB, B system 2	$N_{A,2}$
8	EB, connection	$N_{B,2}$
9	$V_2 - V_2^0 = 0$	$(T_{1,A})^{\text{rsvr}}$
10	$p_1 - p_2 = 0$	$(V_{1,A})^{\text{rsvr}}$
11	$\bar{s} = \text{const}$	$(N_{1,A})^{\text{rsvr}}$
12	Heat transport eq.	$(T_{2,A})^{\text{rsvr}}$
13	Mass transport eq., component A	$(V_{2,A})^{\text{rsvr}}$
14	Mass transport eq., component B	$(N_{2,A})^{\text{rsvr}}$
15	$U_1 + U_2 - U_0 = 0$	$(T_{1,B})^{\text{rsvr}}$
16	$N_{A,1} + N_{A,2} - N_{A,0} = 0$	$(V_{1,B})^{\text{rsvr}}$
17	$N_{B,1} + N_{B,2} - N_{B,0} = 0$	$(N_{1,B})^{\text{rsvr}}$
18	$(T_{1,A})^{\text{rsvr}} - T_1 = 0$	$(T_{2,B})^{\text{rsvr}}$
19	$(V_{1,A})^{\text{rsvr}} - (V_{1,A}^0)^{\text{rsvr}} = 0$	$(V_{2,B})^{\text{rsvr}}$
20	$(\mu_{1,A})^{\text{rsvr}} - \mu_{A,1} = 0$	$(N_{2,B})^{\text{rsvr}}$
21	$(T_{2,A})^{\text{rsvr}} - T_2 = 0$	$\hat{Q}$
22	$(V_{2,A})^{\text{rsvr}} - (V_{2,A}^0)^{\text{rsvr}} = 0$	$\hat{Q}_1$
23	$(\mu_{2,A})^{\text{rsvr}} - \mu_{A,2} = 0$	$\hat{Q}_2$
24	$(T_{1,B})^{\text{rsvr}} - T_1 = 0$	$\hat{Q}^{\dagger}$
25	$(V_{1,B})^{\text{rsvr}} - (V_{1,B}^0)^{\text{rsvr}} = 0$	$\hat{N}_A$
26	$(\mu_{1,B})^{\text{rsvr}} - \mu_{B,1} = 0$	$\hat{N}_{A,1}$
27	$(T_{2,B})^{\text{rsvr}} - T_2 = 0$	$\hat{N}_{A,2}$
28	$(V_{2,B})^{\text{rsvr}} - (V_{2,B}^0)^{\text{rsvr}} = 0$	$\hat{N}_B$
29	$(\mu_{2,B})^{\text{rsvr}} - \mu_{B,2} = 0$	$\hat{N}_{B,1}$
30	-	$\hat{N}_{B,2}$